Function of DNA Ligase III in the Repair of Radiation induced DNA Double Strand Breaks via alternative Pathways of Non-homologous End-Joining functioning as Backup

Inaugural-Dissertation

zur

Erlangung des Doktorgrades

Dr. rer. nat.

der Fakultät für Biologie

an der

Universität Duisburg-Essen

vorgelegt von

Katja Paul

aus Bautzen

Februar 2013

Die der vorliegenden Arbeit zugrunde liegenden Experimente wurden am Institut für Medizinische Strahlenbiologie der Universität Duisburg-Essen durchgeführt.

1. Gutachter: Prof. Dr. Georg Iliakis

2. Gutachter: Prof. Dr. Hemmo Meyer

Vorsitzender des Prüfungsausschusses: PD Dr. Jürgen Thomale

Tag der mündlichen Prüfung: 8. Mai 2013

Das Große ist nicht dies oder das zu sein, sondern man selbst zu sein.

Søren Kierkegaard (1813-1855)

Parts of the results in this thesis have been published:

Arakawa, H., Bednar, T., Wang, M., Paul, K., Mladenov, E., Bencsik-Theilen, A.A., and Iliakis, G. (2012). Functional redundancy between DNA ligases I and III in DNA replication in vertebrate cells. Nucleic Acids Res *40*, 2599-2610.

Paul, K., Wang, M., Mladenov, E., Bencsik-Theilen, A.A., Bednar, T., Wu, W., Arakawa, H., and Iliakis, G. (2013). DNA ligases I and III cooperate in alternative non-homologous end-joining in vertebrates. PLoS One *8*, e59505.

Table of contents

Acknowledgements

Work supported by the Bundesministerium für Bildung und Forschung (BMBF) 02NUK001B entitled “Strahleninduzierte DNA Schäden: Wechselwirkung verschiedener Reparaturwege”. This project was integrated into the Kompetenzverbund Strahlenforschung (KVSF).

I am very grateful to my mentor, Prof. Dr. George Iliakis, for giving me the opportunity to perform my Ph.D. at the Institute of Medical Radiation Biology. I would like to thank him for his continued support throughout the years not only on scientific but also on personal matters. It was a great honor and a pleasure for me to work as a member of such a fantastic team.

I would like to thank Prof. Dr. Hemmo Meyer for his readiness to function as reviewer.

Special thanks go to Dr. Hiroshi Arakawa for his brilliant expertise in gene targeting, as well as for the development of the well thought out targeting strategies that led to the generation of the mutants used in the present work.

I would like to also thank Dr. Minli Wang for the nice introduction into DT40 experimentation and for passing on their secrets.

I am also indebted to Theresa Bednar for her help and contribution to this work.

I am grateful to Dr. Emil Mladenov for the critical reading of this thesis and the useful suggestions on structure and interpretation.

It would be a grave omission not to mention the valuable assistance of Ms. J. Müller in administrative issues, of Malihe Mesbah and Tamara Mussfeldt on all kinds of technical support and of Ms. B. Lander for her superb lab organization. Without their help the laboratory would certainly quickly disintegrate.

I am very thankful to all my friends and colleagues in the lab, especially the Cooking evening group. Thank you girls – the evenings are unforgettable and time would not be the same without you.

Above all, however, I would like to thank my family and all my friends in my personal life. My parents, for never giving up promoting and encouraging me all along the way. Jessica, who accepted neglecting her for the last several months and of course Klaus, for being patient, understanding and boundlessly supportive during this difficult and seemingly endless time.

List of abbreviations

~	Approximately
°C	Degree Celsius
4HT	4-Hydroxytamoxifen
53BP1	P53 Binding Protein 1
6-4PP	6-4 pyrimidine-pyrimidone photoproduct
A	Ampere
aa	Amino acid
Ab	Antibody
ADP	Adenosine diphosphate
AI	Apoptotic index
AID	Activation-induced cytidine deaminase
Al	Aluminum
ALV	Avian Leukosis Virus
AMP	Adenosine monophosphate
A-NHEJ	Alternative NHEJ
ATM	Ataxia-telangiectasia-mutated
ATP	Adenosine triphosphate
ATR	Ataxia-telangiectasia and RAD3 related kinase
BER	Base excision repair
BLM	Bloom’s syndrome protein
B-NHEJ	Backup NHEJ

bp	Base pair
BRCA1	Breast cancer susceptibility protein 1
BRCA2	Breast cancer susceptibility protein 2
BRCT	BRCA1 C-terminal domain
BSA	Bovine serum albumin
bsr	Blasticidin
CC	Catalytic core
Cdc9	Cell division cycle protein 9
cDNA	Complementary DNA
Chk	Chicken
cln	Clone
cm	Centimeter
CML	Chronic myeloid leukemia
CNS	Central nervous system
CO_2	Carbon dioxide
CPD	Cyclobutane pyrimidine dimer
Cre	Causes recombination
CS	Class switch
CSR	Class switch recombination
CtIP	C-terminal binding interacting protein
d	day
DAPI	4',6-Diamidino-2-phenylindole
DBD	DNA-binding domain

DDR	DNA damage response
Deq	Dose equivalent
DLB	DNA loading buffer
D-loop	Displacement loop
DMEM	Dulbecco's modified eagle medium
DMSO	Dimethyl sulfoxide
DNA	Deoxyribonucleic acid
DNA-PK	DNA-dependent protein kinase
DNA-PKcs	DNA-dependent protein kinase catalytic subunit
D-NHEJ	DNA-PK dependent non-homologous end-joining
Ds	Double strand
DSB	DNA double strand break
DTT	Dithiothreitol
e.g.	Exempli gratia
EDTA	Ethylenediaminetetraacetic acid
et al.	Et alii
EtBr	Ethidium bromide
eV	Electronvolt
FACS	Fluorescence activated cell sorting
FANCM	Fanconi anemia, complementation group M
FBS	Fetal bovine serum
FDR	Fraction of DNA released
Fe	Iron

g	Gravity
GeV	Gigaelectronvolt
gpt	Guanine-hypoxanthine phosphoribosyl transferase
Gy	Gray
h	Hour
H	Hydrogen
H_2O	Water
He	Helium
HEPES	4-(2-hydroxyethyl)-1-Piperazineethanesulfonic acid
HKG	Housekeeping gene
HR	Homologous recombination
HRP	Horseradish peroxidase
HRR	Homologous recombination repair
i.e.	Id est
Ig	Immunoglobulin
IR	Ionizing radiation
kg	Kilogram
LET	Linear energy transfer
LIG1	DNA ligase I
LIG3	DNA ligase III
LIG4	DNA ligase IV
LMDS	Locally multiply damaged site
M	Molar (mol/l)

mA	Milliampere
MC	Methylcellulose
MEF	Mouse embryonic fibroblast
Mer	Mutated estrogen receptor
Mev	Megaelectronvolt
min	Minute
ml	Milliliter
mm	Millimeter
mM	Millimolar
MMEJ	Microhomology-mediated end-joining
MRN	Mre11/Rad50/Nbs1
MTS	Mitochondrial targeting signal
mts-hLIG1	Human LIG1 with a mitochondrial targeting signal
NBS	Nijmegen breakage syndrome
NBS1	Nibrin
NER	nucleotide excision repair
NHEJ	Non-homologous end-joining
NLS	N-lauryl sarcosine
nm	Nanometer
nM	Nanomolar
NTase	Nucleotidyltransferase
O_2	Oxygen
OB-fold	Oligonucleotide/oligosaccharide binding

OH	Hydroxyl
OH•	Hydroxyl radical
PARP1	Poly (ADP-ribose) polymerase 1
PBMC	Peripheral blood monocytes
PBS	Phosphate-buffered saline
PCNA	Proliferating cell nuclear antigen
PCR	Polymerase chain reaction
PFA	Paraformaldehyde
PI	Propidium iodide
PIP	PCNA-interacting peptide
PMSF	Phenylmethylsulfonyl fluoride
pol	Polymerase
PVDF	Polyvinylidene difluoride
Rad51/54	Radiation protein 51/54
RECQ1	RecQ-like helicase 1
RNA	Ribonucleic acid
ROS	Reactive oxygen species
RPA	Replication protein A
rpm	Rounds per minute
RT	Room temperature
RTEL1	Regulator of telomere elongation helicase 1
RT-PCR	real-time PCR
SDS	Sodium dodecyl sulfate

SDSA	Synthesis-dependent strand annealing
Ser	Serine
ss	Single strand
SSB	DNA single strand break
SSBR	single strand break repair
TBP1	TATA-binding protein 1
Tris	Tris(hydroxymethyl)-amino methane
UV	Ultraviolet light
WRN	Werner syndrome protein
wt	Wild type
XRCC1/4/5/6	X-ray repair cross-complementing protein group 1/4/5/6
ZnF	Zinc finger
α	Alpha
β	Beta
β-ME	β-Mercaptoethanol
γ	Gamma

1 Introduction

1.1 Preamble/Background

It is broadly acknowledged that among the lesions that may be induced in the DNA, the most critical biological effects are generated by those affecting both strands of the deoxyribonucleic acid (DNA). Such lesions risk the genome, whose maintenance of utmost importance for every organism is. Damage in the genome of eukaryotic cells can be generated by ionizing radiation (IR) (Ward, 1988) or could emerge as consequence of exposure of cells to a variety of exogenous DNA damaging agents like cosmic and terrestrial radiation, chemical compounds (Sato et al., 1983) and radiomimetic drugs (Ackland et al., 1988; Elmroth et al., 2003). Lesions in the DNA can also appear as a result of endogenous cellular processes such as spontaneous chemical alterations in biological molecules, reactive oxygen species (ROS), by-products of intracellular metabolism (Helleday et al., 2007) and faults of biochemical processes related to DNA metabolism, such as DNA replication (Arnaudeau et al., 2001). The final event in all of the above situations can be the generation of DNA double strand breaks (DSBs). In contrast to the randomly induced DSB induced by the above mentioned processes, DSBs can also be generated by programmed events in essential cellular processes such as meiosis (Richardson et al., 2004), or V(D)J- and class switch (CS) recombination during the maturation of lymphoid cells (Bassing et al., 2002; Petersen et al., 2001).

As a result of ionizing radiation exposure to a dose of 1 Gy of X-rays, over 1000 single strand breaks (SSBs), an equal number of base damages, but only 20-40 DSBs are generated (Ward, 1990). DSBs are one of the most severe DNA lesions and, if left unrepaired, can lead to permanent cell cycle arrest, induction of apoptosis, or cell killing (Olive, 1998). If these lesions are misrepaired, they can result in mutations, chromosome rearrangements and carcinogenesis (Jackson, 2002) through translocations, inversions, or deletions (van Gent et al., 2001). Over the evolution, cells have developed sophisticated and efficient mechanisms to detect and eliminate DSBs by the activation of DNA damage

response (DDR) mechanisms. DDR includes a repair network efficient enough to deal with the abundance of DNA lesions generated by ionizing irradiation and helps thus to maintain genomic integrity.

Eukaryotic cells utilize at least two major repair pathways to restore the duplex structure of their genome: homologous recombination repair (HRR) and non-homologous end-joining (NHEJ). These mechanistically distinct pathways are not biochemically equivalent, have different substrate requirements, operate with different kinetics and fidelity, and are utilized differently throughout the cell cycle (Tamulevicius et al., 2007). Such repair activities are supported by an extensive network of signaling proteins, which registers DSBs and coordinates repair with the activation of checkpoints that arrest the normal progression through the cell cycle to provide time for repair (Elledge, 1996; Niida and Nakanishi, 2006). On which basis the cell decides to use HRR or NHEJ for the repair of a certain DSB is still an area of active investigation. Recent studies suggest that components of one repair pathways may regulate key events of the other pathway, thus shifting pathway use. Hence, the Ku70/80 complex together with the DNA Ligase IV complex are thought to be key suppressors of DNA end-resection, which is needed to initiate HRR (Zhang et al., 2007).

In the following chapters, the basics of radiation physics are outlined together with a description of the basic properties and characteristics of the DSB repair pathways, with particular emphasis on the role of DNA ligases in the process. This generates the foundation and the theoretical background for the work performed as part of this thesis outlined in the following sections.

1.2 Ionizing radiation and the induction of DNA damage

1.2.1 Physics of ionizing radiation

In this thesis X-rays were used to generate DNA damage and investigate cellular repair pathways engaged. To facilitate understanding of the mechanisms of DNA damage induction by X-rays, I present here a short introduction into the physics of ionizing radiation. In physics, ionizing radiation (IR) describes any process in which energy emitted by an object travels through a medium or space, and is finally absorbed by another object, thus resulting in excitation or ionization of its atoms. There are several forms of electromagnetic radiation that are classified by the frequency and energy of their wavelengths. A photon is the basic “unit” of all forms of electromagnetic radiation. The electromagnetic spectrum consists of radio waves, microwaves, infrared radiation, visible light, ultraviolet radiation (UV), X-rays and γ-rays; they all vary in their frequency and wavelength, and hence in the energy of constituting photons. In general, photons of high wavelength and low frequency have low energy contrary to those of low wavelength and high frequency, which have high energy (Konkow, 2012).

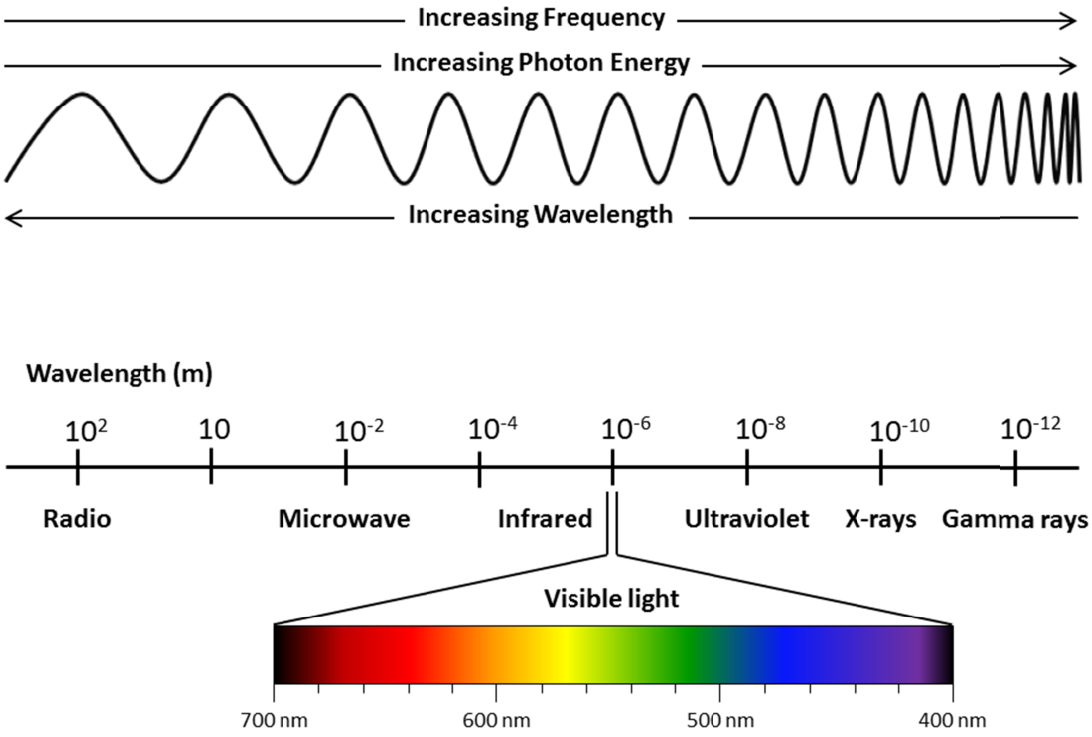

Figure 1: Illustration of the electromagnetic spectrum. Showing the relative connection among energy, wavelength and frequency, with visible light spectrum expanded.

Some types of radiation have enough energy to ionize atoms or molecules. This energy threshold is not precisely defined but one definition suggests that radiation with a photon energy less than 10 electronvolts (eV) should be considered as non-ionizing, whereas about 33 eV are required to disrupt the chemical bond of water molecules under the conditions encountered in biological systems (Hall and Giaccia, 2006). Generally, this implicates an electron being “kicked out” of an atom's electron shell, which will give the atom a positive charge. Radiation with sufficient energy to generate this effect is then referred to as ionizing radiation (Konkow, 2012).

It is common to classify ionizing radiation as either electromagnetic or particulate. X-rays or γ-rays are a form of electromagnetic radiation that do not differ in their nature or basic properties, however particulate radiations include electrons, protons, α-particles, neutrons and heavy charged particles. Moreover, the action of radiation can be classified as directly or indirectly

ionizing. Directly ionizing radiation constitutes charged particles that have sufficient kinetic energy to disrupt atomic structure of the absorber, directly producing chemical and biological changes within the absorber. In contrast, electromagnetic radiation is considered indirectly ionizing, as it deposits the majority of its energy through the production of secondary electrons (see below) (Konkow, 2012).

Radiation is measured in units of Gray (Gy) describing the amount of energy absorbed per unit mass of matter. The unit of 1 Gy corresponds to 1 J/kg (Hall and Giaccia, 2006). The absorbed energy, deposited by IR, is not distributed at random but tends to localize along the tracks of directly ionizing particles in a pattern that is determined by their type, energy and speed (Mothersill and Seymour, 2006). One can distinguish between densely and sparsely ionizing radiation depending on the ionization patterns it generates. This property is described by the parameter linear energy transfer (LET) that is defined as the energy that an ionizing particle deposits along the track (keV/µm) as it traverses matter. LET also reflects the pattern of ionizations a type of radiation generates. Sparsely ionizing radiation is of low LET, whereas densely ionizing radiation is of high LET (Konkow, 2012).

It is important to note that the biological effects of a type of radiation depend strongly on its LET, and increases with increasing LET. X-rays and γ-rays are mostly low LET radiations, whereas charged particles are generally high LET radiations, e.g. α-irradiation is a high LET radiation with low penetration depth (Hall and Giaccia, 2006). For charged particles, the density of ionizations decreases as the particle energy increases (Konkow, 2012). Figure 2 presents track-structure segments of different ions in water.

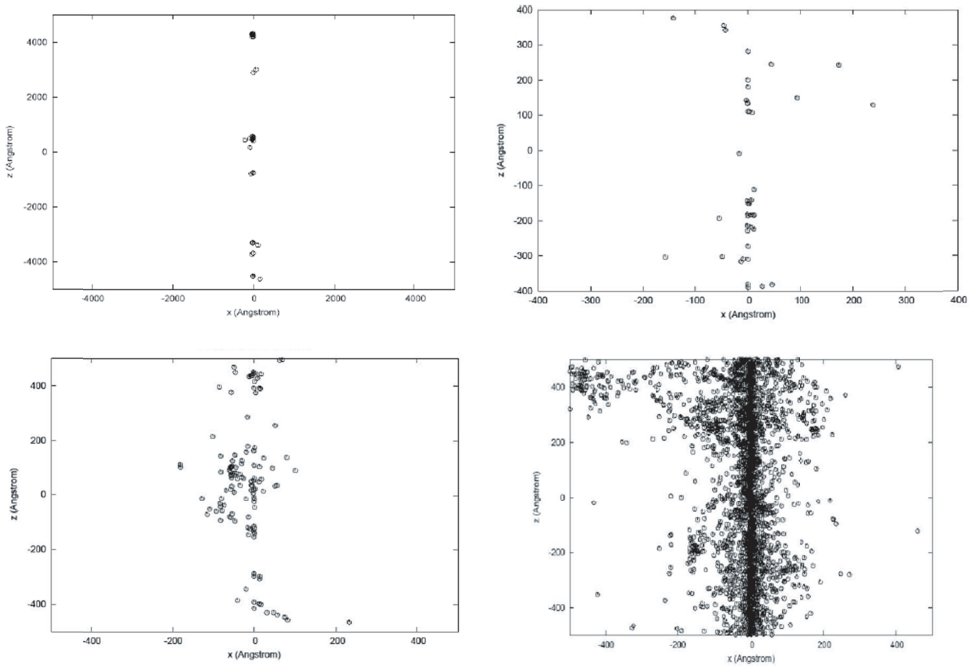

Figure 2: 2D projection of track-structure segments in liquid water for different ions with same velocity (115MeV/nucleon), as calculated with the PARTRAC code (from top to bottom and from left to right: H, He, C and Fe; note the different scale for the proton track) (Ballarini et al., 2008).

Notably, each particle has a distinct track structure (i.e. distribution of ionizations along its path) with randomly varying distances between the ionizations that decreases as the particles lose energy along their tracks (Konkow, 2012). Densely ionizing charged particles and electrons near the ends of their tracks display large increases in the density of ionizations, and as a result multiple ionizations occur in a rather small volume (Nikjoo et al., 1994; Nikjoo and Goodhead, 1991). At the same absorbed dose, the biological effects of high LET radiations are stronger compared to those of low LET radiations (Kadhim et al., 2006). It is generally assumed that this is because high LET radiation deposits most of its energy in ways producing highly clustered damage in the DNA, or in other cellular structures and molecules (Goodhead and Nikjoo, 1989).

1.2.2 DNA damage induction by IR

In our studies X-rays were used to induce DSBs and investigate their repair Cells absorb the energy of ionizing radiation, and sustain a variety of damages in all of their constituent molecules (DNA, proteins and lipids). For that reason the principal target of our interest is considered to be the DNA, where the action of radiation can be direct or indirect. Direct radiation action is the dominant process for high LET radiations and implies that the atoms of the target itself, e.g. the DNA, are ionized (Konkow, 2012). On the other hand, in the indirect action of radiation, which is more relevant after exposure to sparsely ionizing radiation, ionization occurs in the water producing hydroxyl radicals (OH•), which can then diffuse away from the site of their production and damage chemically the DNA (Goodhead, 1994, 1995). Figure 3 illustrates schematically the direct and indirect action of IR.

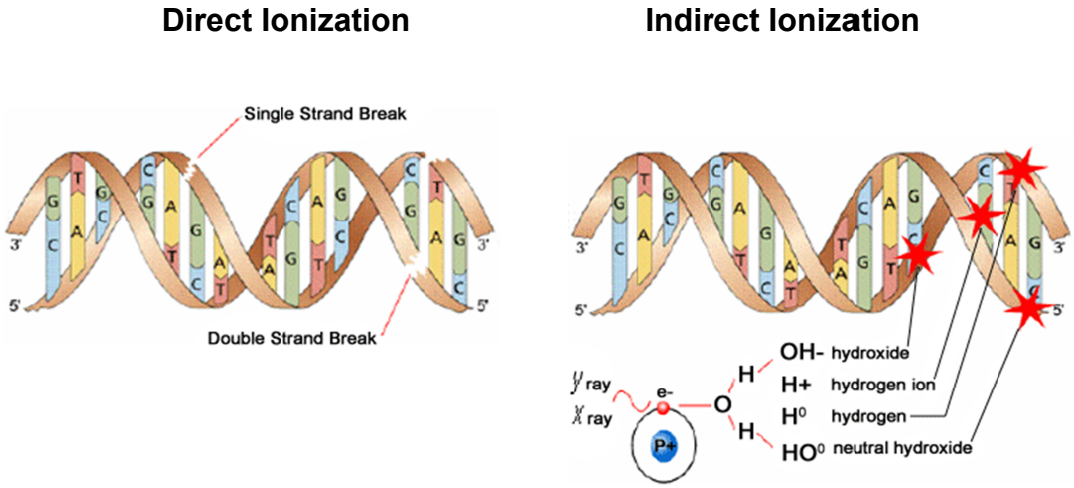

Figure 3: IR can directly or indirectly act on target molecules like the DNA (from the Canadian Nuclear Association website).

The effects of radiation are stochastic and can generate a variety of different DNA damage types, such as DNA base damages (e.g. abasic sites, oxidized purines and oxidized pyrimidines) (Sutherland et al., 2000) as well as regular and oxidized apurinic and apyrimidinic sites (Paap et al., 2008)), DNA backbone breaks (Sancar et al., 2004), alkali labile lesions (Lafleur et al., 1979) and heat

labile sites (Singh et al., 2009) together with many crosslinks between different chromatin associated proteins and the DNA (Konkow, 2012).

Lesions in the DNA backbone include abasic sites, single strand (ss) and double strand (ds) DNA breaks. As mentioned above, each Gy of X-rays induces around 20-40 prompt DSBs, ~1000 single strand breaks (SSBs) and an equal number of base damages (Ward, 1990). SSBs have small biological consequences, since they can be repaired very fast by using the complementary strand as a DNA template. However, if SSBs occur opposite to each other, or are separated by up to ten base pairs (bp) on opposite sides of the DNA strand, a DSB is generated. If this lesion is left unrepaired or is misrepaired it could lead to genomic instability, cell death, carcinogenesis or mutations as well. In summary, DNA damage produced by direct or indirect radiation action leads to changes in the character and the properties of the molecule, and impairs thus its function as carrier of genetic information. As a result, cell death, mutation and/or transformation can ensue (Konkow, 2012).

1.3 Non-Ionizing radiation

Beyond the ability of photons to ionize atoms, within the electromagnetic spectrum photons with energies below 10 eV are considered as non-ionizing (Figure 1). This means that i.e. UV radiation with wavelengths longer than 124 nanometers (nm) is non-ionizing radiation. Instead of “kicking-out” an electron and producing charged ions, this form of electromagnetic radiation has sufficient energy only for excitations, i.e. the movement of an electron to a higher energy state.

The electromagnetic spectrum of UV lies between X-rays and visible light with wavelengths between 40 and 400 nm (30-3 eV). The UV spectrum is divided into Vacuum UV (40-190 nm), Far UV (190-220 nm), UVC (220-290 nm), UVB (290-320), and UVA (320-400 nm). However, the UV spectrum from 3 to 10 eV, although technically designated as non-ionizing, can produce photochemical reactions to many molecules and is doing far more damage than can be accounted for simple heating effects. Since UV light is able to produce free

radicals, it is capable of non-thermal damage in biological systems that have some of the biological features of ionizing radiation. UVC also induces helix distorting DNA lesions like cyclobutane pyrimidine dimers (CPDs) and 6-4 pyrimidine-pyrimidone photoproducts (6-4PPs) between adjacent pyrimidine residues.

1.4 Eukaryotic DSB repair and its regulation

After DNA damage induction cells start to eliminate the generated DSBs by the activation of their DNA repair machinery. Higher eukaryotic cells utilize two main repair pathways to remove DSBs from their genomes – NHEJ and HRR. The fundamental difference between these two repair pathways is that HRR requires a homologous template to restore accurately the DNA sequence around the break, whereas NHEJ simply rejoins the two ends of the DSB (Essers et al., 2000). Consequently, HRR ensures correct repair of the DSB by using either an undamaged sister chromatid or a homologous chromosome as a repair template (Khanna and Jackson, 2001); on the other hand, NHEJ rejoins the two DNA ends without any requirement for homology (Karran, 2000), hence the term “non-homologous end-joining” (Weterings and Chen, 2008). Repair of DSBs by NHEJ is usually accompanied by limited or extensive additions or deletions of nucleotides at the junction, also in order to produce ligatable ends. The result is altered sequence of the repaired DNA molecule - due to the fact that NHEJ does not restore sequence information in the damaged DNA molecule, although it restores its molecular integrity (Iliakis et al., 2004; Lieber, 2010). Thus, DSB repair by NHEJ is considered as error-prone.

The relative contribution of the two repair pathways to the repair of DSBs is likely to be determined by the phase of the cell cycle and the presence of a homologous DNA template, although the importance and usage of NHEJ varies greatly among species (Karran, 2000). As NHEJ has no need for a DNA template, it can operate throughout the cell cycle, although it is thought to dominate DSB repair in the G1-phase of the cell cycle, where HRR activity is limited. In contrast, HRR is restricted to S- and G2-phases of the cell cycle,

where a sister chromatid is available and can be used as a repair template (Krüger et al., 2004; Moynahan and Jasin, 2010). Figure 4 presents the function of the two DSB repair pathways throughout the cell cycle with their dependency on DNA template (Konkow, 2012).

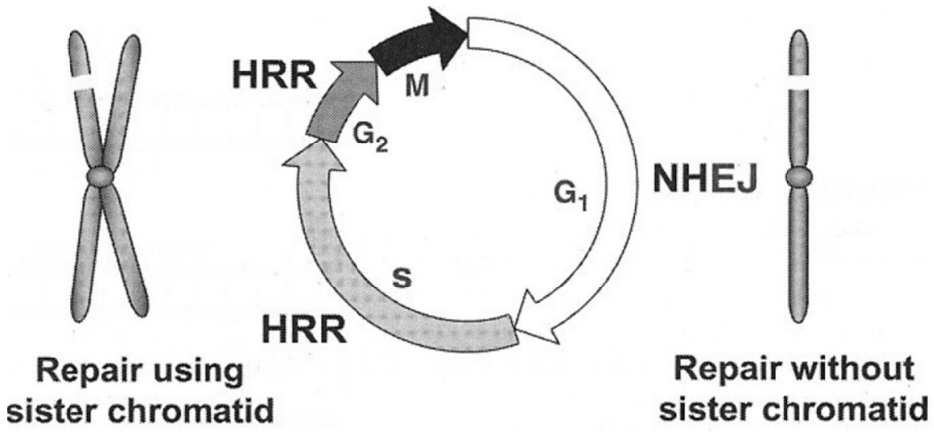

Figure 4: Illustration shows the two major DSB repair pathways with its dependency on DNA template and their occurrence in different cell cycle phases (Hall and Giaccia, 2006).

In theory, HRR could also occur in diploid G1-phase cells, using the existing copy of the chromosome as repair template. However, this seems unlikely due to the fact that homologous chromosomes are usually not directly available owing to the locally distinct nuclear chromosome compartmentalization. It is therefore believed that NHEJ is the prevailing repair pathway during G1/G0- and M-phases of the cell cycle (Lee et al., 1997), whereas HRR is the main repair pathway during S- and G2-phases of the cell cycle, although the NHEJ could be as efficient in S and G2 as well (Rothkamm et al., 2003). In the next section the processes of HRR and NHEJ are described in detail.

1.5 Homologous Recombination Repair (HRR)

HRR is a universal process for repairing DNA DSBs; it is highly conserved from bacteria to mammals and found in all forms of live. The fundamental characteristic of this pathway is that it requires a template DNA sequence homologous to the one which contains the DNA damage for an accurate restoration of the DNA molecule (Essers et al., 2000). This suggests that HRR in principle could occur in G1 phase as well, by using the homologous chromosome (Johnson and Jasin, 2000). However, it is thought that HRR is used preferentially in late S and G2 phase of the cell cycle taking advantage of the sister chromatid present (Krüger et al., 2004; Lee et al., 1997). In bacteria and yeast HRR is the main repair pathway despite the fact that HRR is a relatively slow but error-free process; its contribution in vertebrate cells remains uncertain. HRR may either repair only on a small fraction of DSBs, or may act in a process at a step after an initial end-joining by NHEJ (Iliakis et al., 2004). Yet, the evidence that HRR is functional in vertebrates is strong (Moynahan and Jasin, 2010).

Homologous recombination is a versatile process utilized in several biological processes other than DSB repair. It is involved in meiotic cross over, which is responsible for the rearrangement of alleles in gametes. It is necessary for proper chromosome segregation and is important for mating type switching in yeast and epitope class switching in the majority of organisms.

The process of HRR is schematically shown in Figure 5 and involves in principle the following steps: initial processing of DNA ends, search for homology, strand invasion into the intact homologous double helix and formation of Holiday junction, DNA synthesis with the associated branch migration, and final resolution of the Holiday junction (Kinner et al., 2008).

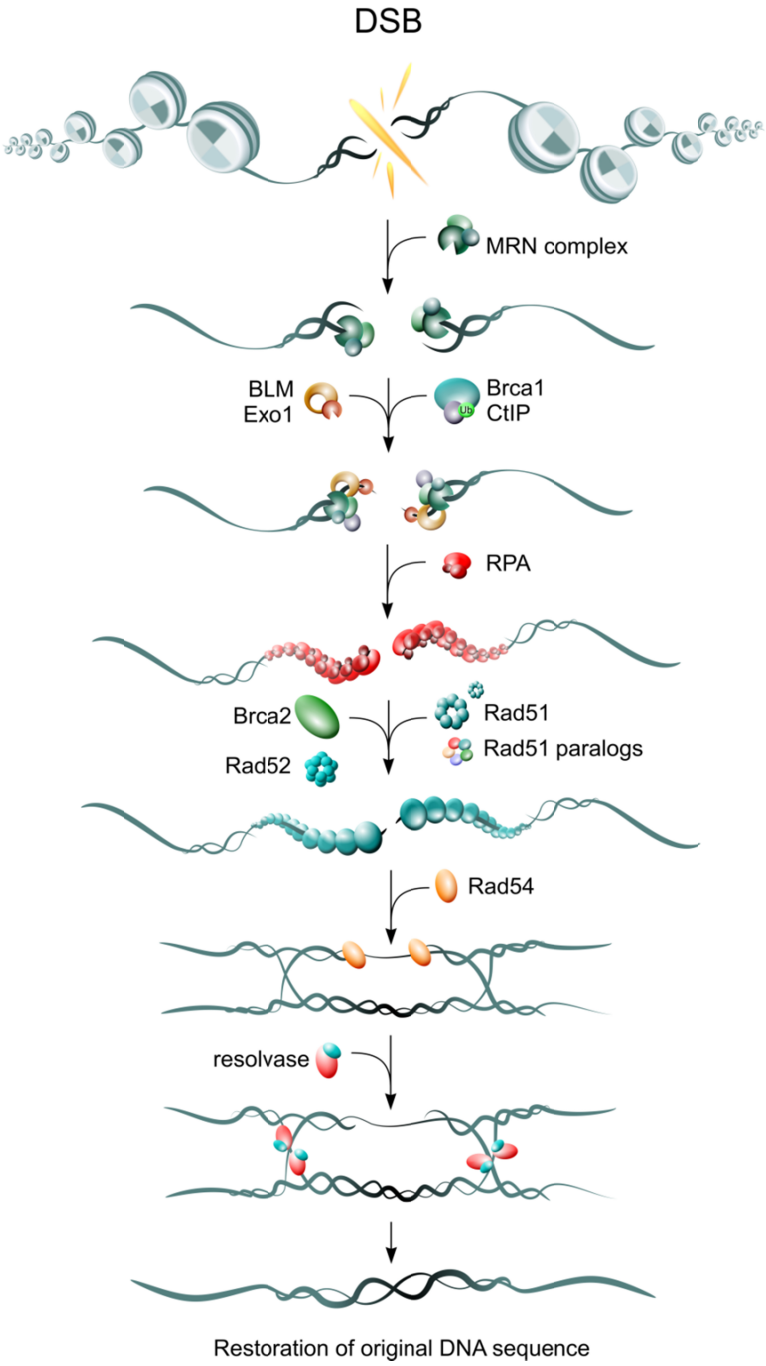

Figure 5: Schematic diagram of main players involved in HRR. (with friendly assistance: Emil Mladenov, Institute of Medical Radiation Biology, University of Duisburg-Essen Medical School, 45122 Essen, Germany)

The initial step of HRR comprises a 5' to 3' end-resection at the break promoted by the Mre11/Rad50/Nbs1 (MRN) complex, the C-terminal binding interacting protein (CtIP) and a helicase activity of Bloom's syndrome protein (BLM) (Nimonkar et al., 2008) resulting in 3' single-stranded (ss) overhangs (Limbo et

al., 2007; Sartori et al., 2007; Takeda et al., 2007). The produced 3' ss tails are recognized and bound first by the eukaryotic ssDNA binding replication protein A (RPA) to be protected from degradation and to avoid secondary structure formation (Sleeth et al., 2007; Wold, 1997). BRCA1 mediates the recruitment of BRCA2 to the DSB. BRCA2 is required for loading of Rad51 on RPA-coated ssDNA overhangs which is supported by the assistance of Rad51 paralogs. In yeasts Rad52 is thought to displace RPA and promote the binding of Rad51 to ssDNA, whereas in vertebrates this role is taken over by BRCA2. The Rad51 nucleoprotein filament interacts with Rad54 and promotes searching for homology, unwinding of duplex DNA (Symington, 2002) and catalyzes strand invasion into the homologous duplex DNA.

In the course of this process Rad51 is displacing the original strand of the duplex and forms a displacement loop (D-loop) by creating a Holiday junction (Baumann et al., 1996). The 3'-end of the invading strand primes for DNA synthesis of the template duplex and can be extended by branch migration. At the end of HRR, the predominant pathway appears to be synthesis-dependent strand annealing (SDSA), where the newly synthesized strand is reversed to anneal to the other original DNA end, resulting in a non-crossover outcome with no change to the template DNA.

When a double Holiday junction is formed, a number of proteins are involved in resolving the D-loop and may function to mediate SDSA and to suppress crossovers. The main class are resolvases which functions *in vitro* are associated to human FANCM, metazoan RTEL1, mammalian RECQ1 and BLM, as well as to Rad54 (Heyer et al., 2010). It is still not known whether the final ligation step of the remaining nicks after disrupting D-loops is completed by DNA Ligase I (LIG1) and its interaction partner proliferating cell nuclear antigen (PCNA). Also Ligase III/XRCC1 (LIG3/XRCC1) could be implicated in this process. Alternatively resolvases themselves ligate and restore DNA integrity at the DNA ends.

Consistent with the described intricacy of this pathway, HRR is a rather slow process. In yeast it takes up to 72 h to repair DSBs during the plateau phase of growth, but it is important to point out that HRR has very high fidelity and the

ability to restore the sequence around the DSB. The proteins involved in HRR are known to be expressed in the majority of mammalian cells and HRR have been confirmed in all organisms, from bacteria to yeast to human and the deficiency of HRR results in many organisms in embryonic lethality. Hence it is assumed HRR plays an important role in the removal of breaks, especially those arising from failures during DNA replication, although the real contribution to ionizing radiation induced DSB repair is only partially defined.

1.6 Non-homologous End-joining (NHEJ)

In cells of higher eukaryotes the predominant pathway to repair DSBs is thought to be NHEJ, which does not depend on extensive regions of homology (Jeggo, 1998). It simply restores efficiently genome integrity by joining of two broken ends without ensuring restoration of the original sequence in the vicinity of the break (Lieber et al., 2003; Valerie and Povirk, 2003; Weterings and van Gent, 2004). NHEJ enzymes are able to function on a diverse range of overhang variation, DNA end sequence, and DNA end chemistry and convert them to joined products with about the same efficiency in vivo.

In general it requires enzymes to recognize breaks, a nuclease for processing the damaged end, DNA polymerases to synthesize and fill-in new DNA, and finally a ligation enzyme for subsequent restoration of DNA integrity (Lieber, 2010). DNA-dependent protein kinase catalytic subunit (DNA-PKcs) and Ku are the key proteins to direct the end-joining to the DNA-PK dependent non-homologous end-joining pathway (D-NHEJ) in a coordinated fashion (Perrault et al., 2004). There is evidence that cells of higher eukaryotes with defects in D-NHEJ rejoin the majority of DSBs using an alternative repair pathway (Wang et al., 2003) that is not utilizing any of the HRR-associated activities (Iliakis et al., 2004). This pathway is therefore termed backup NHEJ (B-NHEJ).

The “multiple” discoveries in NHEJ repair led to a variety of terms which are used to describe it. To simplify differentiation between the two NHEJ pathways I will refer the frequently called canonical or classical NHEJ as D-NHEJ, since its dependence on DNA-PKcs. For the recently identified alternative NHEJ

(A-NHEJ, or alt-NHEJ) the term microhomology-mediated end-joining (MMEJ), Ku-independent end-joining, Ligase IV (LIG4)-independent NHEJ, and our proposed term backup NHEJ is used (Corneo et al., 2007; Liang et al., 2008; Ma et al., 2003; Wang et al., 2003). We prefer and I will use here the term B-NHEJ instead of A-NHEJ because this form of end-joining only comes to the fore when D-NHEJ is defective. Thus, it appears to operate as a “true” backup rather than an equal, alternative partner. However, it cannot be excluded that the failures during D-NHEJ repair, even in the presence of HRR, could lead to initiation of B-NHEJ activities.

1.6.1 DNA-PK dependent non- homologous End-joining (D-NHEJ)

D-NHEJ operates very efficiently in all phases of the cell cycle and is able to remove the majority of IR induced DSBs with very fast half times of 15–30 minutes (Windhofer et al., 2007a).

Like most of the DNA repair processes, D-NHEJ requires different steps and activities. Therefore a set of enzymes is needed for recognition of the break and holding the broken ends in proximity, a nuclease to resect damaged ends, a DNA polymerase to fill the gap with new DNA, and a DNA ligase to rejoin two ends and restoring DNA strand integrity. An outline of the in D-NHEJ involved main steps and players is given in Figure 6.

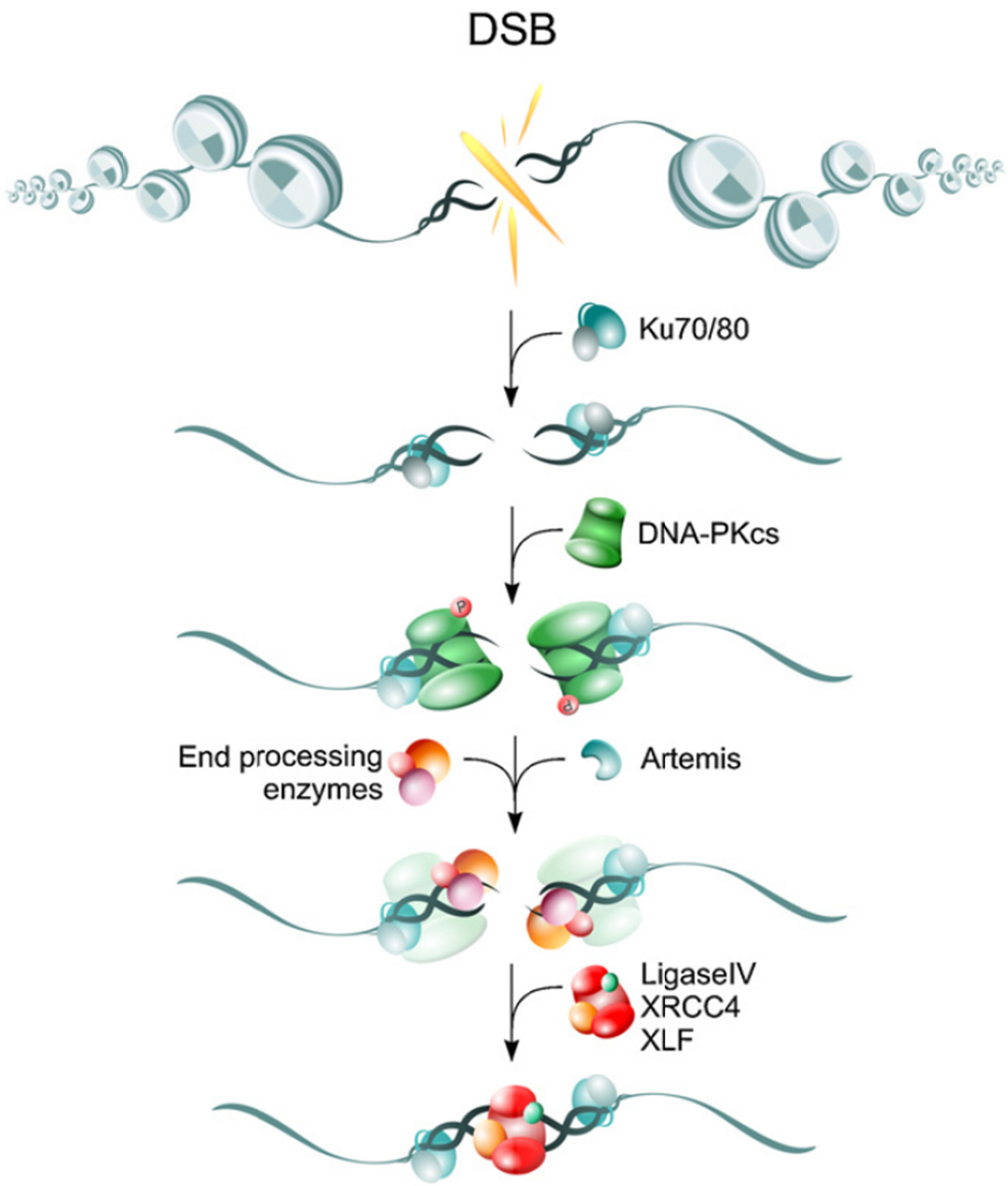

Figure 6: Outline of the main players and steps of D-NHEJ. (Mladenov and Iliakis, 2011)

The first protein which binds to DSB ends on the basis of its abundance of about 300.000 molecules per cell and due to its high affinity for free DNA ends, is thought to be Ku (Mimori and Hardin, 1986; Mladenov and Iliakis, 2011). Ku is a heterodimer, comprising of the two subunits Ku70 and Ku80, encoded by the XRCC5 and XRCC6 genes. Ku binds to DNA ends as an open ring structure and recruits DNA-PKcs to generate the active DNA-PK holoenzyme, which

results in the activation of DNA-PKcs kinase activity (Walker et al., 2001). This enables phosphorylation of various proteins involved in this pathway including DNA-Pkcs itself. Several enzymes that are able to either remove or fill-in ssDNA regions or non-compatible overhangs have been identified. For instance, Artemis bound to DNA-PKcs functions as a endonuclease to allow end-resection of damaged overhangs (Ma et al., 2002). During this step of D-NHEJ, occasional loss of nucleotides is possible (Valerie and Povirk, 2003). Polymerase λ and μ are both able to bind Ku by the virtue of their BRCT domains and aid repair by catalyzing DNA polymerization. In the end of D-NHEJ a final ligation of the two ends occurs in a coordinated fashion by the LIG4/XRCC4 complex, which is also a phosphorylation target of DNA-PK (Leber et al., 1998), with its associated cofactor XLF (Ahnesorg et al., 2006).

When the two ends from the same DSB are rejoined, integrity of the DNA molecule is restored. Each Ku bound to DNA end can function as an anchor where the nuclease, polymerase and ligase are able to accumulate. Recruitment of these enzymes can be performed in any order (Lieber, 2008; Ma et al., 2004). This flexibility displays the basis of the diverse outcomes from this pathway, where limited to extensive deletions or additions of nucleotides at the joined region arise (Lieber, 2010).

In addition to the outlined proteins of HRR and D-NHEJ, numerous other proteins are involved as components of the process that signals the presence of damage in the DNA and activates the cellular responses to this damage. These proteins include Histone H1, phosphorylated histone H2AX, a variant form of histone H2A, and 53BP1. They all can be modified or can be translocated to specific nuclear locations in response to DNA damage induction. As a result they locate actual sites of DNA damage and their presence is indicative of ongoing DSB repair. Anyhow, defects in these proteins do not cause dramatic defects in DSB repair and cells have similar repair kinetics compared to those obtained in wild type cells (Riballo et al., 2004).

1.6.2 Backup Pathway (B-NHEJ)

Both DNA repair pathways outlined above are generally active in higher eukaryotes. This redundancy generates problems and raises the questions as to how or what determines their selection? Which are the underlying mechanisms involved in coordination of pathway selection and what is their relative contribution to the outcome of DNA repair?

The situation became even more complicated after our studies with cells defective in components of D-NHEJ, which show a residual repair activity that removes the majority of induced breaks albeit with much slower kinetics (Figure 7). The results in wild type (wt) cells revealed biphasic kinetics of DSB rejoining with a fast component, acting within 5 to 30 minutes, and a slow component, acting from 2 to 20 hours after irradiation to remove the remaining DSBs (DiBiase et al., 2000; Iliakis et al., 1991). A deficiency in DNA-PK does not significantly influence the overall repair kinetics, but the contribution of the slower component of DSB rejoining is increased from 17 to 72 %.

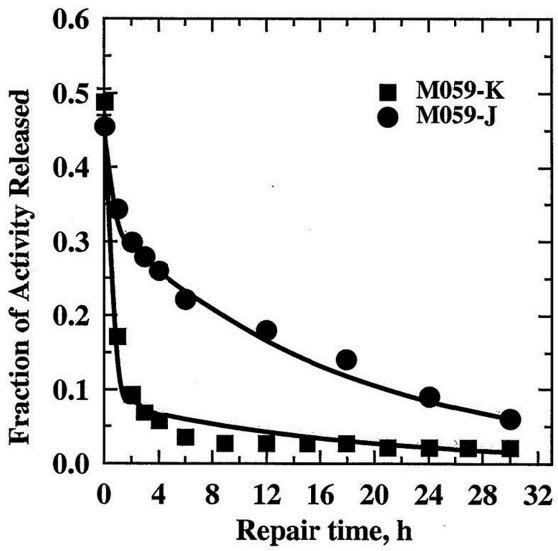

Figure 7: The role of B-NHEJ in cells deficient in D-NHEJ. Rejoining of DSBs in exponentially growing wt (M059K) and D-NHEJ deficient (M059J) cells measured with pulsed-field gel electrophoresis (PFGE) (DiBiase et al., 2000).

This observation directs to the hypothesis that higher eukaryotes are capable to remove the majority of DSBs utilizing a constitutive and inherently slow end-joining mechanism when the fast DNA-PK component is inactive (DiBiase et al., 2000). Similar results regarding end-joining activity have been reported for cells defective in LIG4 (Wang et al., 2001b), the Ku heterodimer (Wang et al., 2001a) and other proteins of D-NHEJ. The same effect was observed in wt cells treated with chemicals inhibiting DNA-PKcs activity.

The first thought which comes in mind from such results is that the slow repair component observed in DNA-PK deficient cells reflects HRR. To address this question, an extensive study was performed using DT40 mutant cells (Wang et al., 2001a). DT40 cells are chicken B-lymphocytes that have a 1000-fold upregulated HR. This ability is frequently used for targeted integration and inactivation of specific genes, resulting in a relatively easy generation of different mutant cell lines (Figure 8). As I will show later, we took extensive advantage of this property of DT40 in the present work.

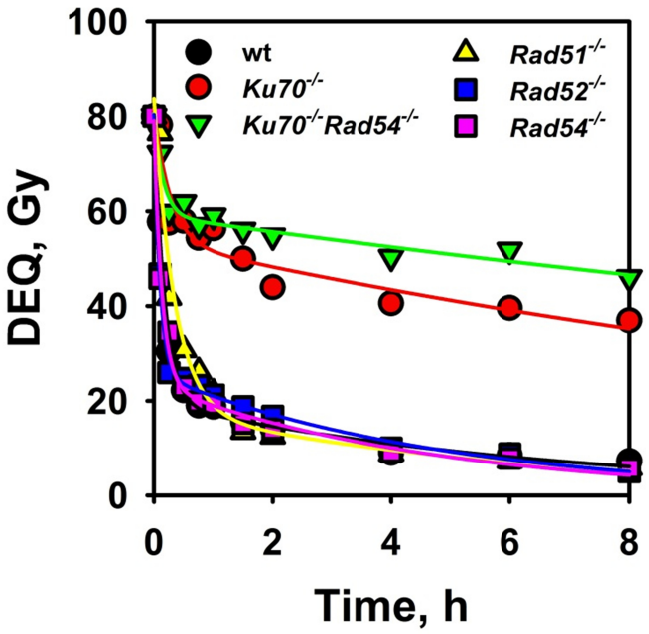

Figure 8: The role of B-NHEJ in cells deficient in D-NHEJ and HRR. Rejoining of DNA DSBs in DT40 cells deficient for D-NHEJ, HRR and double mutants for D-NHEJ and HRR as measured by pulsed-field gel electrophoresis (PFGE) (edited from (Wang et al., 2001a)).

The results of mutants with defects in Rad52 epistasis group of proteins involved in HRR displayed identical repair kinetics in PFGE experiments as wt cells. Furthermore, DT40 wt cells, despite their upregulated HR, show no difference in DSB repair kinetics and additional defects of D-NHEJ on top of HRR deficiency displayed no marked extra defect in DSB repair capability as measured by PFGE (Perrault et al., 2004). Thus, the residual end-joining activity cannot be attributed to HRR.

Together, these results point to an alternative end-joining pathway in higher eukaryotes that operates with slower kinetics and mainly as a backup for D-NHEJ and is therefore termed B-NHEJ. This pathway is a distinct form of end-joining and is likely to be an evolutionarily older pathway with less optimized synapsis mechanisms that rejoins DNA ends with slower half-times of 2 to10 h. It is anticipated that the rapid DNA end-joining of D-NHEJ kinetically suppresses the slower alternative pathway (Perrault et al., 2004).

When D-NHEJ is chemically or genetically compromised, it contributes significantly to the overall repair, fixes the majority of breaks and restores genome integrity, albeit with increased probability for errors (Bennardo et al., 2008; Iliakis et al., 2004). The slower kinetic and suboptimal synapsis mechanism gives more room and time for exchanges through the incorrect joining of DNA ends, leading to the formation of chromosomal aberrations during the repair of IR-induced DSBs. This observation places B-NHEJ at the center of carcinogenesis.

Further investigations led to the discovery that alternative pathways of NHEJ are implicated in telomere maintenance (Rai et al., 2010), and can also robustly substitute for class switch recombination (CSR) (Soulas-Sprauel et al., 2007; Yan et al., 2007) and V(D)J recombination in D-NHEJ deficient cells (Corneo et al., 2007; Jones and Simkus, 2009; Lee et al., 2004).

It was also found, albeit not as a necessary pathway requirement, that the use of microhomologies to some extend facilitates B-NHEJ. This characteristic led to a multitude of terms used for this repair pathways, like alternative NHEJ (A-NHEJ or alt-NHEJ) and microhomology-mediated end-joining (MMEJ), which are used to describe this distinct form of end-joining (Corneo et al., 2007; Liang

et al., 2008). Since it mainly functions as a backup for D-NHEJ and only comes to the forefront when D-NHEJ is compromised, we prefer and will use here the term B-NHEJ (Iliakis, 2009).

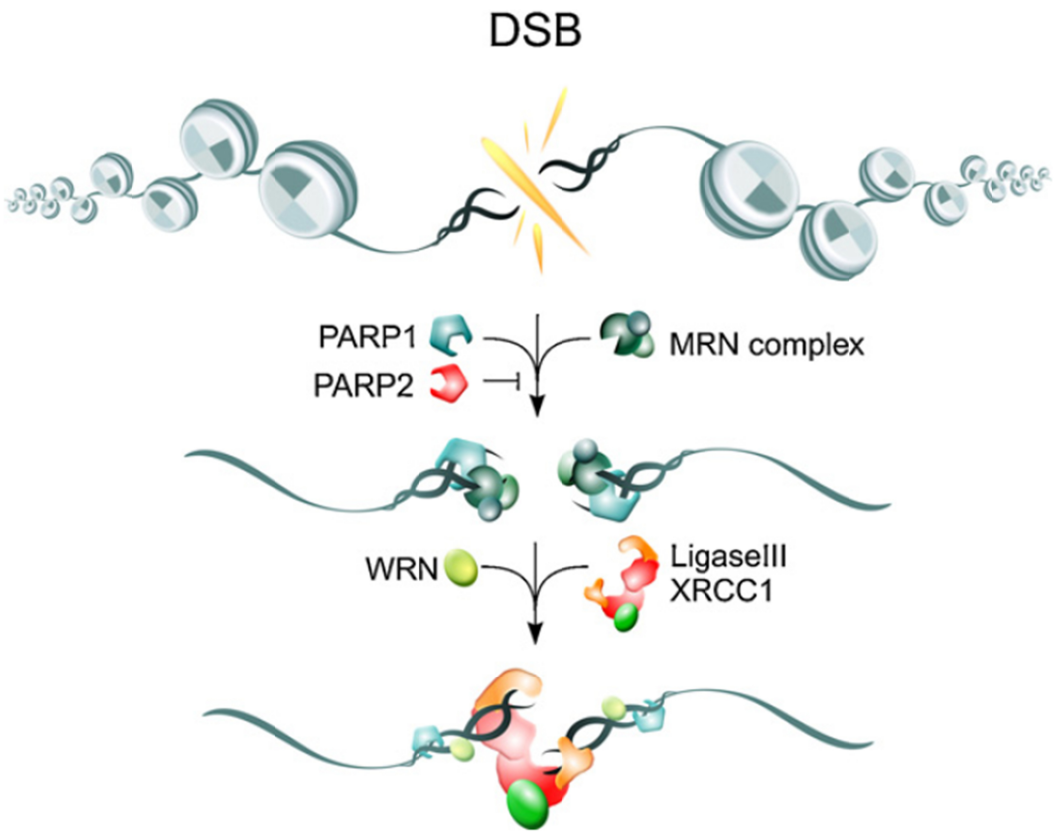

Figure 9: Outline of the main players and key steps of B-NHEJ. (Mladenov and Iliakis, 2011)

The characterization of enzymatic activities contributing to B-NHEJ, the coordination of their functions and their interactions with components of D-NHEJ and HRR has evolved as a prime area of current research in the field. Genetic and biochemical studies indicate that DNA Ligase III (LIG3) is implicated in DNA ligation in B-NHEJ, the last step of the end-joining reaction (Wang et al., 2001b). And interestingly, even low levels of LIG3 are sufficient for effective end-joining (Windhofer et al., 2007a).

LIG3 functions in a complex with X-ray repair complementing defective repair in Chinese hamster cells 1 (XRCC1) and is regulated by poly (ADP-ribose) polymerase 1 (PARP1) (McKinnon and Caldecott, 2007).

Hence, as a component of B-NHEJ, PARP1 might compete with Ku for DNA ends, where the much higher affinity of Ku for DNA ends provides a kinetic basis for the backup character of B-NHEJ (Wang et al., 2006). Another plausible cause for this backup character comes from the fact that the LIG3/XRCC1/PARP1 complex is also involved in other DNA repair activities, such as repair of SSBs and base damages, which are present in great excess in addition to DSBs and compete for PARP1 and furthermore for LIG3 (Audebert et al., 2004; Wang et al., 2006).

In addition to the function of Ku in the recruitment of DNA-PKcs some results strongly suggests that Ku may act as an alignment factor by transiently holding the DNA ends together, thus allowing the polymerase to prime DNA synthesis prior to ligation (Feldmann et al., 2000).

Besides, there is evidence that histone H1, the MRN complex and Werner syndrome proteins (WRN) are involved in B-NHEJ since they are recruited to DSBs (Davies and Chen, 2010; Rosidi et al., 2008; Sallmyr et al., 2008). H1 also helps to align DNA ends prior to ligation and enhances end-joining *in vitro* by LIG3 and LIG4 (Rosidi et al., 2008). Moreover, during V(D)J recombination, NBS1 is required for B-NHEJ of hairpin coding ends, whereas it shows a role in preventing B-NHEJ of signal ends and in coordinating four-ended inversional recombination events (Deriano et al., 2009). Since the inhibition of MRE11 in D-NHEJ mutants decreases end-joining frequency, the results suggest an essential function of MRN in B-NHEJ and that processing of DNA ends is a step in this repair pathway (Dinkelmann et al., 2009; Rass et al., 2009). In chronic myeloid leukemia (CML) cells, WRN is upregulated together with LIG3 and remodels under these conditions a complex to be recruited to DSBs (Sallmyr et al., 2008).

Significantly, B-NHEJ has a marked dependence on growth state (Windhofer et al., 2007b). Whereas its activity is reduced in G1-phase cells and nearly abrogated in resting cells, it is markedly increased during the G2 phase of the cell cycle, suggesting that suppression of growth signaling significantly compromises DSB repair by B-NHEJ (Wu et al., 2008).

Despite the potential consequences of B-NHEJ function on genome integrity, little is known about the underlying molecular mechanisms, their regulation, integration into the cellular DSB processing apparatus, as well as their interaction with components of D-NHEJ and HRR.

It is thus possible that in certain cases, even in repair proficient cells D-NHEJ fails somehow and thereby permits B-NHEJ to substitute for it. Likewise, DNA end-resection during B-NHEJ that generates single stranded DNA regions might facilitate the use of microhomology and may generate interdependencies with HRR. Since DNA end-processing and the use of homology is an important component of HRR, it would be of high interest to investigate to what extend irregular HRR events allow, or even initiate the function of B-NHEJ (Mladenov and Iliakis, 2011).

1.7 DNA Ligases

In the end of all DSB repair pathways, breaks in the phosphodiester backbone of the DNA are rejoined by DNA ligases. DNA Ligases are versatile enzymes and most organisms have multiple ligation enzymes that either function in DNA replication and join Okazaki fragments or are dedicated to particular DNA repair pathways, such as nucleotide excision repair (NER), base excision repair (BER), single strand break repair (SSBR), or the repair of DSBs via NHEJ (Shuman and Glickman, 2007; Tomkinson et al., 2006). Furthermore, breaks that are formed during the discontinuous DNA synthesis on the lagging strand of the replication fork and during recombination, are also rejoined by DNA ligases (Ellenberger and Tomkinson, 2008). By the feature of their enzymatic action DNA ligases are nucleotidyltransferases (NTases) that utilize ATP to catalyze the formation of a phosphodiester bonds by an a universal three sequential step reaction (Figure 10) (Shuman, 2009).

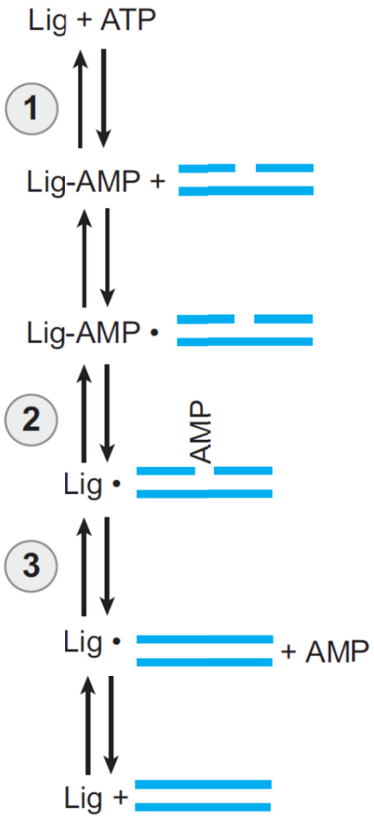

Figure 10: Enzymatic steps of DNA ligation. (Ellenberger and Tomkinson, 2008)

Thereby, during the first step of ligation, an adenylate group, adenosine 5'-monophosphate (AMP) is transferred and a phosphoamide bond (P-N) is formed between the α-amino group of the conserved lysine residue at the active site and the 5' phosphate of AMP. This activated enzyme-NMP adduct is generated in the absence of nucleic acid as substrate. In the second step, the 5' phosphate group of NMP is transferred from the active site lysine to a phosphorylated DNA 5' end, forming a pyrophosphate linkage (5'P-5'P). Adenylation of the DNA activates the 5' phosphate of a DNA substrate for phosphodiester bond formation. In step 3, the 3' hydroxyl group of the adjacent DNA strand displaces AMP from the 5' phosphorylated DNA end by nucleophilic attack and covalently joins the DNA ends of the two strands together (Tomkinson et al., 2006). This reaction sequence is practically irreversible and it is likely that most of the ligase enzymes within the cell are adenylated and therefore ready to react. Adenylation of the enzyme also enhances the

specificity of binding to DNA substrates, an activity known as nick sensing (Ellenberger and Tomkinson, 2008).

Early biochemical and immunological studies showed that eukaryotic cells contain multiple ligase species (Lindahl and Barnes, 1992), which have been recently extensively characterized (Ellenberger and Tomkinson, 2008). The DNA ligases encoded by the human *LIG1*, *LIG3*, and *LIG4* genes serve as the prototypic members of the three families of eukaryotic DNA ligases. These enzymes share a similar catalytic region that is flanked by distinct N- and C-terminal regions. Homologue products of the *LIG1* and *LIG4* genes appear to be present in all eukaryotes. In contrast, the *LIG3* gene appears to be restricted to vertebrates.

Central element in all these enzymes is the catalytic core consisting of the N-terminal NTase domain that is flexibly tethered through a polypeptide linker to a C-terminal oligonucleotide/oligosaccharide binding (OB)-fold domain (Figure 11).

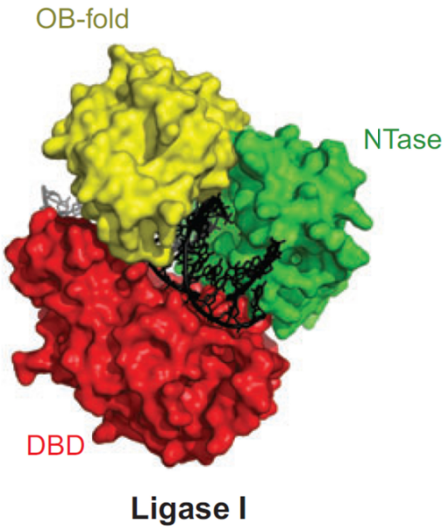

Figure 11: Anatomy of mammalian DNA Ligase I bound to DNA. A conserved catalytic core, consisting of the NTase domain (green) and OB-fold domain (yellow), contacts the 3'-OH and 5'-PO4 ends of DNA during steps 2 and 3 of the end-joining reaction (Figure 10). An additional DNA-binding domain (DBD) (red) in each enzyme interacts with DNA, completing the ring-shaped structure. (Ellenberger and Tomkinson, 2008)

The NTase domain harbors the adenylate- binding pocket composed of six peptide motifs which display active-site residues. Motif I (KxDGxR) contains the conserved lysine to which AMP gets covalently linked in the first step of the ligation reaction. The amino acids (aa) of motifs I, Ia, III, IIIa, IV, and V just contact AMP and play essential roles in one or more steps of the ligation process. The OB-fold domain (OBD) consists of a five stranded antiparallel β-barrel plus an α-helix that assist the transfer of AMP to the active-site lysine of the NTase domain and subsequently undergo a large rotation, bind double stranded DNA and contact the 3'-OH and 5'-PO_4 ends of DNA during the last two steps of ligation.

Recent advances in the structure of DNA ligases reveal that all ligases except the simplest viral ligases completely encircle the DNA substrate using a multidomain architecture with sufficient flexibility to open and close around the DNA. Furthermore, rearrangements at the locus of the active site display an adaptive development throughout the multisteps of DNA ligation reaction. By extending this central core with different additional domains the different eukaryotic DNA ligase species have evolved functionally optimizing to completely encircle the DNA substrate. Besides, the unique regions flanking the conserved catalytic domain of eukaryotic ligases mediate protein-protein interactions and target each isoenzyme for a particular aspect of DNA metabolism and repair.

Ligases of mammals own an additional N-terminal DNA-binding domain (DBD) that interacts with the minor groove and contacts the DNA upstream and downstream of the nick for efficient ligation activity. It stabilizes the DNA in an under wound conformation where the minor groove is enlarged, exposes the ligatable DNA ends and makes protein-protein interactions with the catalytic core forming a ring shaped structure that encircles the DNA (Cotner-Gohara et al., 2008; Pascal et al., 2004).

The main characteristics of the DNA ligase proteins encoded by the genes *LIG1*, *LIG3*, and *LIG4* are introduced in the next sections.

1.7.1 DNA Ligase I

The DNA ligase I (LIG1) family is thought to play the central role in DNA replication. The *LIG1* gene encodes a 919 aa polypeptide with endowed functionality by characteristic domains, divergent among species and dispensable for catalytic activity (Figure 12).

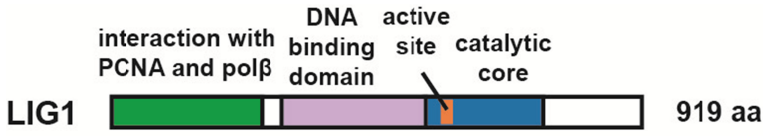

Figure 12: Domain structure of DNA ligase I (Arakawa et al., 2012).

This N-terminal region contains amino acid sequences targeting LIG1 to DNA replication factories through specific protein-protein interactions with PCNA and polymerase ß (polß) (Cardoso et al., 1997; Montecucco et al., 1998; Montecucco et al., 1995). Further regulation of the functions of this domain is requirement for nuclear localization and is also subject to posttranslational modification, since Serine residues at positions 51, 76, and 91 are phosphorylated by cyclin dependent kinases (CDKs), and Ser66 is phosphorylated by casein kinase II (CK2) (Ferrari et al., 2003; Montecucco et al., 1998; Rossi et al., 1999; Song et al., 2007).

The dedicated function of LIG1 family to DNA replication is emphasized in *S. cerevisiae*, since in yeast the corresponding homolog *CDC9* is an essential gene (Hartwell, 1974; Johnston, 1979; Johnston and Nasmyth, 1978). It was therefore expected that inactivation of the vertebrate *LIG1* gene would be incompatible with survival. Indeed, inactivation of both *LIG1* alleles in mouse embryonic stem cells is lethal (Petrini et al., 1995). Notably, however, mouse embryos harboring homozygous deletions of the 3'end of the *LIG1* gene were found to develop normally until midgestation (Bentley et al., 2002; Bentley et al., 1996). Mouse embryonic fibroblast (MEF) cell lines generated from such embryos proliferate normally, show normal sensitivity to DNA damaging agents, but have a defect in Okazaki fragment joining and increased genomic instability (Bentley et al., 2002; Bentley et al., 1996).

The LIG1 deficient cell line 46BR has been established from the single documented case of a human with a *LIG1* mutation (Barnes et al., 1992; Webster et al., 1992). 46BR cells show no obvious defects in proliferation but show a marked defect in Okazaki fragment joining (Henderson et al., 1985; Lönn et al., 1989) and hypersensitivity to UV-light suggesting a function of LIG1 in NER (Aboussekhra et al., 1995). In addition, these cells are hypersensitive to ionizing radiation (IR) (Bentley et al., 2002; Bentley et al., 1996), as well as to simple alkylating agents due to a defect in long-patch subpathway of BER (Levin et al., 2000). Although the above results suggest that in vertebrates another ligase could substitute for LIG1 in DNA replication, the identity of this ligase remains conjectural.

1.7.2 DNA Ligase IV

The second family of ligases found in all eukaryotes is that of DNA Ligase IV (LIG4) and the main function attributed to these polypeptides is the ligation step during the repair of DNA double strand breaks (DSBs). This function of the 912 aa long protein is supported, both in yeast and in vertebrates, by a C-terminal extension of the central core with two tandemly arrayed BRCT motifs (Figure 13) (Schär et al., 1997; Teo and Jackson, 1997; Wei et al., 1995; Wilson et al., 1997).

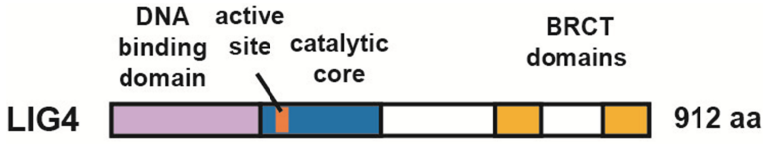

Figure 13: Domain structure of DNA ligase IV (Arakawa et al., 2012).

The BRCT domain fold is comprised an approximately 100 aa tandem repeat in which a central 4-stranded β-sheet flanked by a single α-helix on one side and two α-helices on the opposite side. In general the domain architecture of BRCT domains is remarkably diverse since they range from isolated individual domains to multiple tandem BRCT repeats, or even as fusions with other functional domains (Leung and Glover, 2011).

Although the C-terminal extension of the catalytic region of DNA ligase IV contains two adjacent BRCT domains, LIG4 interacts with XRCC4 independent of phosphorylation (Critchlow et al., 1997; Grawunder et al., 1997) through an unusually long linker region. It mediates the contact between the two proteins by forming a distinct clamp structure of LIG4 that wraps around the linear XRCC4 tails to stabilize the interaction and become integrated in NHEJ pathway of DSB repair (to be termed here D-NHEJ) (Dore et al., 2006). D-NHEJ in vertebrates also comprises XLF, and the DNA dependent protein kinase (DNA-PK) complex, consisting of the Ku heterodimer and the catalytic subunit, DNA-PKcs. LIG4 is one of the targets of DNA-PK (Wang et al., 2004). Through this domain structure and possibly through adaptations in its central core, LIG4 has the unique ability of joining DNA ends that are non-complementary (Gu et al., 2007).

The predominant function of LIG4 in DSB repair is further supported by the phenotype of its inactivation in the mouse. Embryonic lethality occurs late, after multiple normal DNA replication cycles and is caused by massive apoptosis in the central nervous system (CNS) (Barnes et al., 1998; Frank et al., 1998; Frank et al., 2000). Life births are possible when CNS apoptosis is rescued by concomitant loss of either p53 or ATM function (Frank et al., 2000; Lee et al., 2000; Sekiguchi et al., 2001), but *LIG4*$^{-/-}$*p53*$^{-/-}$ MEFs are highly radiosensitive and show defects in DSB repair due to the D-NHEJ defect.

Although LIG4 is firmly linked to D-NHEJ, it remains open whether it can substitute for the functions of other ligases. Also, the possible substitution of LIG4 functions by other DNA ligases has not been formally demonstrated.

1.7.3 DNA Ligase III

The DNA Ligase III (LIG3) family is particularly notable. First, the *LIG3* gene is newer evolutionary and appears restricted to vertebrates (Ellenberger and Tomkinson, 2008). Second, it is capable of generating four distinct DNA ligase polypeptides (Figure 14) (Ellenberger and Tomkinson, 2008).

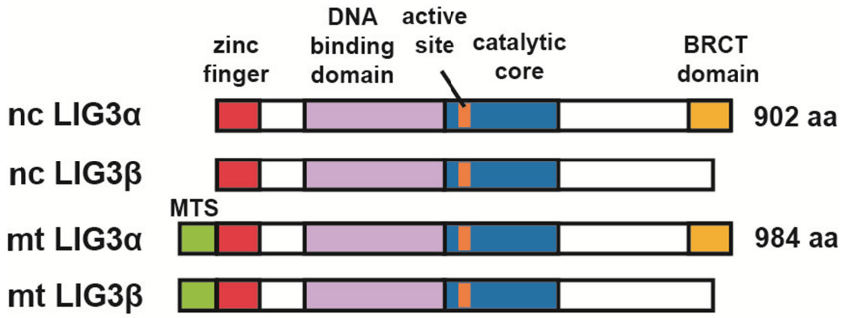

Figure 14: Domain structure of DNA ligase III (Arakawa et al., 2012).

Nuclear and mitochondrial versions of LIG3α are ubiquitously synthesized from *LIG3* mRNA by an alternative translation initiation mechanism (Lakshmipathy and Campbell, 1999; Perez-Jannotti et al., 2001). Thus, the mitochondrial DNA ligation functions are transferred from *LIG1* in lower eukaryotes to *LIG3* in vertebrates (De and Campbell, 2007). In addition, a germ-cell-specific alternative splicing mechanism that replaces the terminal 3'-coding exon of LIG3α by a shorter exon lacking the BRCT domain generates LIG3β (Mackey et al., 1997; Perez-Jannotti et al., 2001).

A unique feature of the ligases encoded by *LIG3* is an N-terminal zinc finger domain that binds to nicks and gaps in DNA and serves as a nick sensor. In LIG3 the overall topology of this domain is a highly extended version of the "treble-clef" zinc finger motif (Sri Krishna et al., 2003) the essential features of which comprise two zinc ligands positioned either side of a β-hairpin (a knuckle) and two positioned at the N-terminal turn of a α-helix (Kulczyk et al., 2004). This domain is not required for DNA nick joining by LIG3, but it significantly broadens the substrate range of the enzyme. The zinc finger stimulates the catalytic efficiency of single strand ligation and improves dramatically intermolecular

ligation of blunt-ended DNA molecules. To explain the stimulation of DNA end-joining by the zinc finger it is proposed that the zinc finger and catalytic core with the DBD of LIG3 engage the ends of a nicked DNA substrate in a sequential manner, like the blades of a jackknife that can open and close (Figure 15) (Cotner-Gohara et al., 2008).

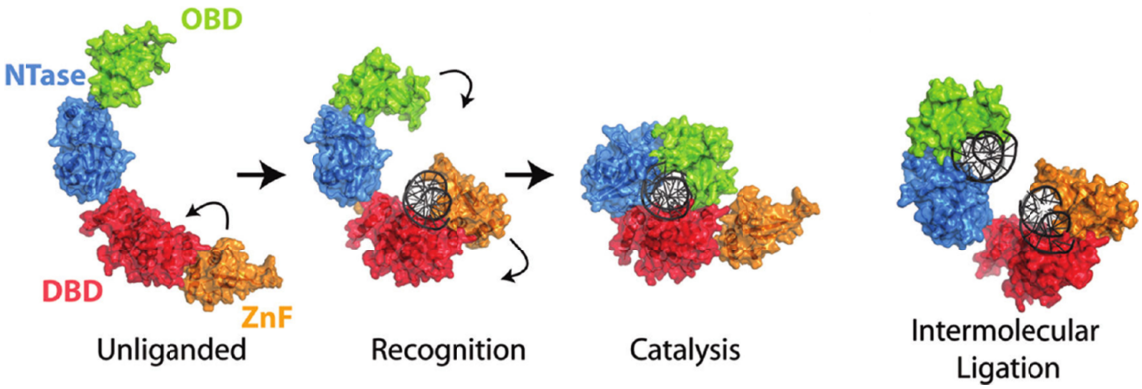

Figure 15: Jackknife model of DNA recognition by LIG3. (Cotner-Gohara et al., 2010)

This “jackknife model" posits that the two DNA-binding modules of LIG3 engage the ends of the DNA substrate at different times during the end-joining reaction. The zinc finger -DBD forms a crescent-shaped surface used for DNA end-recognition which switches to a ring formed by the NTase and OBD domains for catalysis of nick ligation reaction. When joining DSBs, two independent DNA-binding modules of LIG3, the zinc finger-DBD and the catalytic core could allow the enzyme to bind two DNA ends simultaneously for intermolecular ligation (Cotner-Gohara et al., 2010).

Moreover, the 77 C-terminal residues that are unique to LIG3α constitute a BRCT motif mediating the interaction with XRCC1; this interaction stabilizes LIG3 and mediates some of its functions (Caldecott et al., 1995; Caldecott et al., 1994; Dulic et al., 2001; Mackey et al., 1997; Nash et al., 1997).

Biochemical and cell biology studies link the nuclear LIG3α and XRCC1 to the short patch subpathway of BER (Frosina et al., 1996) and the repair of single strand breaks (Okano et al., 2003; Okano et al., 2005). Nuclear LIG3α is also a

key component of a NER subpathway that operates in dividing cells, but is particularly important for the repair of UV lesions in non-dividing cells (Moser et al., 2007). There is also evidence that LIG3α is a component of B-NHEJ (Wang et al., 2005).

Although the confirmed specific functions of the peptides generated by the *LIG3* gene appear restricted to DNA repair, deletion of *LIG3* has consequences significantly more severe than deletion of either *LIG1* or *LIG4* and causes early embryonic lethality that cannot be rescued by deletion of p53 (Puebla-Osorio et al., 2006). Whereas this result may be explained by the function of LIG3α in mitochondria DNA metabolism (Lakshmipathy and Campbell, 1999), or in BER and other repair pathways, this observation is intriguing and requires further in depth investigation.

Because the *LIG3* gene is only present in vertebrates, the use of genetically tractable lower eukaryotes, such as *S. cerevisiae*, to delineate their cellular functions is ruled out. Moreover, conclusions regarding the cellular functions of *CDC9* and *DNL4* genes, the yeast homologs of mammalian *LIG1* and *LIG4*, cannot be extrapolated to mammalian cells because of their larger repertoire of DNA ligases that generates new ways of functional substitution. Finally, the nuclear and mitochondrial roles of LIG3α and LIG3β together with the lethal phenotype of *LIG3* deletion generate urgent requirements for conditional gene targeting strategies.

2 Scope and aims of the work

The genome of eukaryotic cells is under the continuous attack of deleterious environmental factors like cosmic and terrestrial radiation and of byproducts of the intracellular metabolism, such as reactive oxygen species and replication errors. They all can lead to the generation of DNA double strand breaks (DSBs), highly cytotoxic lesions, whose misrepair causes mutations and lethality. Biochemical and genetic studies support the view that the majority of DNA DSBs induced in the genome of higher eukaryotes by ionizing radiation (IR) are removed by two pathways of non-homologous end-joining (NHEJ) termed D-NHEJ and B-NHEJ. While D-NHEJ depends on the activities of the DNA-dependent protein kinase (DNA-PK) and DNA ligase IV/XRCC4, B-NHEJ utilizes, at least partly, the DNA Ligase III/PARP-1/XRCC1 repair module and histone H1 as an alignment factor.

DNA ligase III (LIG3) is, besides ligase I and IV, one of three known mammalian DNA ligases, and interestingly, it is restricted to vertebrates. Thus, genetically tractable lower eukaryotes such as *S. cerevisiae* cannot be used to delineate the functions of the *LIG3* gene.

The *LIG3* gene of higher eukaryotes generates four distinct DNA ligase polypeptides in the form of nuclear and mitochondrial versions of DNA LIG3α and LIG3β. The mitochondrial and nuclear versions of LIG3α are generated from *LIG3*α mRNA by an alternative translation initiation mechanism. The mitochondrial form is distinguished by an N-terminal mitochondrial targeting signal (MTS) that is proteolytically removed during transport into mitochondria. The N-terminal mitochondrial leader sequence is a unique characteristic of DNA LIG3 that is not shared by any of the other remaining ligases. Hence LIG3 is the only DNA ligase present in mammalian mitochondria participating in all important aspects of DNA metabolism including repair and replication of mitochondrial DNA.

The debate about backup pathways of NHEJ, which our laboratory started over ten years ago, is now a hot topic of DDR. Numerous studies suggest the alternative use of B-NHEJ whenever D-NHEJ is compromised.

Thus, the overarching aim of this study was to define the functions of DNA ligases in B-NHEJ, especially of LIG3 and LIG1. Therefore we generated a series of knockout and knock-in mutants in the DT40 system in cooperation with Hiroshi Arakawa from Helmholtz Center Munich. While *LIG1*$^{-/-}$ and *LIG4*$^{-/-}$ mutants are viable and grow normally, *LIG3* knockout is lethal. Therefore, conditional knockout models were developed and combined with knockouts of all other DNA ligases.

The generated mutants and wild type (wt) cells were tested after induction of the conditional knockout of LIG3 by treatment with 4-hydroxytamoxifen (4HT) on their growth characteristics and survival, and with special emphasis the effect of LIG3 knockout induction on mitochondria function. In addition, real time PCR and an *in vitro* end-joining assay were used to define a timeframe after 4HT treatment where DSB repair experiments could be performed.

DSB repair in the different mutants was measured in exponentially growing cells and measured using pulsed-field gel electrophoresis, colony formation assay and γ-H2AX foci formation and decay. Special emphasis was given to the mutants *LIG1*$^{-/-}$*LIG4*$^{-/-}$ and *LIG3*$^{-/-}$*LIG4*$^{-/-}$*mts-hLIG1*, where the only remaining DNA ligase for DSB repair by B-NHEJ were LIG3 and LIG1, respectively.

3 Materials and Methods

3.1 Materials

Table 1: Laboratory Apparatus.

Apparatus	Provider
Aluminum filter	GE Healthcare, USA
Cell counter, Multisizer™ 3 and Coulter Z2	Beckman Coulter, Germany
Centrifuge, Avanti™ J-20 XP	Beckman Coulter, Germany
Centrifugal elutriation rotor, JE-6	Beckman Coulter, Germany
Centrifugal rotor, JA 25.50	Beckman Coulter, Germany
Centrifuge, Rotana 460 R	Hettich, Germany
Cooling unit (external), DC10-K20	Thermo Fischer Scientific, Germany
Dry Block Heater/Cooler	HLC, Oehmen, Germany
Electrophoresis chambers, Horizon 11•14 and 20•25	Life Technologies™, USA
Electrophoresis chamber, Mupid-One	Advance Co. Ltd., Japan
Electrophoresis Power Supply, EPS 301	Amersham, GE Healthcare, USA
Falcon™ Express™ Pipet-Aid®	BD Biosciences, Germany
Flow cytometer, Epics XL and Gallios	Beckman Coulter, Germany
FluorImager, Typhoon 9400	Molecular Dynamics, Germany
GloMax® 20/20 Luminometer	Promega, Germany
iBlot® Dry Blotting System	Invitrogen, Life Technologies, Germany
Inverted phase contrast microscope	Olympus, Germany
Laminar flow hood, HeraSafe	Heraeus, Thermo Scientific, Germany
LC Carousel Centrifuge 2.0	Roche Diagnostics, Germany
Licox CMP Oxygen Monitor	Integra LifeSciences, Germany
LightCyler 2.0	Roche Diagnostics, Germany
Magnetic stirrer, MR Hei-Standard	Heidolph, Germany
MCO-18 O_2/CO_2 incubators	Sanyo, Germany
Metafer Slide Scanning Platform	MetaSystems, Germany
Metafer SlideFeeder	MetaSystems, Germany
Micro Centrifuge, IR	Carl Roth, Germany
NanoDrop™ 2000	Thermo Scientific, Germany
Nucleofector® 2b Device	Amaxa, Lonza, Germany
Odyssey® infrared imaging system	LI-COR Biosciences, Germany
Oxygen catheter microprobe, CC1SB	Integra LifeSciences, Germany
pH-Meter, FE20 – FiveEasy™ pH	Mettler Toledo, Germany
Pipettes, Pipet-Lite™	Mettler Toledo, Germany
Power supply, PowerPac™ Basic	Bio-Rad, Germany

PTB dosimeter	Physikalisch-Technische Bundesanstalt, Germany
Pump drive, MCP Standard	Ismatec®, Idex Health & Science, Germany
Pumphead, Easy-Load® II	Ismatec®, Idex Health & Science, Germany
SDS-PAGE apparatus	Bio-Rad, Germany
SDS-PAGE mini gels, Mini PROTEAN	Bio-Rad, Germany
Seifert Isovolt 320 HS X-ray tube	Seifert, GE Measurement & Control, USA
Rocky shaker	Oehmen, Germany
Tabletop centrifuge, Biofuge fresco	Heraeus, Thermo Scientific, Germany
Thermo-mixer	Eppendorf, Germany
Ultracentrifuge, Optima Max	Beckman Coulter, Germany
Ultracentrifuge rotor, MLN80	Beckman Coulter, Germany
UV spectrophotometer	Shimadzu, Germany
Vacuum gas pump	VWR, Germany
Vortexer, IKA MS 3 basic	IKA, Germany
Water bath	GFL, Germany
Weighing balance, 572-43	Kern, Germany
Weighing balance, VWR-124	Sartorius, Germany

Table 2: Disposable Products and Commercial Kits.

Disposable Product / Commercial Kit	Provider
0.5, 1.5 and 2 ml reaction tubes	Greiner, Germany
2, 5, 10, 25 ml pipette	Greiner, Germany
3 mm diameter glass tubes	CM Scientific Ltd., UK
4.2 ml, 6.3 ml or 8 ml ultracentrifuge tubes	Beckman
12 ml non-cap tubes	Greiner, Germany
15 and 50 ml tubes	Greiner, Germany
20 mm glass cover slips	Invitrogen, Life Technologies, Germany
35 mm glass coverslip bottom dishes	MatTek Corporation, USA
60, 100 mm bacteria dishes	Greiner, Germany
150 mm culture dishes	TPP, Switzerland
CellTiter-Glo® Luminescent Cell Viability Assay	Promega, Germany
Cuvettes, Q-VETTES Halbmikro	Ratiolab®, Germany
Dialysis membrane, Spectra/Por® MWCO: 6-8,000	Spectrum® Laboratories, USA
ECL+ chemiluminescence detection Kit	GE Healthcare, Germany
Filter tips	Greiner, Germany
fluorescence microscope, AxioImager Z2	Zeiss, Germany
Glass flasks, beakers and cylinders	Schott Duran, Germany
High pure RNA isolation kit	Roche Diagnostics, Germany
ImmunoSelect® Adhesion Slides	Squarix, Germany
Maxima First strand cDNA Synthesis Kit	Fermentas, Thermo Scientific, Germany
Microscope Slides, H872	Carl Roth, Germany
Minisart®, 0.45 µm sterile filter	Sartorius, Germany
MitoTracker® Green FM and Deep Red FM	Invitrogen, Life Technologies, Germany
NucleoBond Xtra Midi/Maxi Plus EF purification kit	Macherey-Nagel, Germany
NucleoSpin Tissue Kit	Macherey-Nagel, Germany
PAP pen for immunostaining	Sigma-Aldrich, Germany
Peha-soft® nitrile FINO gloves	Hartmann, Germany
Phase Lock Gel, 1.5 ml Heavy	Eppendorf, Germany
Pipettes	Greiner, Germany
Pipette tips	Greiner, Germany
LightCycler® capillaries	Roche Diagnostics, Germany
LightCycler® FastStart DNA Master^{PLUS} SYBR Green I Kit	Roche Diagnostics, Germany
iBlot® blotting stacks, Nitrocellulose and PVDF	Invitrogen, Life Technologies, Germany

Table 3: Chemical Reagents

Chemical	Provider
1,4 Dithiothreitol	Carl Roth, Germany
Agarose, LE	Lonza, Germany
Ampicillin	Carl Roth, Germany
ATP	Sigma-Aldrich, Germany
β-Mercaptoethanol	Sigma-Aldrich, Germany
Blasticidin S	InvivoGen, Germany
Boric acid	Carl Roth, Germany
Bovine serum albumin fraction IV	Carl Roth, Germany
Bromophenol blue	Sigma-Aldrich, Steinheim, Germany
Caspase Inhibitor III, BOC-D-FMK	Calbiochem®, Merck Millipore, Germany
Chicken serum	Gibco®, Life Technologies, Germany
Chloramphenicol	Carl Roth, Germany
Chloroform	Sigma-Aldrich, Germany
Coomassie brilliant blue R 250	SERVA, Germany
Crystal violet	Merck, Germany
CsCl	Crescent Chemical, USA
DAPI	Sigma-Aldrich, Germany
Dimethyl sulfoxide	Sigma-Aldrich, Germany
Dulbecco's Modified Eagle Medium: Nutrient Mixture F-12	Gibco®, Life Technologies, Germany
Ethanol	Sigma-Aldrich, Germany
Ethidium bromide	Roth, Germany
EDTA	Roth, Germany
Fetal bovine serum	Biochrom, Germany; PAA, Coelbe, Germany; Gibco®, Life Technologies, Germany
G418	InvivoGen, Germany
Gelatin	Calbiochem®, Merck Millipore, Germany
GeneRuler™ 1 kb DNA Ladder	Fermentas, Thermo Scientific, Germany
GeneRuler™ 100 bp Plus DNA Ladder	Fermentas, Thermo Scientific, Germany
Glycerol	Carl Roth, Germany
GlutaMAX™	Gibco®, Life Technologies, Germany
HCl	Carl Roth, Germany
HEPES	Carl Roth, Germany
LB agar	USB®, Affymetrix®, USA
LB medium	USB®, Affymetrix®, USA
KCl	Carl Roth, Germany
KH_2PO_4	Carl Roth, Germany
KOH	Carl Roth, Germany
Low melting agarose	Carl Roth, Germany
Lysozyme	Sigma-Aldrich, Germany

Methanol	Sigma-Aldrich, Germany
Methylcellulose	Sigma-Aldrich, Germany
$MgCl_2$	Merck, Darmstadt, Germany
Minimum Essential Medium	Gibco®, Life Technologies, Germany
NaCl	Carl Roth, Germany
NaF	Carl Roth, Germany
$NaHCO_3$	Carl Roth, Germany
NaH_2PO_4	Merck Millipore, Germany
Na_2HPO_4	Carl Roth, Germany
NLS	Merck, Heidelberg, Germany
Non-fat dry milk	Carl Roth, Germany
*Not*I	Fermentas, Thermo Scientific, Germany
NU7441, KU-57788	Tocris Bioscience, USA
Orange G	Carl Roth, Germany
Paraformaldehyde	Carl Roth, Germany
Phenol	Carl Roth, Germany
Phosphoric acid	Carl Roth, Germany
Phenylmethylsulfonyl fluoride	Carl Roth, Germany y
Poly-L-lysine	Biochrom AG, Berlin, Germany
Primer	Invitrogen, Germany
ProLong® Gold antifade reagent	Invitrogen, Germany
Propidium iodide	Sigma-Aldrich, Germany
Protease, from *Streptomyces griseus*	Sigma-Aldrich, Germany
Puromycin	InvivoGen, Germany
RIPA buffer	Thermo Scientific, Germany
RNase A	Sigma-Aldrich, Germany
Rotiphorese® Gel 30 (37.5:1)	Carl Roth, Germany
Page Ruler, Prestained Protein Ladder	Fermentas, Thermo Scientific, Germany
*Sal*I	Promega, Germany Fermentas, Thermo Scientific, Germany
Sodium dodecyl sulfate	Carl Roth, Germany
Streptomycin	Calbiochem®, Merck Millipore, Germany
Sucrose	Sigma-Aldrich, Germany
SYBR Gold	Molecular Probes, Life Technologies, Germany
Tetramethylethylenediamine (TeMeD)	Sigma-Aldrich, Germany
Tris base	Carl Roth, Germany
Triton X-100	Sigma-Aldrich, Germany
Trypsin	Biochrom, Germany
Tween 20	Carl Roth, Germany
Xylene Cyanol	Sigma-Aldrich, Germany

3.2 Methods

3.2.1 Cell culture

DT40 cells are suspension cells and were grown in D-MEM/F12 supplemented with 10% fetal bovine serum (FBS), 1% chicken serum, 50 µM β-mercaptoethanol (β-ME) at 41ºC in a humidified SANYO MCO-18 O_2/CO_2 incubator with 5% CO_2 and 95% air. Cells were grown in 100 mm bacteria dishes with 10 ml growth medium and maintained in the logarithmic phase of growth through routine passaging by dilution with fresh medium.

When frozen stocks of cells were taken to subculture, they were passaged at least two times before being used in experiments and were discarded after approximately one month or about 40 passages. In all experiments exponentially growing cells were used unless otherwise indicated. The distribution of cells throughout the cell cycle was routinely measured by flow cytometry.

3.2.2 Drug treatments

All inhibitors used were dissolved in dimethyl sulfoxide (DMSO), and were applied to culture medium 1 h before irradiation unless otherwise indicated. Table 4 lists all inhibitors with their mechanism of action and the concentrations used.

Table 4: Used inhibitors with mode of action and final concentrations

Drug	Description	Final Concentration
Caspase Inhibitor III (BOC-D-FMK)	A synthetic peptide that irreversibly inhibits activity of caspase family proteases and blocks apoptosis	100 µM
NU7441 (KU-57788)	Highly potent and selective DNA-PK inhibitor	10 µM

3.2.3 Parental Cell line

Mutants analyzed here were derived from the DT40-Cre1 cell line. The primary DT40 cell line was established in the laboratory of Eric. H. Humphries from an Avian Leukosis Virus (ALV) induced B cell lymphoma in the Bursa of Fabricius from a female White Leghorn chicken (Baba et al., 1985) and derived its official name LSCC-DT40 due to the proposed unified designation system for avian tumor transplants and cell lines (Witter et al., 1979).

The DT40-Cre1 cell line used here conditionally express Cre recombinase to allow genome editing, and v-myb to enhance gene conversion (Arakawa et al., 2012; Arakawa et al., 2002; Arakawa et al., 2001). Cre recombinase is expressed from a human β-actin promoter as a chimera, MerCreMer, between a mutated estrogen receptor (Mer), only responding to 4HT (Zhang et al., 1996), and Cre recombinase (Arakawa et al., 2002; Arakawa et al., 2001). In the absence of 4HT, MerCreMer is efficiently sequestered by heat shock proteins in the cytoplasm. This interaction is rapidly disrupted upon administration of 4HT and causes the translocation of the protein to the nucleus, where Cre exerts recombination activity at loxP sites. Cells are also *AID*$^{-/-}$ and carry a deletion in the pseudo V locus of the non-rearranged Ig light chain locus. Furthermore, the non-rearranged V-intervening-sequence is replaced by a rearranged VL light chain gene together with DsRed as a hypermutation reporter. Thus, the full description of the parental cell line is DT40-*AID*$^{-/-}$*IgL*^{dual}; and is referred here as DT40 (Arakawa et al., 2012).

3.2.4 Targeting strategies and mutants

While LIG4 is solidly implicated in the D-NHEJ pathway of DSB repair, the responsible ligase for B-NHEJ is less well characterized. Early work from our laboratory, as well from the laboratories of other investigators, provides strong biochemical evidence for the putative involvement of LIG3 in B-NHEJ. However, the biological significance of these observations remains less well characterized. To investigate the individual functions and possible functional overlap among DNA ligases, we developed in a higher eukaryotic cell system a comprehensive gene targeting strategy to study the ligation requirements of DNA replication and repair (Arakawa et al., 2002; Arakawa et al., 2004). For this study the majority of mutant was generated at the Institute for Molecular Radiobiology, Helmholtz Center Munich by Dr. Arakawa and they were functionally characterized for their DSB repair ability as part of the present work. Mutants generated in Essen are mentioned explicitly.

Since the *LIG3* gene has not been described in DT40, we started with a phylogenetic tree analysis of the ligase genes using the neighbor joining method and organisms for which sequences were available. While *LIG1* and *LIG4* can be detected in all eukaryotes from yeast to plants and animals, *LIG3* is only found in vertebrates, including the chicken. Surprisingly, our homology search uncovered a previously undetected *LIG3* homolog in Drosophila. Notably, despite extensive homology search, we were unable to identify in higher eukaryotes including the chicken, genes of the DNA ligase family, other than *LIG1*, *LIG3* and *LIG4*.

The six amino acids of the active site are highly conserved across species including the bacteriophage T4, emphasizing its importance in enzyme activity. In an effort to minimize the risk of residual activity, we constructed targeting vectors deleting a substantial portion of the core region including the enzyme active site of *LIG1*, *LIG3*, and *LIG4* (Figure 16).

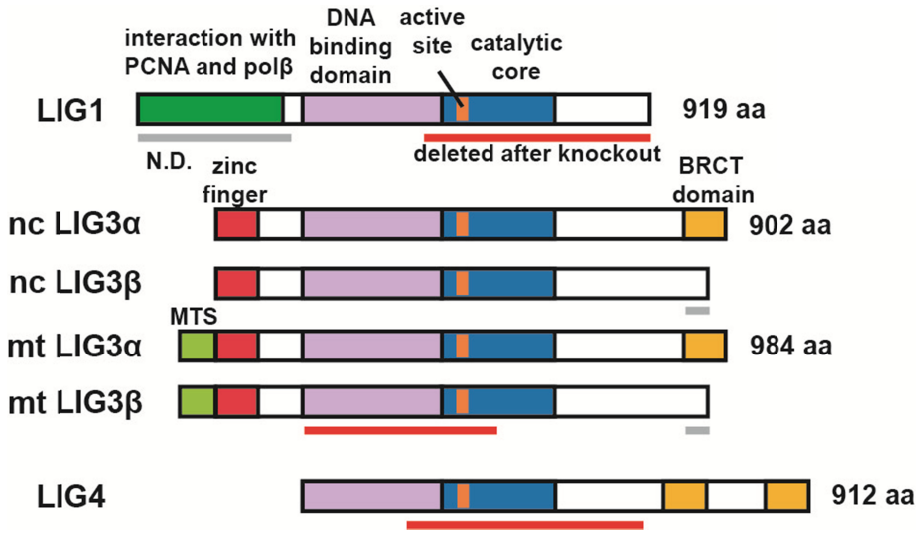

Figure 16: Comparison of DNA ligases and targeting strategies: Domain structure of chicken DNA ligases (Arakawa et al., 2012). Nc: nuclear; mt: mitochondrial. Red bars indicate regions deleted in the mutants generated. The β form of LIG3 is inferred, as the corresponding exon could not be identified.

3.2.4.1 Targeting of *LIG3*

First focus of our study was the elucidation of *LIG3* function using reverse genetics. Since blast algorithms failed to unambiguously define in the chicken *LIG3* locus the LIG3β-specific exon, we confined our studies to LIG3α. The chicken *LIG3* gene encodes a nuclear polypeptide of 902 aa and shares 76% identity and 84% similarity with the human enzyme (922 aa). A mitochondrial polypeptide is generated from the same transcript using a second start codon that adds the 82 aa mitochondria targeting signal (MTS).

LIG3 targeting using conventional strategies readily generated *LIG3*$^{+/-}$ cells, but *LIG3*$^{-/-}$ mutants could not be recovered. We therefore took advantage of the Cre/loxP system to generate conditional mutants. Using the vector *pLig3Lox3Bsr* we first conservatively knocked-in three loxP sites into one allele of the endogenous *LIG3* gene and selected blasticidin S (bsr) resistant cells. In this way, *bsr*-free cells retaining all *LIG3* exons, *LIG3*$^{+/2loxP}$, are recovered by limited dilution and PCR screening after a short treatment with 4HT. In these clones, the remaining two loxP sites mediate upon further treatment with 4HT the removal of *LIG3* exons 6-9, encoding the DNA binding domain and the

5'-half of the catalytic core including the enzyme active site. Follow up of locus editing by PCR shows excision of the drug resistance cassette 8 h after addition of 4HT and of the floxed *LIG3* exons within 4-8 h (Arakawa et al., 2012).

In the conditional *LIG3*$^{+/2loxP}$ cells, the second allele is targeted with the vector *pLig3Gpt* deleting a segment from the middle of exon 4 up to exon 10 and inserting an in-frame stop codon into exon 3, as well as the xanthine-guanine phosphoribosyl transferase (*gpt)* resistance cassette. This cassette is subsequently excised by limited Cre induction with 4HT. In this way, the mutant *LIG3*$^{-/2loxP}$ is generated in which the conditional *LIG3* allele can be excised upon further treatment with 4HT (Arakawa et al., 2012; Paul et al., 2013).

In addition to the above nuclear form of LIG3, the mitochondria form made from the same mRNA supports replication and repair of the mitochondria DNA. In an effort to separate the nuclear and mitochondrial functions of LIG3, we inactivated the M2 translation initiation site in the second allele of the *LIG3*$^{+/2loxP}$ mutant using the targeting vector *pLig3M2IBsr*. The vector introduces an inactivating mutation in the M2, while preserving M1, translation initiation site. Following excision of the *bsr* drug resistance cassette from the second allele, a mutant is generated expressing constitutively only the mitochondrial form of LIG3 (*LIG3*$^{-/M2I}$) (Paul et al., 2013).

3.2.4.2 Targeting of *LIG1*

Conditional targeting strategies similar to those described for *LIG3* were also employed for *LIG1* to account for the possibility that the *LIG1* knockout is lethal as well (Arakawa et al., 2012). In the bursal cDNA database, we identified an incomplete chicken *LIG1* cDNA sequence encoding the 658 C-terminal amino acids. The amino acid sequence of chicken LIG1 derived from this cDNA shared 66% identity and 81% similarity with the human enzyme. Therefore, we deduced the numbering of amino acids and exons of the entire chicken *LIG1* locus from that of human and used it to construct appropriate targeting vectors. The first *LIG1* allele was targeted using the vector *pLig1Lox3Bsr* containing the *LIG1* exons 12-28 and the *bsr* drug resistance cassette, in addition to the three

loxP sites. This allowed the generation of the conditional mutant *LIG1*$^{+/2loxP}$. The second *LIG1* allele was disrupted with the *pLig1Puro* targeting vector, which deletes the same *LIG1* region and generates the *LIG1*$^{-/2loxP}$ mutant. Treatment of this mutant with 4HT deletes exons 17-28 and generates a truncated LIG1 lacking amino acids 509-919, which cover the entire catalytic core including the enzyme active site (red bar in Figure 16). 4HT-induced locus-editing reactions were confirmed also for this ligase by PCR (Arakawa et al., 2012).

3.2.4.3 Targeting of *LIG4*

For the inactivation of *LIG4 w*e employed a conventional knockout strategy (Arakawa et al., 2012). The amino acid sequence of chicken LIG4 has 75% identity and 85% similarity with the human enzyme. The chicken *LIG4* gene does not contain introns and is composed of a single exon. The vector *pLig4Bsr* was therefore designed to delete the entire coding sequence of one *LIG4* allele, while allowing at the same time recycling of the selection marker. The vector *pLig4Puro4* was designed to delete amino acids 185-614 of the second allele while inserting an in frame stop codon after codon 184. Integration of this vector deletes the entire catalytic core including the LIG4 active site. The latter vector also allowed recycling of the selection marker. Successive targeting and the selection-marker-recycling steps were again confirmed by PCR reactions (Arakawa et al., 2012).

3.2.4.4 Targeted integration of overexpression vectors

In case of targeted integration of overexpression vectors we wanted to ensure consistent expression of transgenes and constructed the expression vector, *pChr8RsvLoxIresBsr*, which can be targeted into a defined intergenic locus on chromosome 8, as previously described (Arakawa et al., 2012; Paul et al., 2013). The vector integrates without destroying or grossly disturbing nearby genes. Transgene expression is driven by the Rous sarcoma virus (RSV)

promoter and is followed by an internal ribosome binding site (IRES), the *bsr* selection marker and the SV40 polyA signal. The yeast *LIG1* homolog, *CDC9* and the human *LIG1* with a mitochondrial leader sequence (*mts-hLIG1*) genes were cloned into this vector and knocked into DT40 (Arakawa et al., 2012; Paul et al., 2013).

3.2.4.5 Synopsis of the generated mutants

For a conclusive elucidation of the contributions of LIG1 and LIG3 to DSB repair, we generated a large set of knockout and knock-in mutants in chicken DT40 cells. This set of mutants (summarized in Table 5) includes, in addition to knockouts for individual DNA ligases, also double and triple ligase knockout mutants, as well as ligase knock-in mutants in appropriately selected genetic backgrounds (Paul et al., 2013).

Table 5: A summary of the key features of knockout, conditional knockout and knockin DT40 mutants used in the present study (Paul et al., 2013).

Cell line	Feature
***LIG1*$^{-/-}$ •**	*LIG1* knockout
***LIG3*$^{-/2loxP}$ •**	*LIG3* conditional knockout
***LIG3*$^{-/-}$ ***	*LIG3* knockout
***LIG3*$^{-/M2I}$ •**	nuclear *LIG3* knockout
***LIG4*$^{-/-}$ •**	*LIG4* knockout
***LIG1*$^{-/-}$*LIG4*$^{-/-}$ •**	*LIG1* knockout; *LIG4* knockout
***LIG3*$^{-/2loxP}$*LIG4*$^{-/-}$ •**	*LIG3* conditional knockout; *LIG4* knockout
***LIG3*$^{-/-}$*LIG4*$^{-/-}$ ***	*LIG3* knockout; *LIG4* knockout
***LIG3*$^{-/M2I}$*LIG4*$^{-/-}$ •**	nuclear *LIG3* knockout; *LIG4* knockout
***LIG3*$^{-/-}$*Cdc9* •**	*LIG3* knockout overexpressing *CDC9* (yeast *LIG1*)
***LIG3*$^{-/2loxP}$*LIG4*$^{-/-}$*mts-hLIG1* +**	*LIG3* conditional knockout; *LIG4* knockout overexpressing human mitochondrial *LIG1*
***LIG3*$^{-/-}$*LIG4*$^{-/-}$*mts-hLIG1* * +**	*LIG3* knockout; *LIG4* knockout overexpressing human mitochondrial *LIG1*

***** Deletion of the conditional allele by treatment of the parental cell line with 4HT. Note, not all of the generated mutants are viable.

• Mutants generated by H. Arakawa.

+ Mutants generated by K. Paul.

3.2.5 Cell transfection by electroporation

To generate the above describe mutants two methods of electroporation were used to introduce vector DNA into DT40 cells. (Paul et al., 2013). In the first protocol, electroporation was carried out with cells suspended in complete growth medium. 10^7 cells were electroporated using the GenePulser-Xcell (BIORAD) at 25 µF and 700 V. In the second protocol, 10^6 cells were electroporated in an Amaxa cuvette with program 21 in Buffer B using Nucleofector® II device (Amaxa).

After transfection cells were placed in prewarmed medium and subcloned by limiting dilution in 96 well flat bottom microtiter plates. Therefore, 10 ml medium containing an appropriate number of cells were prepared and 100 µl cell suspension was added to each well of the plate. After 24h 100 µl growth medium with the corresponding selection drug was added. Stable transfectants were selected in 15 µg/ml of blasticidin S, 1 µg/ml mycophenolic acid, or 1 µg/ml of puromycin, as appropriate. After 8 to 10 incubation days subclones were visible as round colonies and were picked from the plate. Targeted clones were screened by PCR (Paul et al., 2013).

3.2.6 Validation of ligase knockouts by PCR

Targeted integration events were screened by polymerase chain reaction (PCR) using primer located upstream of the 5' targeting arm of the construct together with a primer from the resistance marker as previously described (Arakawa et al., 2002; Paul et al., 2013). For this purpose, genomic DNA was isolated according to the protocol using NucleoSpin Tissue Kit (Macherey-Nagel). DNA concentration was determined with a spectrophotometer (NanoDrop; Thermo Scientific).

PCR reactions were performed with 50 ng of genomic DNA and an appropriate primer pair using Expand-Long-Template PCR System (Roche) according to the

protocol of the manufactor. The available primers for PCR screening are summarized in Table 6.

Table 6: Summary of the primer sequences and their direction for targeted integration screening.

Oligo nucleotide	Sequence	Direction
1LI19	CCCCCTTCTACCCCAAATCCTGATAATTTT	For
1LI35	GACAGTGTTGGTGGGATGACACAGGGATCC	For
1LI37	TTTGTAGTCTGCTAGTAAGAAGATTGACAT	For
1LI47	GGGACTAGTTGGTAGGGGCAGTTAGTGCTAGGCT	Rev
1LI5	TCCCGGTGCTGCTGGAGCATGGCCTGGA	For
1LI8	TTGTACTCGCAGGTGAATGCAGCCTCCTCA	Rev
3LI32	GGTTCATGTCTGCAATTAAGTAAAAGTAGC	For
3LI32R	GCTACTTTTACTTAATTGCAGACATGAACC	Rev
3LI34	TTAGCACCAGAATCAGACTTGGAGAGAAAT	For
3LI41	CAACTGCAACATCTAAACTAGTGGAT	Rev
3LI44	CATCCCTCTGCCTGTGCACACGTGGCTGTG	For
3LI62	GGACAGCAAGCAGCCTCCAAGCGGACTGAG	For
4LI18	TGCTTCATCTCTGCCTGAAAGACAATTTCA	For
4LI34	CGGCTGCGCGCGGCGGTTCTTTTCCGACTC	For
4LI39	CTGGATGGTGAACGTATGCAGATGCACAAA	For
4LI40	AATACATCAAACACACAGAAGCAGGTCTGC	Rev
ML29	GGCTAGCGAATTCATAACTTCGTATAGCAT	Rev
BS1	CGATTGAAGAACTCATTCCACTCAAATATACCC	Rev
GP1	TGTTGATATCCCGCAAGATACCTGGATTGA	Rev
PU5	CCCACCGACTCTAGAGGATCATAATCAGCC	Rev
RS16	TGTAGCTTAAATTTTGCTCGCGCACTACTC	Rev
CHR0807	AGATGTGCCCTGGGACAAAGATTCTGGCCA	For
CHR0806	ACGTGTGTCCCATTAGGCAAAACCTTGAGA	For

PCR was performed with the PCR protocol shown in Table 7.

Table 7: PCR protocol for screening of targeted integration.

Temperature	Time	Cycles	PCR step
94°C	240 s	1	Initial Denaturation
94°C	10 s	35	Denaturation
65°C	30 s		Annealing
68°C	90 s		Extension
68°C	420 s	1	Terminal Extension
4°C	hold		Cooling

Reactions were monitored by loading 10 µl of a reaction mixed with 6 x DNA loading buffer (6 x DLB) on an 1% agarose gel. Gel run was performed for 40 min at 100 V with Mupid®-One electrophoresis system (Advance Co. Ltd.). Gels were stained for 30 min in 0.5 x TBE containing 2 µg/ml Ethidium bromide (EtBr) and scanned with a FluorImager (Typhoon, Molecular Dynamics).

3.2.7 Reverse transcription and RT-PCR

Relative expression levels of DNA ligases were measured by real-time polymerase chain reaction (RT-PCR) as recently described (Arakawa et al., 2012; Paul et al., 2013). Therefore, RNA was prepared according to the protocol of the High Pure RNA Isolation Kit (Roche) with the exception that three million cells were used for total RNA isolation. RNA concentration was determined with a spectrophotometer (NanoDrop; Thermo Scientific).

cDNA was prepared from 1 µg total RNA by reverse transcription using the Transcriptor First Strand cDNA Synthesis Kit (Roche) according to the manufacturer's instructions. This cDNA was used as input in real-time PCR reactions.

Realtime-PCR was performed according to the protocol suggested in the LightCycler® FastStart DNA Master^{PLUS} SYBR Green I kit (Roche). Briefly, 1 µl of cDNA, 0.5 µl of sense and antisense primer solution, 2 µl of LightCycler®

FastStart DNA Master^{PLUS} SYBR Green I Master Mix and 6 µl H_2O were mixed together in a 10 µl reaction mixture and put in a LightCycler® Capillary. Glass capillaries were placed in the sample carousel of the LightCycler® (Roche). The settings for the thermal cycles are listed in Table 8 with a following melting curve analysis by increasing the temperature and continuous fluorescence signal measurement.

Table 8: Real-time PCR protocol to measure DNA ligase gene exression.

Temperature	Time	Cycles	PCR step
95°C	600 s	1	Initial Denaturation
95°C	10 s	45	Denaturation
62°C	5 s		Annealing
72°C	10 s		Extension
65°C – 95°C	0.1°C/s		Melting Curves
37°C	30 s		Cooling

The used primer sequences for the different DNA ligases and the utilized Housekeeping gene (HKG) TATA-binding protein 1 (TBP1) are listed in Table 9.

Table 9: Summary of the primer sequences used for real-time PCR.

Oligo nucleotide	Sequence
Chk TBP1-F	CAGCACCAACAGTCTGTCCA
Chk TBP1-R	GGGGCTGTGGTAAGAGTCTG
Chk Lig1-F7	CATCTGCAAGATAGGCACTG
Chk Lig1-R7	CCCAAATCGTCACCAAACAG
Chk Lig3-F	GATGACCCCAGTTCAGCCTA
Chk Lig3-R	GTGGGCTACTTTGTGGGGAA
Chk Lig4-F	CCCCATTAACAGGCAGGATA
Chk Lig4-R	CCACGTTTGTCAGGCTTGTA
Lig1 Hs F1	GAATTCTGACGCCAACATGCA
Lig1 Hs R1	CCGTCTCTCTGCTGCTATTGGA
Lig1 Hs F2	CAGAGGCCAGAAAGACGTG
Lig1 Hs R2	GTCCAGGTCGGGAACCTC

3.2.8 Analysis of cell cycle distribution by flow cytometry

Flow cytometry allows measurement of several different cellular parameters as well as cell sorting on the basis of different properties by assessing fluorescence intensity. This technique is also termed as fluorescence activated cell sorting (FACS). For instance, cell cycle distribution can be evaluated by measuring fluorescence intensity of propidium iodide (PI) bound to DNA, as PI binds to DNA proportionally to its mass. Hence, the fluorescence intensity of PI is proportional to the DNA amount present in a cell. As after replication the DNA amount is doubled, there is twice as much signal generated from a G2-phase cell as compared to G1-phase cell. In this way, it is possible to distinguish cells in different phases of the cell cycle by their detected DNA amount.

Therefore cells were collected by centrifugation and either fixed in 70% ice cold ethanol for at least 15 min or directly stained. Ethanol fixed cells were spun down at 1500 rpm for 5 min and were resuspended in 1x phosphate-buffered saline (PBS; 1.37 M NaCl, 27 mM KCl, 74 mM Na_2HPO_4, 15 mM KH_2PO_4, pH 7.4) containing 40 µg/ml propidium iodide (stock 4 mg/ml in water) and 62 µg/ml RNase A (stock 6.2 mg/ml in 10 mM Tris, 100 mM EDTA, 50mM NaCl, pH 7.6). Cells were incubated at 37ºC for 20 min or at room temperature for 45 min. Unfixed cells were spun down at 1500 rpm for 5 min and were resuspended in buffer for PI-staining without fixation (100 mM Tris pH 7.0, 100 mM NaCl, 5 mM $MgCl_2$, 0.05% Triton X-100) containing also 40 µg/ml PI and 62 µg/ml RNase A and stained at room temperature for ≥10 min.

Measurements of cell cycle distribution were carried out with an Epics XL-MCL (Beckman-Coulter) flow cytometer. During the measurements the cells are suspended within the flow cytometer with Isoton II (135 mM NaCl, 13 mM Na_2HPO_4, 1 mM EDTA, 5 mM KCl, 1.45 mM $NaH_2PO_4 \cdot H_2O$, 7 mM NaF, pH 7.4) to obtain a stream of fluid sheath with single cells. For each sample 10,000 to 20,000 cells were counted and the single cell population was gated to obtain standard histograms. Histogram files (*.HST) were generated by counting the frequency of cells with the same PI signal intensity.

The fraction of cells in the different phases of the cell cycle was calculated using MultiCycle AV software.

3.2.9 Measurement of ATP load

Cellular ATP load was evaluated using the CellTiter-Glo® Luminescent Cell Viability Assay (Promega) to determine the number of viable cells in culture. Applying the reaction mixture results in cell lysis and generation of a luminescent signal proportional to the amount of ATP present. The amount of ATP is directly proportional to the number of metabolically active cells present in culture.

Figure 17: The luciferase reaction. Mono-oxygenation of luciferin is catalyzed by luciferase in the presence of Mg^{2+}, ATP and molecular oxygen (Promega).

Reactions were assembled with 2 x 10^4 cells suspended in 100 µl medium and 100 µl of CellTiter-Glo reagent. After mixing for 30 s, tubes were incubated for 15 min at room temperature and luminescence was quantified using the GloMax® 20/20 Luminometer (Promega).

3.2.10 Measurement of Oxygen Consumption

The amount of oxygen consumed by cells is an indicator of their metabolic rate. As mitochondrial function is responsible for the majority of oxygen consumption within the cell, about 70–90%, any reduction in mitochondrial function can therefore have a major effect upon total oxygen utilization (Chen et al., 2009). The oxygen consumption in DT40 cell suspensions was measured with an oxygen electrode (Oxygen catheter microprobe (CC1SB) attached to a Licox CMP Oxygen Monitor (Integra LifeSciences) in an enclosed glass chamber. Before use, cells were suspended in fresh preheated growth medium at a concentration of 5 x 10^6 cells/ml. During the measurement cells were maintained in a water bath at 41°C and the relative change in oxygen concentration in the glass chamber was manually recorded every 5 min for up to 1 h.

3.2.11 Analysis of mitochondria integrity

To investigate mitochondria integrity in DT40, the MitoTracker Green probe (Invitrogen) was used. MitoTracker Green FM is green-fluorescent mitochondrial stain which appears to localize to mitochondria regardless of mitochondrial membrane potential (Invitrogen). Cells from standard cultures were directly stained with 100 nM MitoTracker Green for 30 min at 41°C. Cells were analyzed in an Epics XL-MCL (Beckman-Coulter) flow cytometer after centrifugation and resuspension in PBS.

3.2.12 Measurement of Apoptotic index

The appearance of cell death is often defined by morphological criteria, whereas pyknosis, or karyopyknosis, followed by karyorrhexis, or fragmentation, is the irreversible condensation of chromatin in the nucleus of a cell undergoing apoptosis. To determine the Apoptotic Index of a sample cells were collected by centrifugation and fixed in 70% ethanol. Ethanol fixed cells were resuspended in 4',6-diamidino-2-phenylindole (DAPI) staining solution (0.1 M Tris, pH 7.0, 0.1 M NaCl, 5 mM $MgCl_2$, 0.05% Triton X-100 and 2 µg/ml DAPI). After incubation for 5 min, an aliquot was analyzed under a fluorescent microscope by counting the fraction of pycnotic and fragmented nuclei within 1000 cells.

3.2.13 Cell fractionation in the different phases of the cell cycle by centrifugal elutriation

Cell populations enriched in G1- or G2-phases of the cell cycle were obtained by centrifugal elutriation – a method for isolating cellular subpopulations on the basis of their sedimentation coefficient (Arakawa et al., 2012; Paul et al., 2013). For elutriation, cells were grown for 24h from a concentration appropriately selected to be exponentially growing and reach approximately 1.5 x 10^6 cells/ml. Cells (2-3 x 10^8) were collected and elutriated at 4°C using a Beckman JE-6 elutriation rotor and a Beckman J2-21M high-speed centrifuge at a flow of 25 ml/min with medium containing 1% FBS (Beckman, Krefeld, Germany). Cells were loaded at 4,100 rpm, and 250 ml fractions collected between 3,300 and 2,200 rpm at 100-rpm steps. Cells were then sequentially elutriated out of the rotor based on their size, with small ones coming out first. In an exponentially growing culture, cell size approximates phases of the cell cycle, with G1-phase cells being small and G2-phase cells being large. Cell-cycle analysis was carried out by flow cytometry for unfixed cells as described above. Usually fractions of highly enriched cells in G1 and G2 cells were used for experiments.

3.2.14 Irradiation of cells

For irradiation experiments regularly exponentially growing cells were used. Since DT40 cells are suspension cells they were irradiated in 60 mm petri dishes in suspension with culture medium. With synchronized cells, enriched cells were resuspended to ~2 x 10^6 cells/ml in fresh growth medium prior to irradiation and were processed as described for exponentially growing cells.

X-rays were generated by an X-ray machine ("Isovolt 320HS", Seifert/Pantak, General Electric-Pantak) with an effective photon energy of approximately 90 keV. The machine was operated at 320 kV and 10 mA using a 1.65 mm aluminum (Al) filter (GE-Healthcare) to absorb soft X-rays. Dosimetry was performed with a PTB dosimeter (Physikalisch-Technische Bundesanstalt, Braunschweig, Germany) that was used to calibrate an in-field ionization monitor. Radiation dose was monthly confirmed with Fricke's chemical dosimetry (Frankenberg, 1969). Cells were exposed to X-rays in petri dishes at a distance of 50 cm to the source at a dose rate of approximately 2 Gy/min and even irradiation was ensured by rotating the radiation table. Immediately after IR exposure cells were returned to the incubator, and at different repair times collected according to the experimental procedure. Unirradiated control cells were treated similarly (sham-irradiated).

3.2.15 Colony Formation Assay

Cell radiosensitivity to killing was determined by their clonogenic survival in the colony formation assay as previously described (Arakawa et al., 2012; Paul et al., 2013). Because DT40 are suspension cells, it is necessary to restrict their movement during the incubation time by seeding them in a viscous growth medium containing 1.5% methylcellulose (MC). Cells are plated in 5 ml MC-medium in dilutions aiming at 100 – 200 colonies per dish and incubated for 10-14 d in a humidified SANYO MCO-18 O_2/CO_2 incubator with 5% CO_2 and 95% air. Colonies are counted without any staining using a reflected-light microscope.

3.2.16 Pulsed-field gel electrophoresis (PFGE)

Asymmetric field inversion gel electrophoresis, a pulsed field gel electrophoresis (PFGE) technique, was developed by Stamato and Denko in 1990 (Stamato and Denko, 1990) and is a specific technique to measure IR-induced DSBs in genomes of cells of higher eukaryotes. This technique takes advantage of the fact that fragmentation of chromosomal DNA by radiation leads to a linear and dose dependent increase in the fraction of DNA that enters the gel, whereas intact mammalian chromosomes are unable to do so. As recently described in detail (Paul et al., 2013), PFGE resolves DNA fragments ranging in size from 0.2-6 Mbp, and detects damage induced by as little as 2 Gy of X-rays, whereas gel electrophoresis with a constant electric field cannot resolve DNA fragments much above 50 kbp.

To evaluate induction of DSBs at different radiation doses (i.e. dose response experiment) cells were resuspended in cold serum-free medium, and mixed with an equal volume of pre-warmed (50°C) serum-free medium containing 1% low melting agarose to reach a final concentration of 7 x 10^6 cells/ml. The cell-agarose suspension was then pipetted into glass tubes with a diameter of 3 mm and placed on ice to allow solidification. Solidified cell-agarose suspension was extruded from glass tubes and cut into 5 mm long cylindrical pieces (plugs) containing approximately 175 x 10^3 cells/plug. Subsequently, agarose plugs were placed in a 60 mm petri dish containing 3ml cold serum-free medium and exposed to different X-ray doses on ice. Plugs were immediately placed in hot lysis buffer (10 mM Tris, 50 mM NaCl, 100 mM EDTA, 2% N-lauryl sarcosine (NLS), pH 7.6 and freshly added 0.2mg/ml protease), and initially incubated at 4°C for 30 min and then at 50°C for 18h (Paul et al., 2013).

For the evaluation of IR induced DSB repair kinetics 16 x 10^6 cells were pre-treated for 1 h in 4 ml medium containing 100 µM Caspase Inhibitor III, cooled to 4°C and irradiated on ice. After irradiation, cells were quickly returned to 41°C for repair. After each repair time interval, cells were collected by centrifugation, washed with PBS and embedded in 0.5% Agarose prepared in fresh serum free growth medium at a final concentration of 7 x 10^6 cells/ml, as

described above. Cells in the plugs were lysed in hot lysis buffer by initially incubation at 4°C for 30 min and then 50°C for 18h. Subsequently, after the lysis step plugs were transferred to washing buffer (10 mM Tris, 100 mM EDTA, 50 mM NaCl, pH 7.6) for 1 h at 37°C and then treated for 1 h with 0.1 mg/ml RNase A in washing buffer at 37°C. To determine the signals generated by non-irradiated cells as background, cells from identically treated non-irradiated cultures were processed at pre-defined times, e.g. 15 min and 4 h (Paul et al., 2013).

AFIGE was carried out in 0.5% agarose (Lonza) and the gels were presatined with 0.5 µg/ml EtBr. The run was carried out in 0.5 x TBE (45 mM Tris, pH 8.2, 45 mM Boric Acid, 1 mM EDTA) at 8°C for 40 h using conventional gel boxes (Horizon 20•25) connected to a switching apparatus. During this time cycles of 50 V (1.25 V/cm) for 900 s in the direction of DNA migration (forward) alternated with cycles of 200 V (5.0 V/cm) for 75 s in the reverse direction. Gels were scanned in the Typhoon and analyzed using the Image-Quant software (GE Biosciences). The fraction of DNA released (FDR) from the well into the lane is a measure of DSBs present and is plotted as a function of dose. FDR was calculated using ImageQuant 5.0 software and FDR values of non-irradiated samples (background) was subtracted from the FDR measured in samples exposed to IR. To obtain dose response curves, induction of DSBs was measured at different radiation doses, and FDR was plotted against radiation dose. In order to facilitate the inter comparison of results obtained by different mutants, and to account for differences in the dose response curves between different cell lines and experiments, repair kinetics are not presented as FDR versus time, but rather as dose equivalent (Deq) versus time. We used dose response curves to deduce Deq values from each FDR value. The obtained repair kinetic curves were fitted using non-linear regression analysis of SigmaPlot 12.0 software. In general, two components, a fast and a slow one, were assumed to exist in the repair curves and fitting algorithms were selected accordingly (Paul et al., 2013).

3.2.17 Immunofluorescence microscopy

For immunofluorescence staining approximately 10^6 cells were spun for 3 min at 1,500 x g on coverslips using cytospin. Cells were washed once with PBS and fixed for 15 min at room temperature with 2% PFA (2% paraformaldehyde in PBS, pH 7.4). Alternatively, cells were collected in cold PBS to 2 x 10^6 cells/ml and 50–100 µl per sample were layered on adhesion slides (ImmunoSelect Adhesion slides, Squarix). Adhesion slides were kept on ice and cells were left to attach for 15 min to the slide surface by gravity. Adhesion slides needed to be prepared using a liquid blocker pen (PAP pen for immunostaining, Sigma-Aldrich) to generate a drawn edge of a hydrophobic circle for every sample. Attached cells were fixed at room temperature for 15 min by adding 2% PFA. Generally, after washing with 1 x PBS, cells were permeabilized for 5 min in P-solution (0.5% Triton X-100 in 100 mM Tris, 50 mM EDTA, pH 7.4) and were blocked in PBG solution (0.5% BSA, 0.2% Gelatin in PBS) overnight at 4°C or 1 h at room temperature.

For visualization of γ-H2AX foci, cells slips were incubated for 90 min at room temperature with an anti-γ-H2AX mouse monoclonal antibody (JBW301, Upstate) diluted 1:200 in PBG solution. Cells were washed three times with 1 x PBS and an anti-mouse IgG antibody, conjugated with AlexaFluor488 (Invitrogen), was added for 60 min at room temperature in 1:400 dilution. Cell nuclei were counterstained for 30 min with DAPI (0.025 µg/ml 4′,6-Diamidin-2-phenylindol (DAPI), 100 mM Tris pH 7.0, 100 mM NaCl, 5 mM $MgCl_2$, 0.05% Tritin X-100), washed once with PBS and mounted using Prolong-Gold Antifade (Invitrogen). Immunofluorescence images were either captured on Leica TCS SP5 confocal scanning microscope using LAS AF software and were further processed using Imaris software (Bitplane), or samples were scanned using a 40x objective in an automated analysis station equipped with a fluorescence microscope (AxioImager Z2, Zeiss) and controlled by Metafer software (MetaSystems). On average, 4000 cells per sample were scored and analyzed using the same software. Using DAPI signal intensity one was able to analyze cell cycle distribution and to distinguish cells separately in the cell cycle (i.e., G1

and early S, termed here as G1) and late in the cell cycle (i.e., late S and G2, termed here as G2).

3.2.18 Live Cell Imaging

To study intracellular localization of LIG3 we used DT40 cells expressing different GFP fusion proteins as described recently (Paul et al., 2013). Cells were placed in glass coverslip bottom dishes and incubated at 41°C in a humidified incubator. DT40 cells expressing a LIG3-GFP fusion protein were directly stained for mitochondria visualization with 150 nM MitoTracker DeepRed (Invitrogen) for 1 h and for nuclei visualization with 1 µg/ml Hoechst 33342 (Invitrogen) for 30 min. Immunofluorescence images of live cells were captured on a Leica TCS SP5 laser scanning confocal microscope using the LAS-AF software (Leica Microsystems) and were further processed using the Imaris software (Bitplane).

3.2.19 In vitro assay of NHEJ

Important insights into the biochemical mechanisms of DSB repair have been obtained using diverse plasmid-based *in vitro* assays. In the majority of in vitro NHEJ assays developed to date, the substrate DNAs used is obtained by restriction enzyme cleavage of plasmid DNA, while end-joining proteins are derived from cell or tissue extracts. Here we use the previously well described plasmid-based assay for DNA end-joining *in vitro* (Iliakis et al., 2005), where whole cell extracts prepared from cells efficiently support the joining in *pSP65* plasmid of *Sal*I-produced DSB ends with 4 nucleotide 5'-cohesive overhangs to generate circles, dimers and multimers by LIG3 (Cotner-Gohara et al., 2010; Wang et al., 2005).

In vitro end-joining was measured with the *pSP65* plasmid (3 kb, Promega) after linearization with *Sal*I. End-joining reactions were performed in NHEJ buffer

(20 mM HEPES-KOH pH 7.5, 10 mM $MgCl_2$, 80 mM KCl, 1 mM ATP, 1 mM DTT) with 50 ng of substrate DNA (*pSP65-Sal*I) and 0.5–2 µg of whole cell extract in a final volume of 20 µl at 25°C for 1 h. Reactions were terminated by adding 5 µl of stop solution (2 µl 5% SDS, 2 µl 0.5 M EDTA and 1 µl protease (10 mg/ml) and incubating for 30 min at 37°C. To the reaction 5 µl of 6 x DNA loading buffer (30% glycerol, 50 mM EDTA pH 8.0, 100 mM Tris-HCl pH 8.0, 0.01% bromophenol blue) was added and half of the reaction was loaded on a 0.7% agarose gel and run at 45 V (2 V/cm) for 4.5 h. Gels were stained with 1:10.000 SYBR Gold (Molecular Probes) and scanned in a FluorImager (Typhoon, Molecular Dynamics). For quantification of rejoining the ImageQuant software (Molecular Dynamics) was used to calculate the percent of input plasmid found in circles, dimers and other higher order multimers.

3.2.20 Plasmid Preparation

The supercoiled plasmid *pSP65* (3 kb; Promega) utilized in the *in vitro* assay of NHEJ was prepared using CsCl/EtBr gradients (Iliakis et al., 2005) or using a NucleoBond Xtra Midi/Maxi Plus EF purification kit (Macherey-Nagel) following the instruction manual (Paul et al., 2013). For CsCl/EtBr gradients, a 1 liter culture of plasmid-transformed E.coli was grown in Lysogeny Broth medium (LB, 10 g/l tryptone, 5 g/l yeast extract, 10 g/l NaCl) containing Ampicillin (Amp, 100 mg/ml in H_2O) in a final concentration of 100 µg/ml to an OD_{600} of 1.0 and then chloramphenicol (Cm, 34 mg/ml in ethanol) to a final concentration of 150 µg/ml was added. Cells were grown overnight and were collected by centrifugation for 30 minutes at 1,300 x g and 4°C. The pellet was resuspended in 10 ml Sucrose/Tris/EDTA solution (25% sucrose, 50 mM Tris-HCl pH 8.0, 40 mM EDTA pH 8.0) and 2 ml of freshly prepared lysozyme (10 mg/ml in Sucrose/Tris/EDTA solution) was added and gently mixed. Cells were incubated for 30 minutes at room temperature and then 4 ml Triton lysis mix (2% Triton X-100, 50 mM Tris-HCl pH 8.0, 40 mM EDTA pH 8.0) was added and mixture was incubated at least 30 min at 37°C with occasional swirling. Subsequently, lysates were centrifuged for 1 hour at 25.000 rpm (48.400 g) in a Beckman

JA25.50 rotor. Supernatant was removed and volume determined to add 0.95 g cesium chloride per ml while making sure that it was completely dissolved. Then 0.1 ml/ml supernatant of EtBr solution (10 mg/ml) was added to the supernatant. Mixture was centrifuged for 20 min in a Beckman JA 25.50 rotor at 7.000 rpm to remove protein and debris. Then it was transferred to an ultracentrifuge tube (Beckman, 4.2 ml, 6.3 ml or 8 ml) and centrifuged for 16 h at 20°C in an ultracentrifuge (Beckman:Optima Max) in a near vertical rotor MLN80 at 70.000 rpm (240.000 x g). Subsequently, the lower band, containing the supercoiled plasmid, was removed and was transferred to a new 4.2 ml ultracentrifuge tube. CsCl/TE solution containing 0.2 mg/ml EtBr was added to fill the tube which was centrifuged again as described above. The lower band was removed and extracted with 1:1 phenol/chloroform twice and precipitated with ethanol overnight at –20°C. Pellet was extracted once more with phenol/chloroform and precipitated with ethanol. The resulting pellet was dissolved in 1 x Tris-EDTA buffer (TE, 50 mM Tris-HCl pH 8.0, 40 mM EDTA pH 8.0). After dialysis against 1 x TE overnight concentration of plasmid was determined with a spectrophotometer (NanoDrop; Thermo Scientific).

3.2.21 Plasmid Digestion

pSP65 was used as a substrate in DNA end-joining reactions after digestion with *Sal*I (Promega/Fermentas) to generate linearized DNA as previously described (Iliakis et al., 2005; Paul et al., 2013). Gel electrophoresis was used to test the completeness of digestion. The completely digested plasmid was again purified with phenol/chloroform extraction, precipitated with isopropanol and the precipitate was washed twice with 70% ethanol. The air-dried plasmid *pSP65-Sal*I was dissolved in 1 x TE buffer aiming a concentration of 50 ng/ml.

3.2.22 Extract preparation

The above described *in vitro* end-joining experiments (see 3.2.19) were performed using whole cell extracts (WCE) (Iliakis et al., 2005; Paul et al., 2013). For the preparation cells were collected, washed once with ice-cold 1 x PBS and subsequently with 5 ml of cold hypotonic buffer (10 mM Hepes-KOH pH 7.5, 5 mM KCl, 1.5 mM MgCl2, 0.2 mM phenylmethylsulfonyl fluoride (PMSF) and 0.5 mM 1,4 Dithiothreitol (DTT)) and centrifuged. The cell pellet was resuspended in three packed volumes of hypotonic buffer and, after 10 min on ice, subjected to three freeze–thaw cycles with liquid nitrogen and a 37°C water bath by keeping carefully ice temperature. Afterwards, 1/5 volume of 3 M KCl was slowly added to the lysate to reach a final concentration of 500 mM KCl. After 30 min incubation at 4°C on a rotation platform, the sample was cleared by centrifugation for 40 min at 14,000 rpm at 4°C. The supernatant was removed as WCE and dialyzed overnight against dialysis buffer (25 mM Hepes, pH 7.5, 10% Glycerol, 400 mM KCl, 1 mM EDTA, 0.2 mM PMSF and 0.5 mM DTT). Dialyzed extracts were cleared by a second centrifugation for 40 min at 14,000 rpm at 4°C and aliquots of the extract were snap frozen and stored at –80°C.

3.2.23 SDS-PAGE and Western blotting

Protein gel electrophoresis under denaturating conditions was carried out using WCE prepared as described above (see 3.2.22). Protein concentration of WCE was determined by colorimetric Bradford assay. WCE were mixed with 2 x Laemmli sample buffer (65 mM Tris-HCl pH 6.8, 10 mM EDTA, 20% glycerol, 3% Sodium dodecyl sulfate (SDS), 0.02% bromophenol blue, 50 µl/ml β-ME), denaturated at 95°C for 5 min and spun down for 1 min at 13,000 x g before electrophoresis. Protein separation was performed by electrophoresis on SDS-polyacrylamide mini gels (“Mini PROTEAN”, Bio-Rad), consisting of a 5% stacking gel and a 10% resolving gel. WCE were loaded with a total protein

amount of ~20 µg on SDS polyacrylamide gels and resolved at a constant voltage of 130 V for 1.5 h at RT (Paul et al., 2013).

For Western blot analysis, proteins were transferred onto 0.2 µm Nitrocellulose or polyvinylidene difluoride (PVDF) membranes using an iBlot dry transfer system (Invitrogen. The self-contained iBlot device uses disposable blotting stacks with integrated nitrocellulose or PVDF membranes that efficiently and reliably blots proteins from polyacrylamide gels on membranes in less than 10 min without the need for additional buffers or an external power supply. Equal loading and transfer efficiency were monitored by immunodetection of GAPDH. After transfer, membranes were incubated in blocking buffer (5% non-fat dry milk in 0.1% Tween-20, 150 mM NaCl, 25 mM Tris-HCl, pH 7.6) for 1-2 h at room temperature. Subsequently, membranes were incubated overnight at 4˚C with primary antibody appropriately diluted in blocking buffer. After three washes for 10 min with TBS-T (0.1% Tween-20, 150 mM NaCl, 25 mM Tris-HCl, pH 7.6), membranes were incubated for 1 h with secondary antibody appropriately diluted in blocking buffer. Membranes were scanned using the Odyssey infrared imaging system (Li-COR) or were developed for chemiluminescence detection by using ECL+ chemiluminescence detection kit (GE Healthcare) as recommended by the manufacturer. Signals were visualized in a VersaDoc imaging system (Bio-Rad) and analyzed with the Quantity one software (Bio-Rad). The following primary antibodies were used: anti-LIG3 (1F3) mouse mAb (GeneTex); anti-LIG1 (10H5) mouse mAb (Santa Cruz), anti-α-Tubulin (AA13) mouse monoclonal (Sigma Aldrich), anti-histone H1 (AE-4) mouse mAb (Acris), and anti-GAPDH mouse mAb (Millipore). The secondary antibody was an anti-mouse IgG conjugated with HRP (Cell Signaling), IRDye680 or IRDye800 (Li-COR) (Paul et al., 2013).

4 Results

Early work from our laboratory, as well from the laboratories of other investigators, provides strong biochemical evidence for the putative involvement of LIG3 in B-NHEJ. Recent studies from our lab showed an impressive functional redundancy between LIG3 and LIG1 in DNA replication (Arakawa et al., 2012). For a conclusive elucidation of the function of LIG1 and LIG3 in DSB repair, we generated a set of conditional knockout, knockout and knock-in mutants in chicken DT40 cells. This set of mutants (summarized in Table 5) includes, in addition to single knockouts for all three DNA ligases, also double ligase knockout mutants, as well as ligase knock-in mutants in appropriately selected, DNA ligase genetic background to study the interplay between DNA ligases in DSB repair.

4.1 LIG1 and LIG4 are not essential for survival of higher eukaryotic cells

As a first step in the characterization of the generated mutants we investigated the consequences of DNA LIG1 and LIG4 depletion in cell growth (Arakawa et al., 2012). For these experiments, the cells were maintained in the logarithmic phase of growth by daily subculturing with fresh growth medium to keep cell density between 1 to 2 x 10^6 cells/ml. The cell cycle distribution of the wild type and mutant cell lines was also measured every day by FACS analysis. The obtained DNA histograms and growth curves for wild type (wt), single *LIG1*$^{-/-}$ or *LIG4*$^{-/}$ mutants and for double *LIG1*$^{-/-}$*LIG4*$^{-/-}$ mutant cells are summarized in Figure 18.

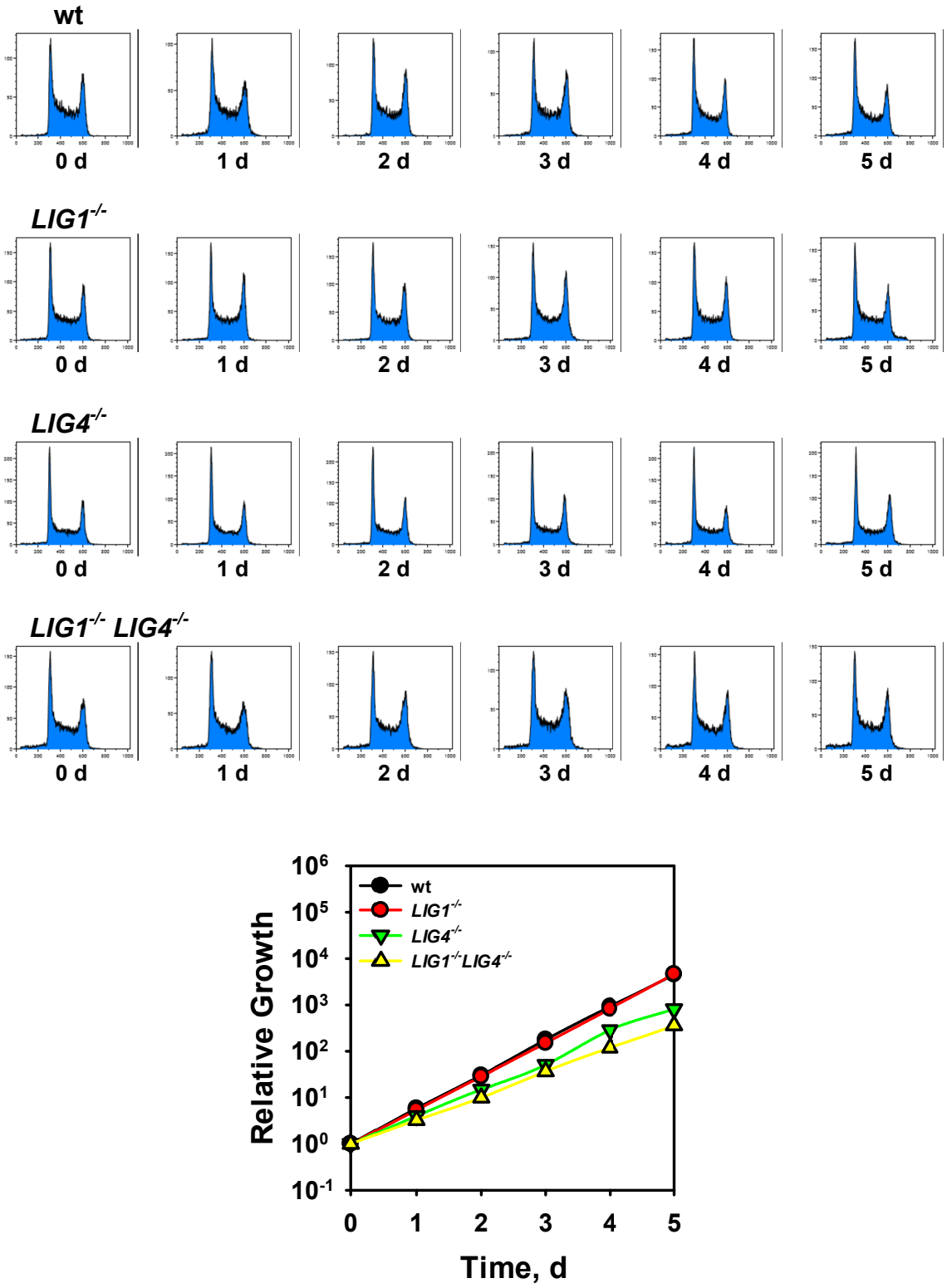

Figure 18: LIG1 and LIG4 are not essential for survival (Arakawa et al., 2012). DNA histograms and growth kinetics of wild type (wt), single knockout *LIG1*$^{-/-}$ and *LIG4*$^{-/-}$, and double knockout *LIG1*$^{-/-}$*LIG4*$^{-/-}$ cells. The cell numbers are calculated relatively to a beginning with one cell.

Whereas the ablation of LIG1 functions does not display a significant effect on cell growth, the growth of *LIG4*$^{-/-}$ cells is distinctly slower as compared to wt and *LIG1*$^{-/-}$ cells, respectively. The growth of the double *Lig1*$^{-/-}$*Lig4*$^{-/-}$ mutant is only slightly further reduced in comparison to *LIG4*$^{-/-}$ cells. From these results it may be concluded that in DT40 LIG3 alone can promote proliferation without having an adverse effect on DNA metabolism and most importantly, it can efficiently substitute, as sole DNA ligase, the DNA replication functions of LIG1.

4.2 LIG3 is essential for survival of higher eukaryotic cells

As a next step we examined the function of the conditional *LIG3*$^{-/2loxP}$ knockout (Arakawa et al., 2012). In these cells one allele is completely eliminated, while the second one contains two loxP sites, which are specifically recognized and cut by the modified Cre recombinase. Cre is constitutively expressed in the cellular cytoplasm and is, upon treatment with 4-hydroxytamoxifen (4HT) translocated to the nucleus. This results in the removal of the 2loxP sites flanked region and in the full *LIG3* knockout upon 4HT treatment. The influence of the LIG3 knockout on cell growth was studied in experiments where exponentially growing *LIG3*$^{-/2loxP}$ and *LIG3*$^{-/2loxP}$*LIG4*$^{-/-}$ cells were incubated with 50 nM 4HT. As a control for the overall effect of 4HT on cell proliferation, wt cells were also treated with 4HT in addition to conditional *LIG3* knockout mutants. Figure 19 summarizes the obtained flow cytometry histograms and growth curves for the indicated treated and untreated cell lines.

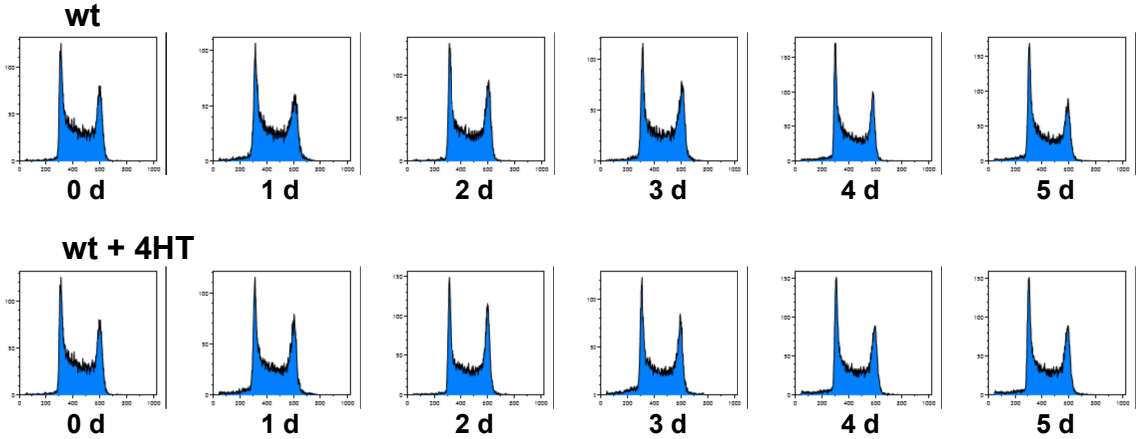

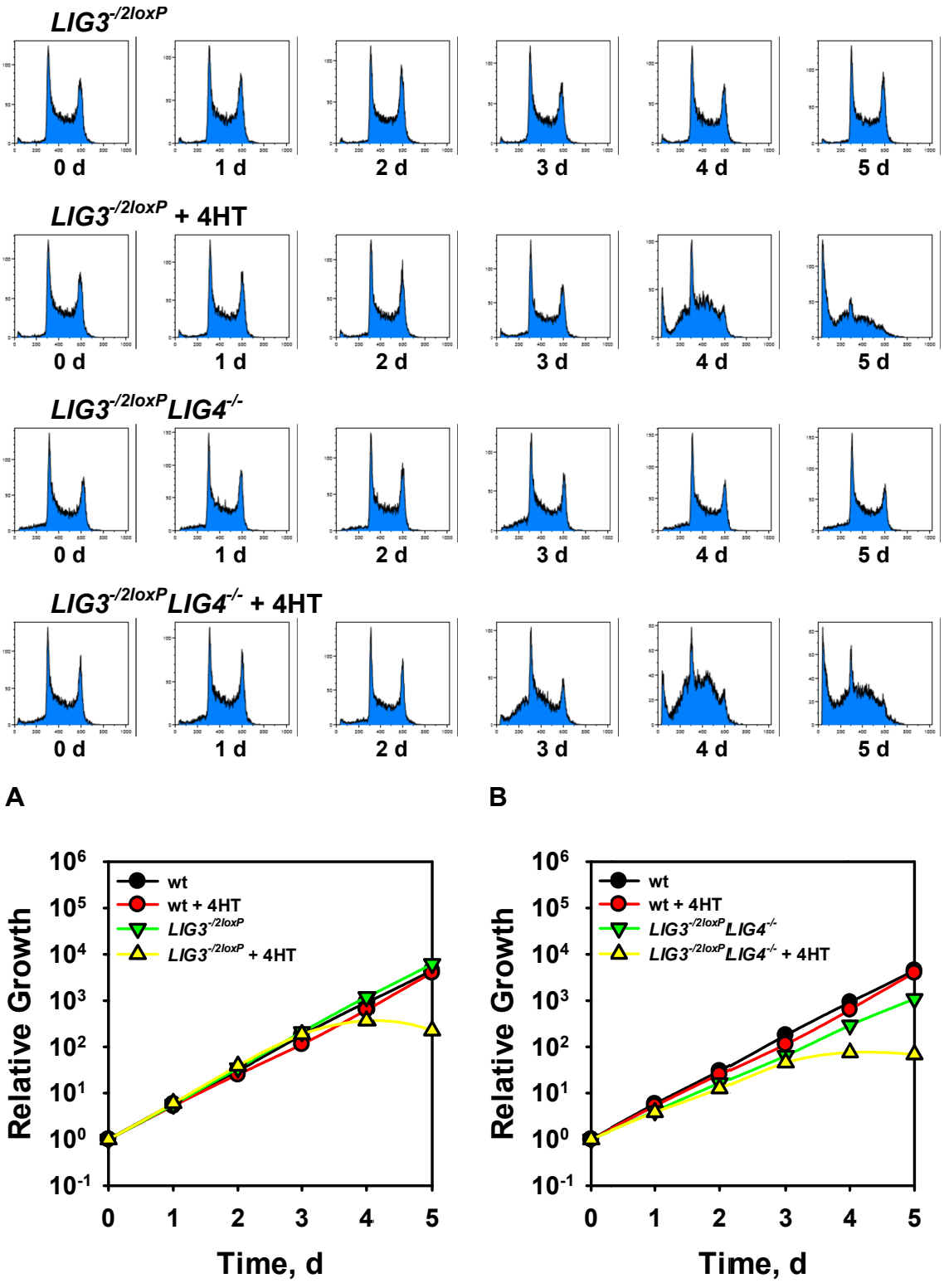

Figure 19: LIG3 is essential for survival (Arakawa et al., 2012). DNA histograms and growth kinetics of treated and untreated *LIG3*$^{-/2loxP}$ (A) and *LIG3*$^{-/2loxP}$*LIG4*$^{-/-}$ (B) cells in comparison to wt.

According to these results, wild type cells grow with similar growth kinetics and show no change in cell cycle distribution in the presence or absence of 4HT, indicating no drug side effects. Nevertheless, in the conditional *LIG3* background, deletion of *LIG3* by 4HT treatment has severe consequences for the cells. Cell growth ceases completely after 4 days and *LIG3*$^{-/2loxP}$ and *LIG3*$^{-/2loxP}$*LIG4*$^{-/-}$ cells start dying (Figure 19A and 19B) (Arakawa et al., 2012). In addition, the flow cytometry results of 4HT treated *LIG3*$^{-/2loxP}$ and *LIG3*$^{-/2loxP}$*LIG4*$^{-/-}$ cells indicate an extensive activation of apoptosis displayed by the increased population of sub-G1 cells and an unusual accumulation of cells in S-phase (Figure 19 upper panel).

For a validation of the results of the conditional knockout system and a more specific determination of LIG3 activity in *LIG3*$^{-/2loxP}$ and *LIG3*$^{-/2loxP}$*LIG4*$^{-/-}$ cells exposed to 4HT, we followed the induction of the conditional *LIG3* knockout measuring *LIG3* mRNA levels using RT-PCR and survival using the colony formation assay (Arakawa et al., 2012; Paul et al., 2013). The results obtained are summarized in Figure 20.

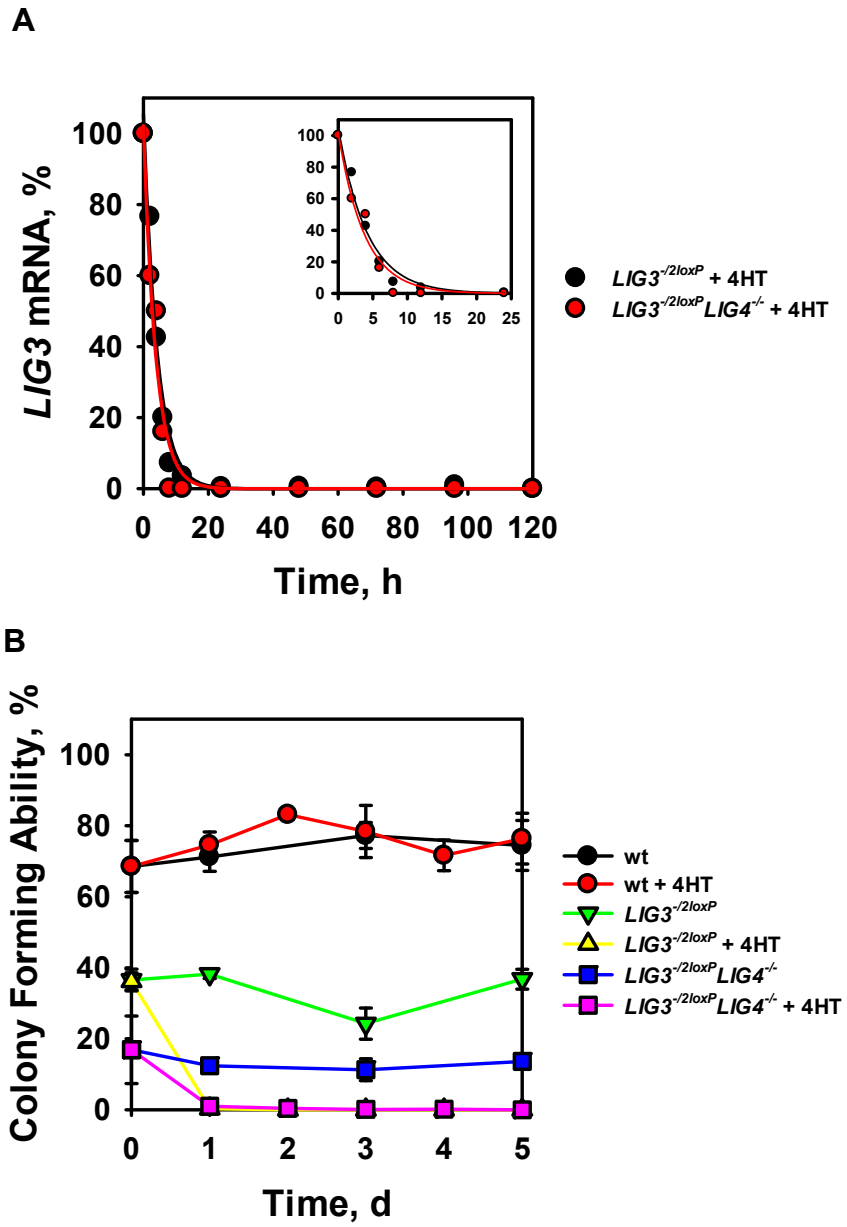

Figure 20: LIG3 is essential for survival (Arakawa et al., 2012). (A) *LIG3* mRNA levels related to levels of untreated cells measured by RT-PCR. (B) Colony forming ability of the indicated mutants treated with 4HT in comparison to their untreated counterparts and wt cells as a control.

Treatment of the cells with 4HT initiates translocation of Cre into the nucleus and excision of the conditional *LIG3* allele. This event results in a rapid reduction of *LIG3* mRNA quantity to undetectable levels 12 h after 4HT induction (Figure 20A) (Arakawa et al., 2012; Paul et al., 2013). Notably, cell viability as measured by colony formation remains unchanged for the duration of the experiment in wt cells treated with 4HT. Similar results are also obtained

with *LIG3*$^{-/2loxP}$ and *LIG3*$^{-/2loxP}$*LIG4*$^{-/-}$ cells grown in the absence of 4HT, although in this case growth is somewhat compromised and survival obviously lower. This suggests effects of *LIG3* haploinsufficiency in conditional *LIG3* mutants. However, colony forming ability in 4HT treated conditional knockout cells drops to zero at the first time point within 24h, while the survival of the untreated control cells, as well as the 4HT treated wt cells, remains unchanged, which may reflect a disconnect between mRNA levels and the stability of the LIG3 protein (Figure 20B) (Arakawa et al., 2012).

In addition, we quantitatively evaluated LIG3 activity in an *in vitro* end-joining assay as a function of time after addition of 4HT to *LIG3*$^{-/2loxP}$ and *LIG3*$^{-/2loxP}$*LIG4*$^{-/-}$ cells (Paul et al., 2013). Due to the assumption that a functional decrease in ligation activity will become apparent after the protein is degraded, the time frame for this experiments was protracted to 120 h after induction with 4HT. Therefore, we prepared whole cells extracts from 4HT treated cells and utilized them in a plasmid-based in vitro assay, detecting mainly LIG3 activity. The ligation substrate in this assay was *pSP65* plasmid DNA, harboring a single *Sal*I restriction endonuclease site. Incubation with *Sal*I results in linearization of the plasmid and the generation of two cohesive 5' overhang DNA ends. The ligation activity of the WCE used in the DNA end-joining reactions generates circles, dimers and multimers (Figure 21). It was initially difficult to monitor LIG3 protein levels by Western blotting, due to the absence of a commercially available antibody raised against the chicken LIG3 protein. This obstacle was eliminated later by optimization of the Western blot procedure with available antibodies raised against hLIG3 peptide (results not shown).

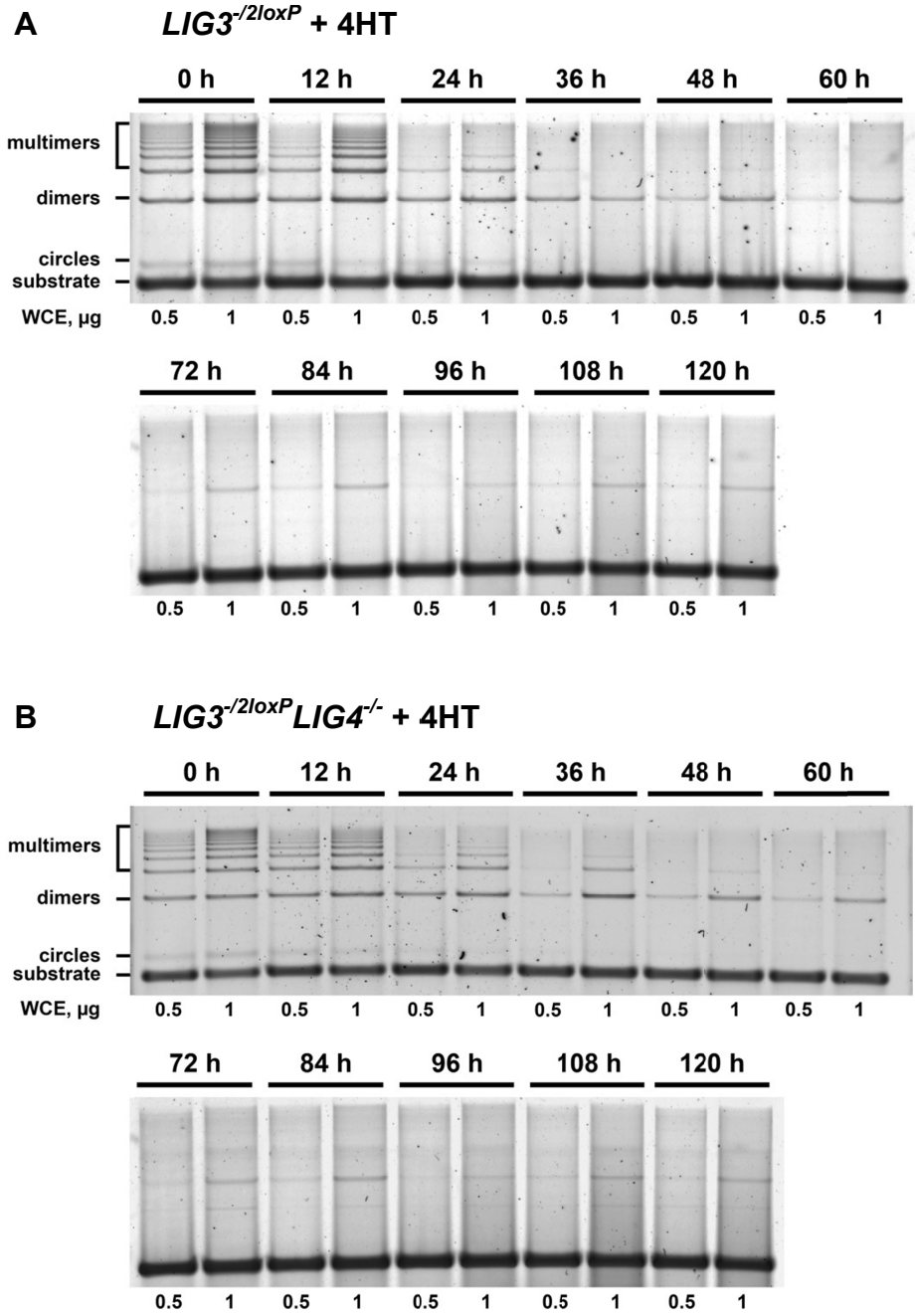

Figure 21: LIG3 function after induction of *LIG3* conditional knockout (Paul et al., 2013). End-joining capacity of 0.5 and 1 µg whole cell extract from 4HT treated *LIG3*$^{-/2loxP}$ (A) and *LIG3*$^{-/2loxP}$*LIG4*$^{-/-}$ (B) cells is shown. Whole cell extracts support the end-joining of *pSP65-SalI* plasmid to generate circles, dimers and multimers.

A gradual reduction in end-joining activity is observed in extracts from *LIG3*$^{-/2loxP}$ cells treated with 4HT (Figure 21A) reflecting the reduction of LIG3 protein activity. The proportion of rejoined *pSP65-SalI* plasmid is markedly reduced already one day later and drops to approximately 10% after two days of 4HT

treatment. A similar initial activity and then reduction in end-joining is also observed in extracts of 4HT treated *LIG3*$^{-/2loxP}$*LIG4*$^{-/-}$ cells (Figure 21B), in line with earlier reports that LIG3 mainly catalyzes end-joining under the conditions employed (Wang et al., 2005). Thus, LIG3 activity measurements using this *in vitro* end-joining assay provide relevant information on the function of the conditional knockout (Paul et al., 2013).

Taken together, the observations show a fast, efficient and complete, Cre nuclease mediated, 4HT induced excision of the second *LIG3* allele and an induction of the complete *LIG3* knockout. Subsequently LIG3 activity is reduced with an associated appearance of cell death. In agreement with earlier reported mouse data (Puebla-Osorio et al., 2006), we conclude that *LIG3* is essential for survival of higher eukaryotic cells (Paul et al., 2013).

Based on the above results we decided to utilize conditional LIG3 knockout mutants in the following repair experiments always after 3 to 3.5 days of 4HT treatment, as at this point LIG3 activity is largely reduced but the cells are still viable to perform experiments (Paul et al., 2013).

4.3 LIG3 knockout lethality is due to a mitochondrial defect

The unique property of the *LIG3* gene of higher eukaryotes to express a mitochondria-specific form raises the possibility that this protein is essential for the maintenance and function of this particular cellular organelle. The lethality observed in the experiments described above could therefore be attributed to specific functions of LIG3 in the mitochondria, which cannot be complemented by any of the other ligases expressed in DT40 cells. To address this question, we tested mitochondria integrity and function in 4HT treated *LIG3*$^{-/2loxP}$ and compared the results obtained with those of wt cells after applying three different assays.

Firstly, we measured the relative oxygen consumption in a sample using an enclosed oxygen electrode. The results are displayed in Figure 22.

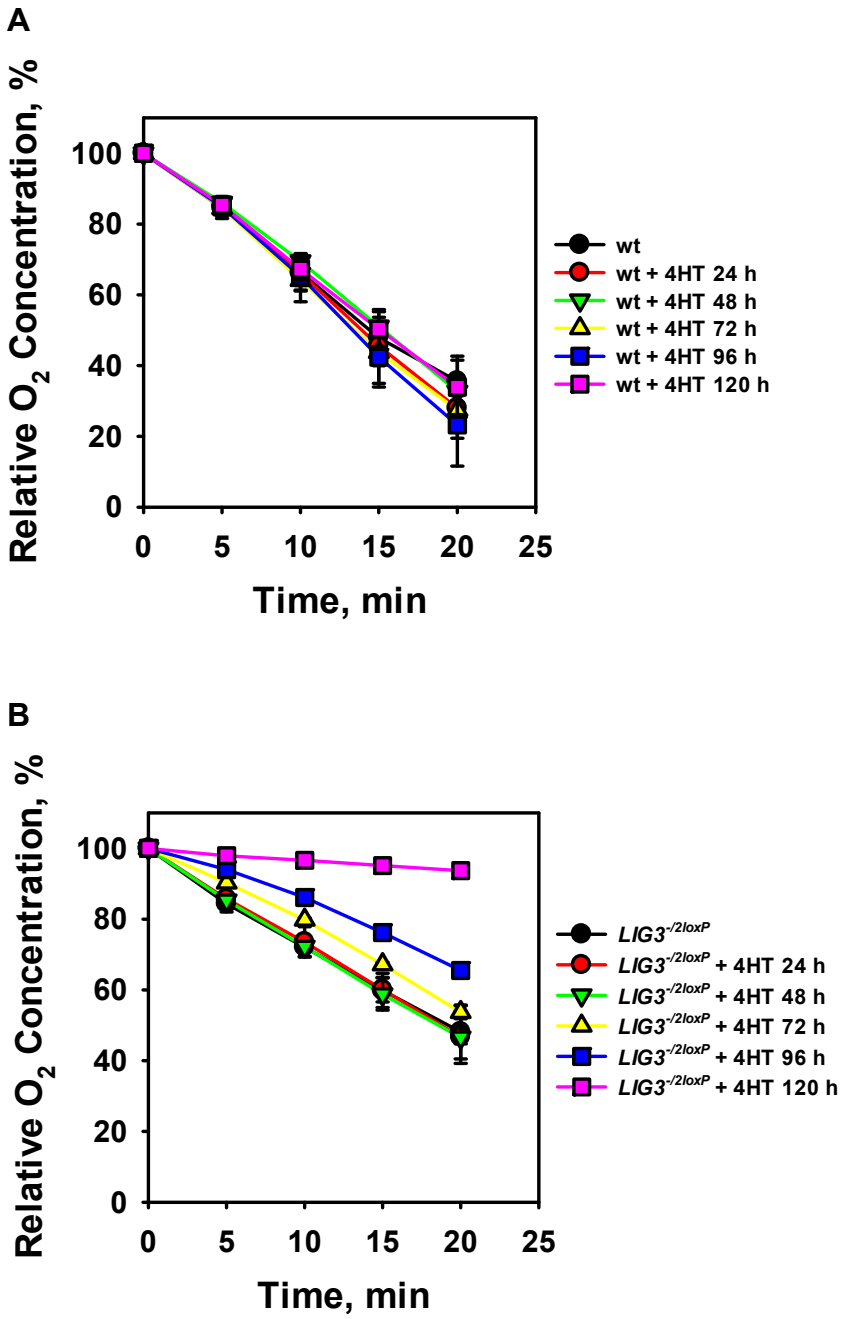

Figure 22: LIG3 knockout lethality is due to a mitochondrial defect. Relative oxygen concentration of 4HT treated wt (A) and *LIG3*$^{-/2loxP}$ (B) cells. Oxygen consumption was measured in a sample using an oxygen electrode attached to a Licox CMP Oxygen Monitor in an enclosed glass tube.

A drop in partial pressure is a direct measure of oxygen consumption by the cells. Wild type cells cause a rapid reduction in dissolved oxygen that remains unaffected by the presence of 4HT. *LIG3*$^{-/2loxP}$ cells show oxygen consumption similar to that of wt cells in the absence of 4HT. But a gradual reduction in oxygen consumption is noted at day three after 4HT treatment – the time point when cells start to die.

Secondly, for a direct measurement of the cellular ATP load in wt and *LIG3*$^{-/2loxP}$ cells at different times after treatment with 4HT we employed a luciferin/luciferase based assay and the acquired results are summarized in Figure 23.

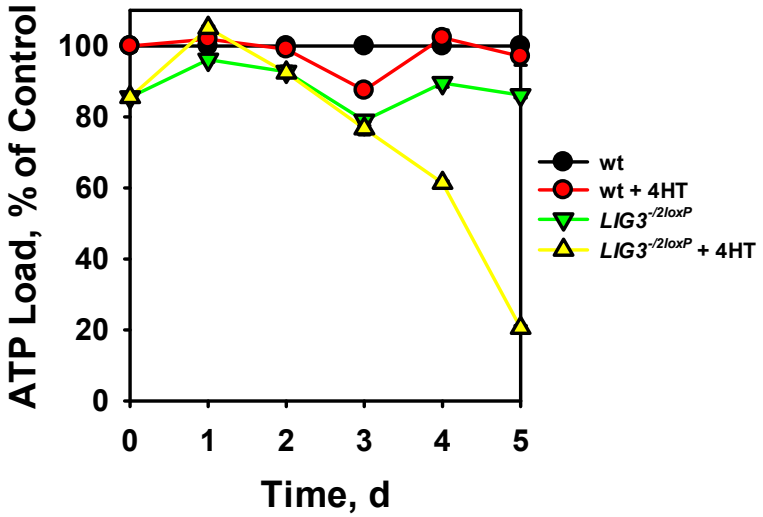

Figure 23: LIG3 knockout lethality is due to a mitochondrial defect. Cellular ATP load in wt and *LIG3*$^{-/2loxP}$ cells after treatment with 4HT evaluated with CellTiter-Glo Luminescent Cell Viability Assay, a luciferin/luciferase based assay which generates a luminescent signal proportional to the amount of ATP present. Each determination was carried out using 2 x 10^4 cells and results shown are referred to ATP levels of untreated wt cells.

Notably, the method used for ATP determination is very sensitive; for example the produced luminescent signal from 50 cells is greater than three times the background signal from serum supplemented medium without cells. The slight changes in ATP levels of 4HT treated wt cells could be ascribed to dilution errors. Compared to wt cells the ATP load of *LIG3*$^{-/2loxP}$ cells is only slightly

lower when measured in the absence of 4HT. ATP levels remain high for up to three days after 4HT treatment and drop rapidly as cells begin to die at day four.

As a third parameter of mitochondrial integrity we employed MitoTracker Green probe to assay for possible transitions in mitochondria amount and membrane potential. Results obtained with the corresponding MitoTracker Green and DNA histograms are shown in Figure 24.

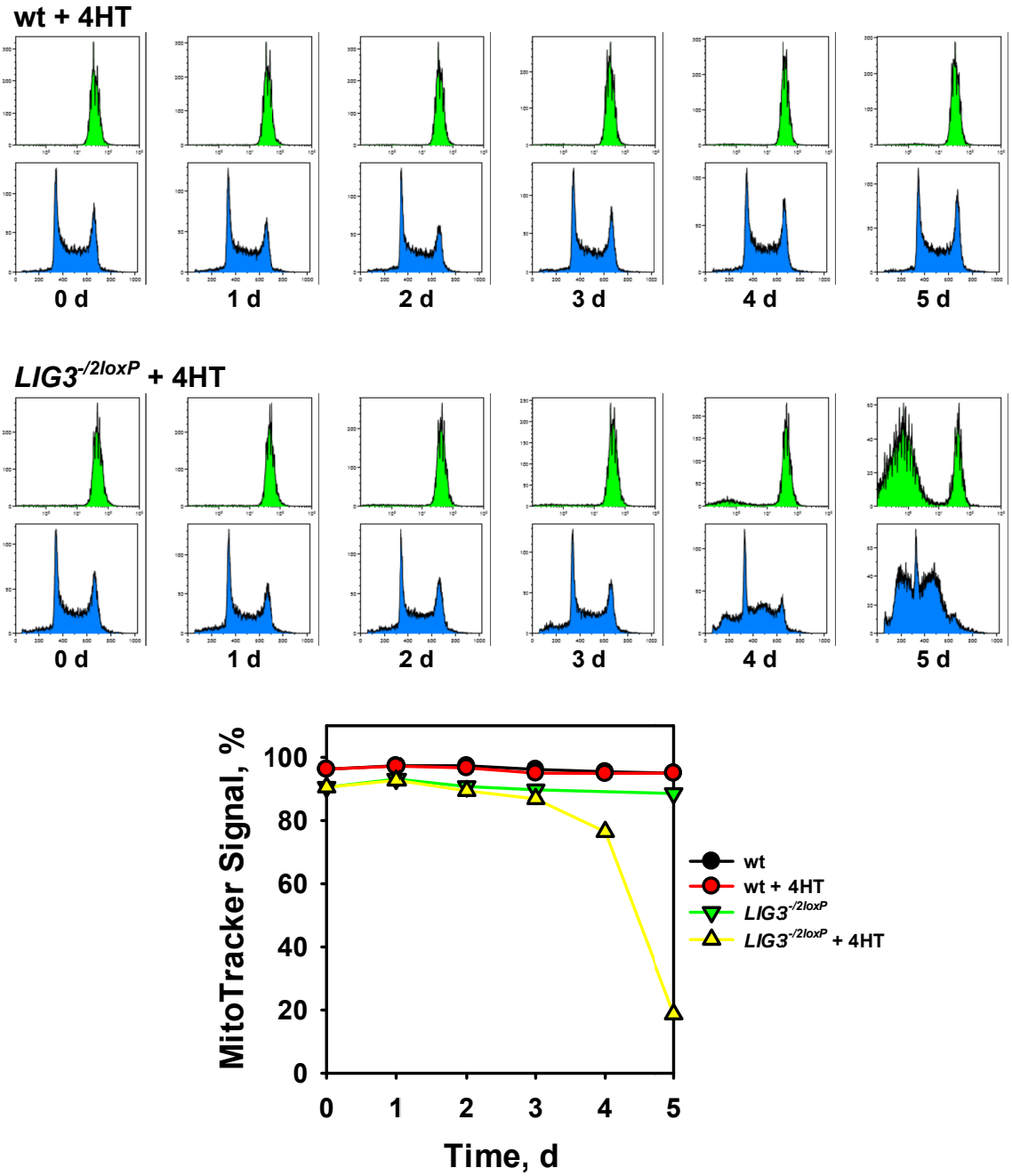

Figure 24: LIG3 knockout lethality is due to a mitochondrial defect. MitoTracker Green probe (green) and DNA histograms (blue) as a function of time after 4HT treatment in wt and *LIG3*$^{-/2loxP}$ cells.

Here again, *LIG3*$^{-/2loxP}$ cells show compared to the wt only slight differences in MitoTracker signal. But in the presence of 4HT the MitoTracker signal drops gradually as cells begin to die after 4 days of 4HT treatment. The results suggest reduction in mitochondria membrane potential in line with oxygen consumption and the ATP load results described above.

As a final parameter we defined the nuclear fragmentation, as a criterion to evaluate cell death by apoptosis after 4HT treatment. This parameter is expressed as apoptotic index (AI) and represents the number of cells with fragmented nuclei as percentage of the total number of cells in the population. The results obtained are summarized in Figure 25.

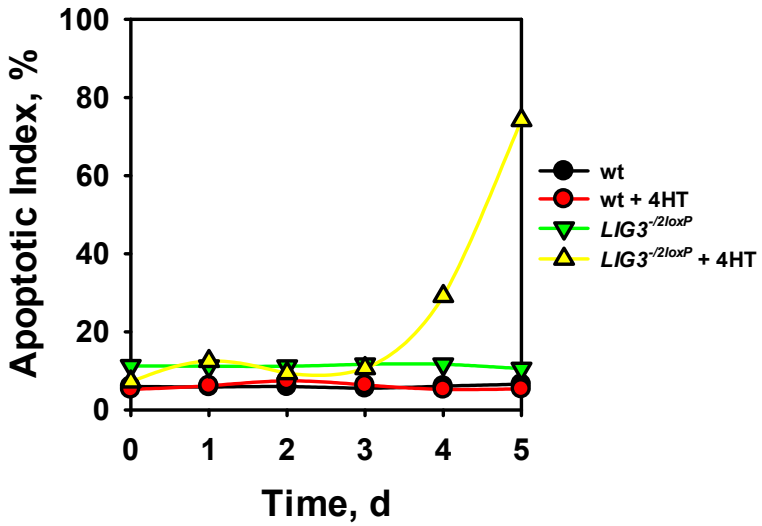

Figure 25: LIG3 knockout leads to apoptosis. Apoptotic index determined by counting the fraction of cells showing nuclear fragmentation among 1000 cells in the population.

Compared to wt cells the AI of *LIG3*$^{-/2loxP}$ cells is only slightly higher in the absence of 4HT. After 4HT treatment the AI of *LIG3*$^{-/2loxP}$ cells increases rapidly from 30% at day four to 80% at day five. Notably, the increase of the AI after four days of 4HT treatment indicates a coincidence between viability loss, on the one hand, and a reduction mitochondria function, on the other hand.

The above outlined results show a timely parallel induction of apoptosis and a deterioration of mitochondria function in LIG3 depleted cells, that makes it difficult to establish cause and effect relationships. Given the fact that even

primary chicken embryo fibroblasts can survive after depletion of their mitochondria (Desjardins et al., 1985), it is possible that what we observe here are LIG3 mediated mitochondria effects that specifically affect apoptosis signaling in the highly pro-apoptotic DT40 cells. According to this interpretation, LIG3 depletion induces lethality in DT40 by interfering with the mitochondrial regulation of apoptosis.

4.4 Knock out of LIG3 has no detectable effect on DSB repair in LIG4 and LIG1 proficient cells

While LIG4 is solidly implicated in D-NHEJ pathway of DSB repair, the ligase responsible for B-NHEJ is less well characterized. Early work from our laboratory, as well from the laboratories of other investigators, provides strong biochemical evidence for the involvement of LIG3 in B-NHEJ (Wang et al., 2005).

As a result of single allele expression, *LIG3* mRNA is in *LIG3*$^{-/2loxP}$ cells 50% reduced (Figure 26A). To examine the effect on DSB processing of a further reduction in LIG3 protein level, we analyzed IR induced DSB repair kinetics using PFGE (Paul et al., 2013). Figure 26B shows the results obtained with *LIG3*$^{-/2loxP}$ cells as compared to wt cells after treatment with 4HT for 3 or 3.5 days, respectively.

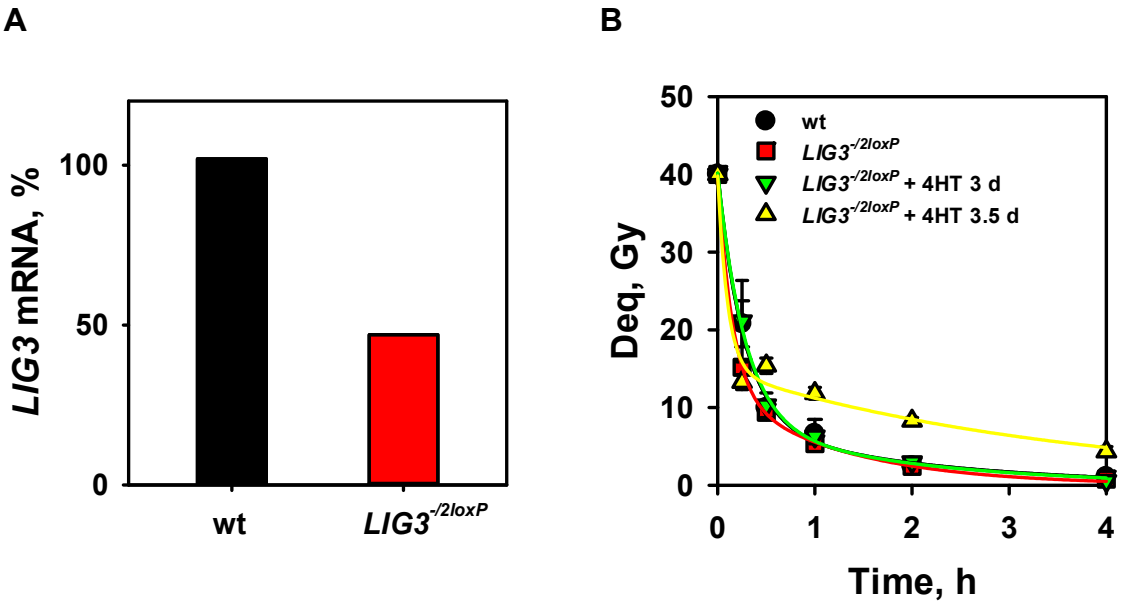

Figure 26: Knockout of LIG3 has not detectable effect on DSB repair (Paul et al., 2013). (A) *LIG3* mRNA levels in wt and *LIG3*$^{-/2loxP}$ cells measured by RT-PCR. (B) Repair kinetics of IR-induced DSBs in asynchronous wt and *LIG3*$^{-/2loxP}$ cells after treatment with 4HT for the indicated periods of time. Results of three determinations from at least two independent experiments were used to calculate the indicated means and standard errors.

Wt DT40 cells efficiently repair DSBs induced by high doses of IR with half times of less than 30 min. Ninety percent of DSBs induced by 40 Gy X-rays are processed in these cells within 1 h, and their number is below the detection limit of PFGE 4 h later. Moreover, *LIG3*$^{-/2loxP}$ cells process DSBs with kinetics indistinguishable from that of wt cells. Since the heterozygous nature of the *LIG3*$^{-/2loxP}$ mutant causes a 50% reduction in LIG3 mRNA and consequently presumably also in LIG3 protein level, we conclude that reductions of this magnitude leave unchanged the ability of the cells to deal with DSBs (Paul et al., 2013).

To examine whether lower levels of LIG3 compromise DSB repair we treated *LIG3*$^{-/2loxP}$ cells with 4HT and analyzed DSB repair efficiency at different times thereafter (Figure 26B). Since cells die after five days as a result of apoptosis (see above 4.3), we carried out experiments within this time frame to avoid complication in the interpretation of the results. The results summarized in Figure 26B indicate that more than 90% reduction in protein activity (Figure 21A) has not detectable effect on DSB repair in DT40 cells. We

conclude that under these conditions other DNA ligases, and predominantly LIG4, carry out repair of DSBs. These results confirm that LIG3 is unlikely to have a primary role in DSB repair and that its task most probably is limited to back up the functions of LIG4 (Paul et al., 2013).

4.5 A contribution of LIG3 in DSB repair is clearly detectable in a *LIG4*$^{-/-}$ genetic background

To study the putative role of LIG3 in B-NHEJ we knocked out *LIG4*, using standard approaches in a wt and *LIG3*$^{-/2loxP}$ genetic background and studied repair of DSBs by PFGE in the presence or absence of 4HT (Paul et al., 2013). The results for *LIG3*$^{-/2loxP}$*LIG4*$^{-/-}$ double mutant cells are shown in Figure 27.

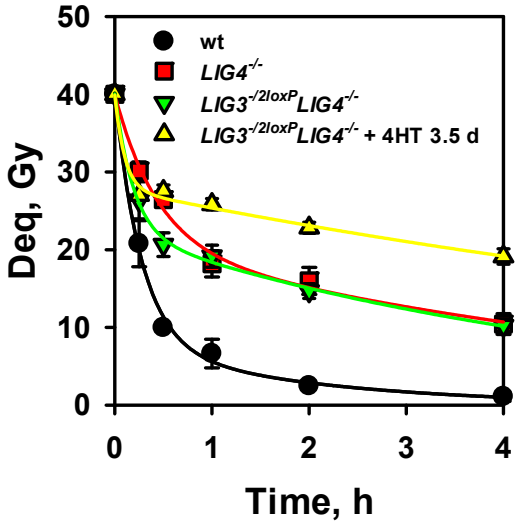

Figure 27: A contribution of LIG3 in DSB repair is clearly detectable in a *LIG4*$^{-/-}$ genetic background (Paul et al., 2013). Repair kinetics of IR-induced DSBs in asynchronous wt, *LIG4*$^{-/-}$ and *LIG3*$^{-/2loxP}$*LIG4*$^{-/-}$ cells after treatment with 4HT for the indicated periods of time. Results of three determinations from at least two independent experiments were used to calculate the indicated means and standard errors.

As expected, *LIG4*$^{-/-}$ cells show, compared to the wt and *LIG3*$^{-/2loxP}$ cells a pronounced defect in DSB repair by the resulting inhibition of D-NHEJ. Despite this repair defect, a robust alternative repair pathway removes ~50% of the generated DSBs within 1h and nearly 80% in 4h. This alternative form of NHEJ must utilize LIG1 or LIG3, the only remaining ligases in this mutant. The repair efficiency in the *LIG3*$^{-/2loxP}$*LIG4*$^{-/-}$ double mutant is similar to that of *LIG4*$^{-/-}$ mutant suggesting that even in this background reduction by 50% of the cellular LIG3 level has no effect on DSB repair capacity. Further reduction of LIG3 by treatment with 4HT for 3.5 days compromises DSB repair. Since the level of LIG3 at the latest time point measured may not be zero, residual DSB repair activity may be attributed to residual LIG3 or to LIG1. This result further demonstrates the contribution of LIG3 to B-NHEJ and confirms earlier observations that even low levels of LIG3 are sufficient to support efficient B-NHEJ (Paul et al., 2013; Windhofer et al., 2007a).

4.6 A double mutant conclusively shows the function of LIG3 in B-NHEJ

For a conclusive elucidation of the function of LIG1 and LIG3 to DSB repair, we generated a set of knockout and knock-in mutants in chicken DT40 cells. This set of mutants (summarized in Table 5) contains, in addition to single knockouts for all three DNA ligases, also double knockout mutants. To study the role of LIG1 in DSB repair we knocked out this ligase in wt and *LIG4*$^{-/-}$ genetic background to generate cells deficient in *LIG1*$^{-/-}$ and *LIG1*$^{-/-}$*LIG4*$^{-/-}$ (Paul et al., 2013).

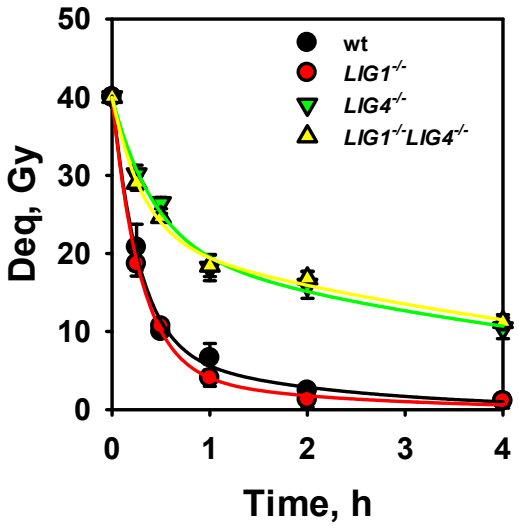

Figure 28: LIG3 repairs DSBs in a *LIG1* and *LIG4* deficient background (Paul et al., 2013). Kinetics of DSB processing in asynchronous wt, *LIG1*$^{-/-}$, *LIG4*$^{-/-}$, and *LIG1*$^{-/-}$*LIG4*$^{-/-}$ cells after exposure to 40 Gy X-rays. Results of three determinations from two independent experiments were used to calculate the indicated means and standard errors.

The results presented in Figure 28 demonstrate that *LIG1*$^{-/-}$ cells repair the generated DSBs with kinetics indistinguishable from those of wt cells. Thus, a contribution of LIG1 to DSB repair is undetectable in the presence of the two other DNA ligases (Paul et al., 2013).

Similarly, *LIG1*$^{-/-}$*LIG4*$^{-/-}$ double knockout cells repair DSBs with kinetics identical to those of *LIG4*$^{-/-}$ cells, showing that a deletion of LIG1 in a *LIG4*$^{-/-}$ background generates no additional DSB repair defect beyond these observed in *LIG4* deficient cells. Thus, the robust processing of DSBs in the *LIG1*$^{-/-}$*LIG4*$^{-/-}$ double mutant must be supported by the only remaining DNA ligase, LIG3 (Paul et al., 2013).

4.7 γ-H2AX foci formation and decay confirms the results of PFGE

PFGE is a reliable method for determination of the induction of DSBs and their physical rejoining, but experiments are carried out at relatively high radiation doses to accommodate the sensitivity of PFGE as method, which might consequences for the results obtained. There are hints that DSB repair pathway selection could be affected by the load of DNA damage registered in the cell and therefore is also relevant to design experiments using lower doses of radiation. We therefore wished to confirm the main conclusions from the PFGE experiments with experiments at low doses. Therefore, we measured γ-H2AX foci formation and decay after irradiation with 0.5 and 1 Gy X-rays (Paul et al., 2013). The kinetics of γ-H2AX foci formation that reflects DSB related signaling and those of the removal of physical breaks measured by PFGE are widely different and have been discussed. Nevertheless, γ-H2AX foci scoring represents an acceptable surrogate for physical DSB determination (Kinner et al., 2008). γ-H2AX are frequently used as markers for DSBs and it has been reported that the number of γ-H2AX foci correlates with the number of DSBs present, and that it increases linearly with radiation dose (Rothkamm and Löbrich, 2003).

The γ-H2AX foci results obtained for wt, *LIG1*$^{-/-}$, *LIG4*$^{-/-}$, and *LIG1*$^{-/-}$*LIG4*$^{-/-}$ cells are displayed in Figure 29.

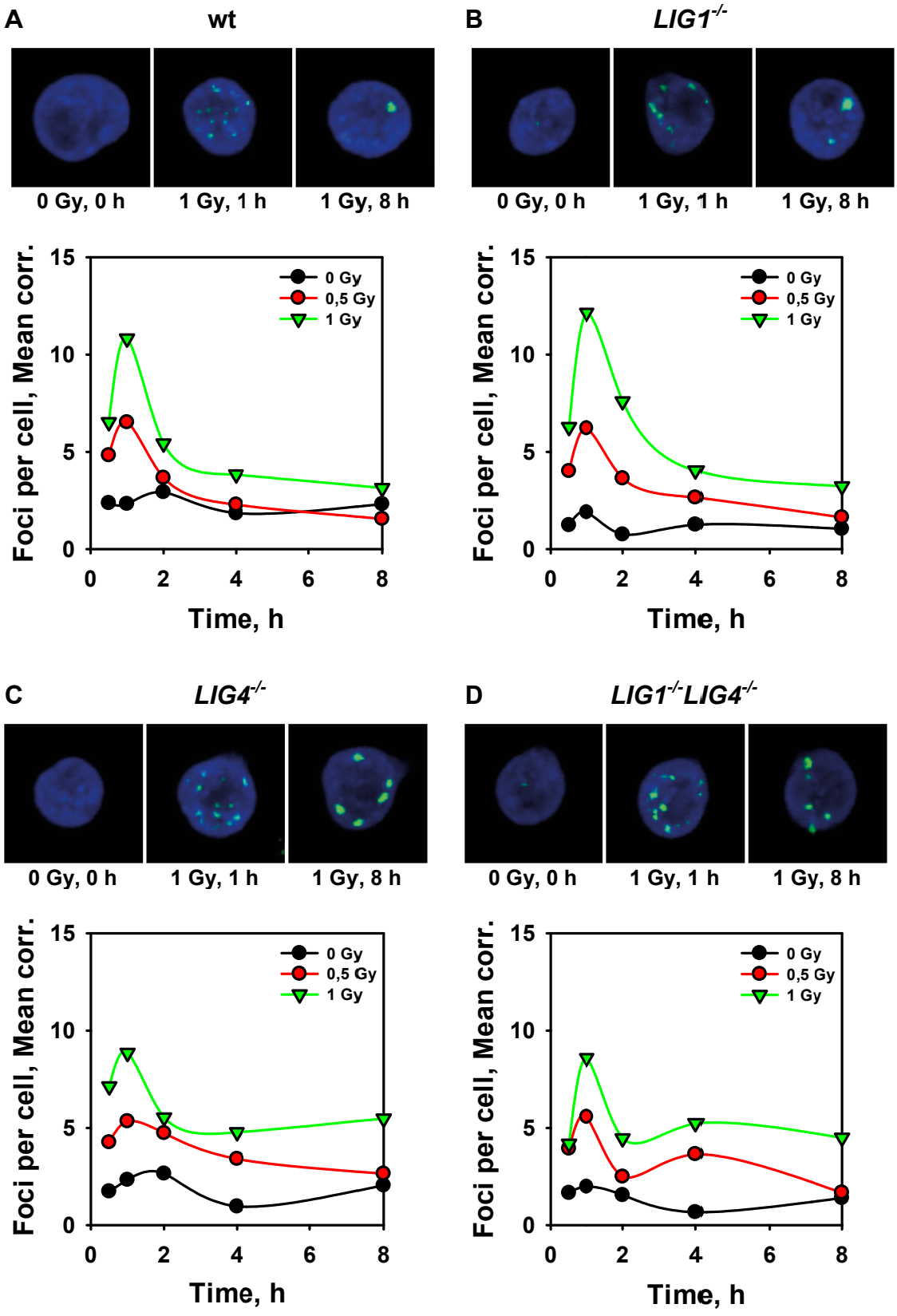

Figure 29: LIG3 supports processing of DSBs also after low doses of X-rays (Paul et al., 2013). Representative images and kinetics of γ-H2AX foci formation and decay in wt (A), single knockout *LIG1*$^{-/-}$ (B), *LIG4*$^{-/-}$ (C), and double knockout *LIG1*$^{-/-}$*LIG4*$^{-/-}$ (D) cells using immunofluorescence microscopy.

As expected, the rate of DSB induction in DT40 cells does not significantly differ between wt and mutant cell lines and is about 9-12 foci per cell, which is two times lower than the γ-H2AX foci yields measured in mouse or human cells. This number correlates with the smaller genome size of DT40 cells; likewise they exhibit a two times lower DNA content. Moreover, DT40 wt cells efficiently repair DSBs at the applied radiation doses, as indicated by the disappearance of γ-H2AX foci after an initial peak reached ~1 h after IR exposure (Figure 29A). The kinetics of γ-H2AX foci formation and decay in *LIG1*$^{-/-}$ cells (Figure 29B) are identical to those of wt cells, confirming the corresponding results with PFGE. The efficiency of γ-H2AX foci decay is reduced in *LIG4*$^{-/-}$ cells (Figure 29C) in line with the expected defect in D-NHEJ. The function of LIG3 in this set-up is confirmed by the results obtained with the double mutant *LIG1*$^{-/-}$*LIG4*$^{-/-}$ (Figure 29D) (Paul et al., 2013). In general, the same pattern of γ-H2AX foci formation and decay, with the initial peak arising 1 h after IR and with a subsequent decay is found in all four investigated mutants.

For a better comparison, we also plotted the remaining γ-H2AX foci scored 8 h after 1 Gy in the different cell lines as a bar graph (Figure 30).

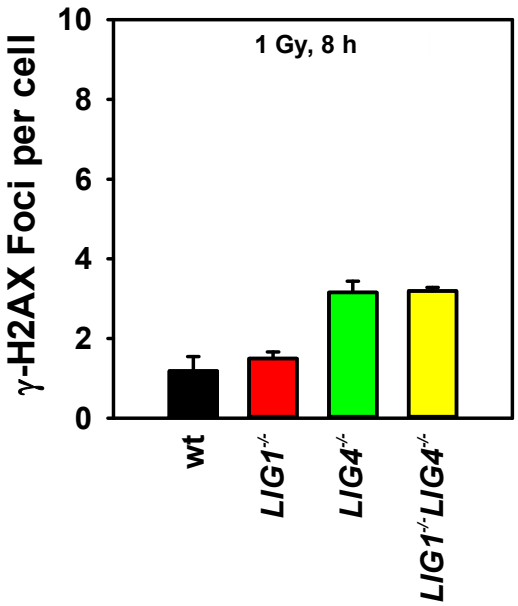

Figure 30: LIG3 supports processing of DSBs also after low doses of radiation (Paul et al., 2013). γ-H2AX foci scored in wt, *LIG1*$^{-/-}$, *LIG4*$^{-/-}$, and *LIG1*$^{-/-}$*LIG4*$^{-/-}$ cells 8 h after exposure to 1 Gy X-rays. Foci measured in non-irradiated control cells have been

subtracted. Results of two independent experiments, in which 8000 nuclei on average were scored, were used to calculate the indicated means and standard errors.

The number of residual γ-H2AX foci 8 h after exposure to 1 Gy is in *LIG1*$^{-/-}$ cells is similar to the wt, suggesting, in agreement with previous PFGE experiments, similar repair capacity. Higher numbers of residual γ-H2AX foci are detected, as expected, in *LIG4*$^{-/-}$ cells, but this repair defect is not further enhanced in the double mutant *LIG1*$^{-/-}$*LIG4*$^{-/-}$ (Paul et al., 2013).

The above observations in aggregate suggest that independently of the applied radiation dose, LIG3, as sole ligase, supports processing of DSBs in D-NHEJ deficient cells and that LIG1 is not required for this function. We further conclude that the DSB repair pathways within which LIG3 operates, process DSBs with kinetics slower than D-NHEJ (Paul et al., 2013).

4.8 A mitochondria specific LIG3 rescues DT40 cells lethality but has no influence on DSB repair

The lethality of *LIG3* knockout limits the conclusive analysis of LIG3 and LIG1 function and their interplay during DSB repair. However, in agreement with recent studies, we observed that DT40 cell lethality associated with LIG3 knockout can be rescued by expressing a mitochondria specific form (M2I). The generated *LIG3*$^{-/M2I}$, mutant carries one null *LIG3* allele and one altered allele that lacks the second translation initiation site (M2I), which is needed to generate the nuclear version of LIG3 (Arakawa et al., 2012). This mutant expresses exclusively the mitochondrial form of LIG3 which can be visualized by immunofluorescence microscopy (Figure 31).

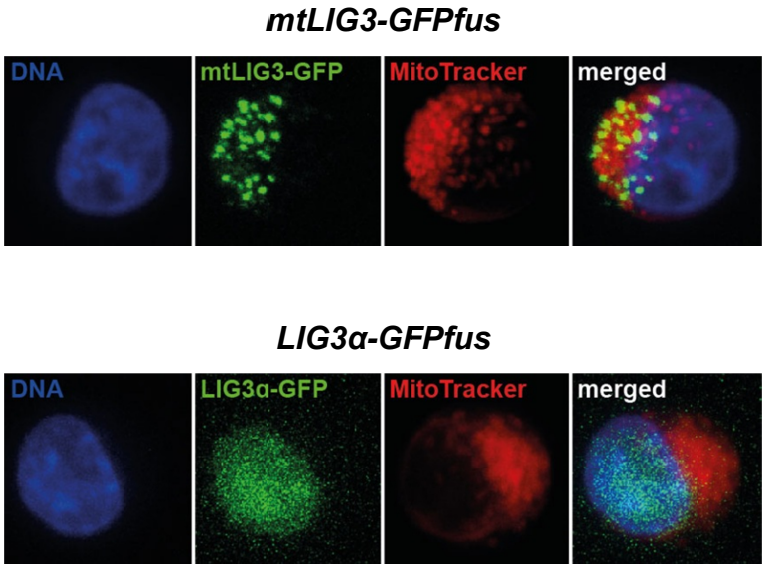

Figure 31: A mitochondria specific LIG3 is able to rescue LIG3 lethality (Paul et al., 2013). Subcellular localization studies by live cell imaging using mtLIG3-GFP and LIG3α-GFP fusion proteins to follow the intracellular distribution of these LIG3 variants and MitoTracker Deep Red to visualize the mitochondria. Cell nuclei were counterstained with Hoechst 33342. Note the colocalization between GFP and Deep Red that indicates the localization of mtLIG3 in the mitochondria.

The intracellular localization studies show through the expression of the tagged proteins mtLIG3-GFP and LIG3α-GFP a clear compartmentalization in the mitochondria by mtLIG3-GFP and a distribution all over the nucleus by LIG3α-GFP, respectively (Figure 31) (Paul et al., 2013).

To compromise D-NHEJ and to further narrow-down the choice of ligases for DSB repair, we knocked out *LIG4* in the *LIG3*$^{-/M2I}$ background to generate the double mutant *LIG3*$^{-/M2I}$*LIG4*$^{-/-}$. Note, in this mutant LIG1 is the only remaining DNA ligase in the nucleus (Paul et al., 2013). The DSB repair kinetics obtained are summarized in Figure 32.

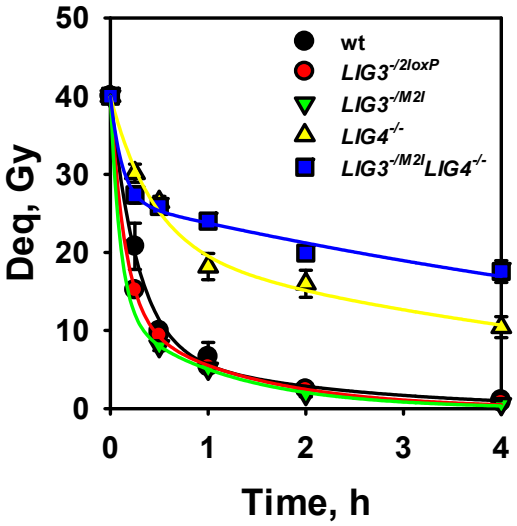

Figure 32: A mitochondria specific LIG3 rescues DT40 cells lethality but has no influence on DSB repair (Paul et al., 2013). Kinetics of DSB repair in wt, *LIG3*$^{-/2loxP}$, *LIG3*$^{-/M2I}$, *LIG4*$^{-/-}$ and *LIG3*$^{-/M2I}$*LIG4*$^{-/-}$ after exposure to 40 Gy X-rays. Results from at least two independent experiments with 4 samples each were used to calculate the indicated means and standard errors.

The resulting mutant *LIG3*$^{-/M2I}$ grows normally (data not shown) and shows normal levels of DSB repair similar to those of wt and *LIG3*$^{-/2loxP}$ cells. Under these conditions, DSB repair is supported by LIG4, LIG1 and, possibly, traces of LIG3 that remain in the cell nucleus.

The double mutant *LIG3*$^{-/M2I}$*LIG4*$^{-/-}$ shows a slightly reduced potential for DSB repair when compared to the single *LIG4*$^{-/-}$ mutant.

These results implicate LIG1 in B-NHEJ taking place in the absence of LIG4 and suggest that the efficiency of LIG1 for this function is lower than that of LIG3. In fact, it is possible that DSB rejoining in this mutant would be further reduced if the function of residual nuclear LIG3 could be inhibited (Paul et al., 2013).

4.9 Deletion of LIG3 reveals a function of LIG1 in the processing of IR-induced DSBs by B-NHEJ

In an effort to generate a better defined system to measure the role of LIG1 in DSB repair we designed and develop a genetic system allowing the complete elimination of LIG3 in DT40 cells. For this purpose, we attempted rescuing the mitochondria function of LIG3, which was found to be essential for cell survival, with the gene *Cdc9*. *Cdc9* is the yeast homolog of LIG1 but functions also in the mitochondria owing to its MT signal. Indeed, *Cdc9* rescues the mitochondria defect and allows us to generate cells entirely lacking LIG3. Since we were not successful in generating the *LIG3*$^{-/-}$*LIG4*$^{-/-}$*Cdc9* double mutant, we utilized a specific DNA-PKcs inhibitor, NU7441, which chemically compromises D-NHEJ to simulate the LIG4 defect (Paul et al., 2013). The obtained DSB repair kinetics of *LIG3*$^{-/-}$*Cdc9* cells are displayed in Figure 33.

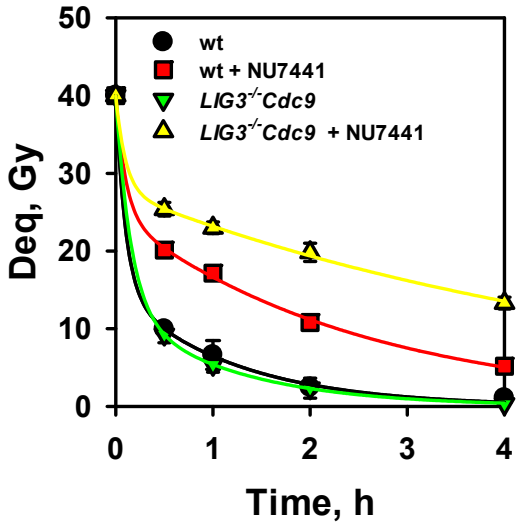

Figure 33: Deletion of LIG3 reveals a function of LIG1 in the processing of IR-induced DSBs by B-NHEJ (Paul et al., 2013). Kinetics of DSB repair in wt and *LIG3*$^{-/-}$*Cdc9* cells measured in the presence or absence of 10 µM NU7441, a DNA-PKcs specific inhibitor. This *LIG3*$^{-/-}$ mutant is viable as a result of the expression of the yeast homolog of LIG1, *Cdc9* (Arakawa et al., 2012). Results from at least two independent experiments with 4 samples each were used to calculate the indicated means and standard errors.

The repair of IR induced DSBs in *LIG3*$^{-/-}$*Cdc9* is identical to wt, owing to the presence of LIG4 in this mutant. As was mentioned above, to study the function of LIG1 alone in this system we used NU7441 to inhibit DNA-PKcs and consequentially also D-NHEJ. The results obtained showed a stronger reduction in DSB repair in *LIG3*$^{-/-}$*Cdc9* cells treated with NU7441 than in NU7441 treated wt cells (Figure 33).

These results confirm that in wt cells, B-NHEJ in the presence of NU7441 is carried out by LIG3 and provide additional evidence that LIG1, in *Lig3*$^{-/-}$*Cdc9* cells treated with NU7441, could be involved in B-NHEJ as well. Thus, we conclude that LIG1 could also support B-NHEJ, albeit with lower efficiency than LIG3 (Paul et al., 2013).

4.10 LIG1 is capable to support B-NHEJ in the absence of LIG3

The structural similarity between LIG1 and LIG3 (Pascal et al. 2004) offers a rationale for the possible functional overlap in the functions between the two enzymes. To further delineate the function of LIG1 in DSB repair by B-NHEJ we wished to generate mutants only expressing LIG1 to avoid possible interferences from any other ligase. For this purpose, we generated mutants expressing human LIG1 with a mitochondrial leader sequence, mts-hLIG1, in a *LIG3*$^{-/2loxP}$*LIG4*$^{-/-}$ background (Paul et al., 2013). In this way we were able to generate seven mutant clones, and their characterization is shown in Figure 34.

A

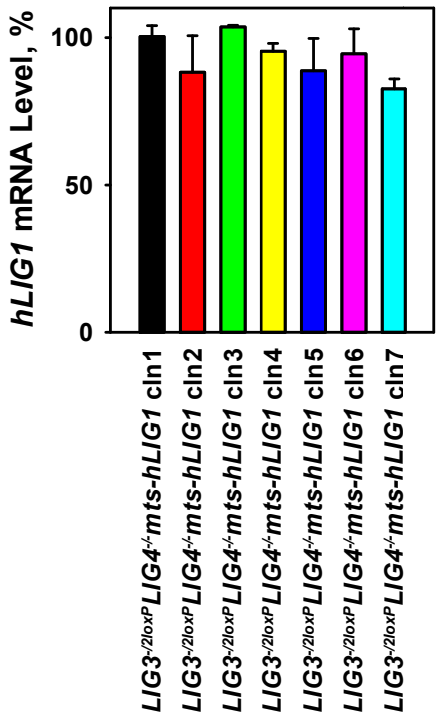
hLIG1 mRNA Level, %
100
50
0
LIG3-/2loxP LIG4-/- mts-hLIG1 cln1
LIG3-/2loxP LIG4-/- mts-hLIG1 cln2
LIG3-/2loxP LIG4-/- mts-hLIG1 cln3
LIG3-/2loxP LIG4-/- mts-hLIG1 cln4
LIG3-/2loxP LIG4-/- mts-hLIG1 cln5
LIG3-/2loxP LIG4-/- mts-hLIG1 cln6
LIG3-/2loxP LIG4-/- mts-hLIG1 cln7

B

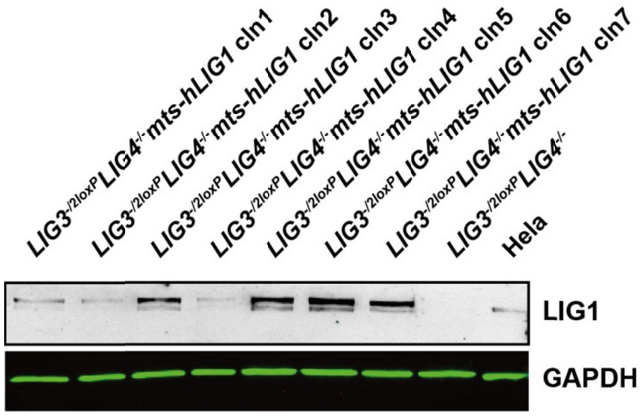
LIG3-/2loxP LIG4-/- mts-hLIG1 cln1
LIG3-/2loxP LIG4-/- mts-hLIG1 cln2
LIG3-/2loxP LIG4-/- mts-hLIG1 cln3
LIG3-/2loxP LIG4-/- mts-hLIG1 cln4
LIG3-/2loxP LIG4-/- mts-hLIG1 cln5
LIG3-/2loxP LIG4-/- mts-hLIG1 cln6
LIG3-/2loxP LIG4-/- mts-hLIG1 cln7
LIG3-/2loxP LIG4-/-
Hela
LIG1
GAPDH

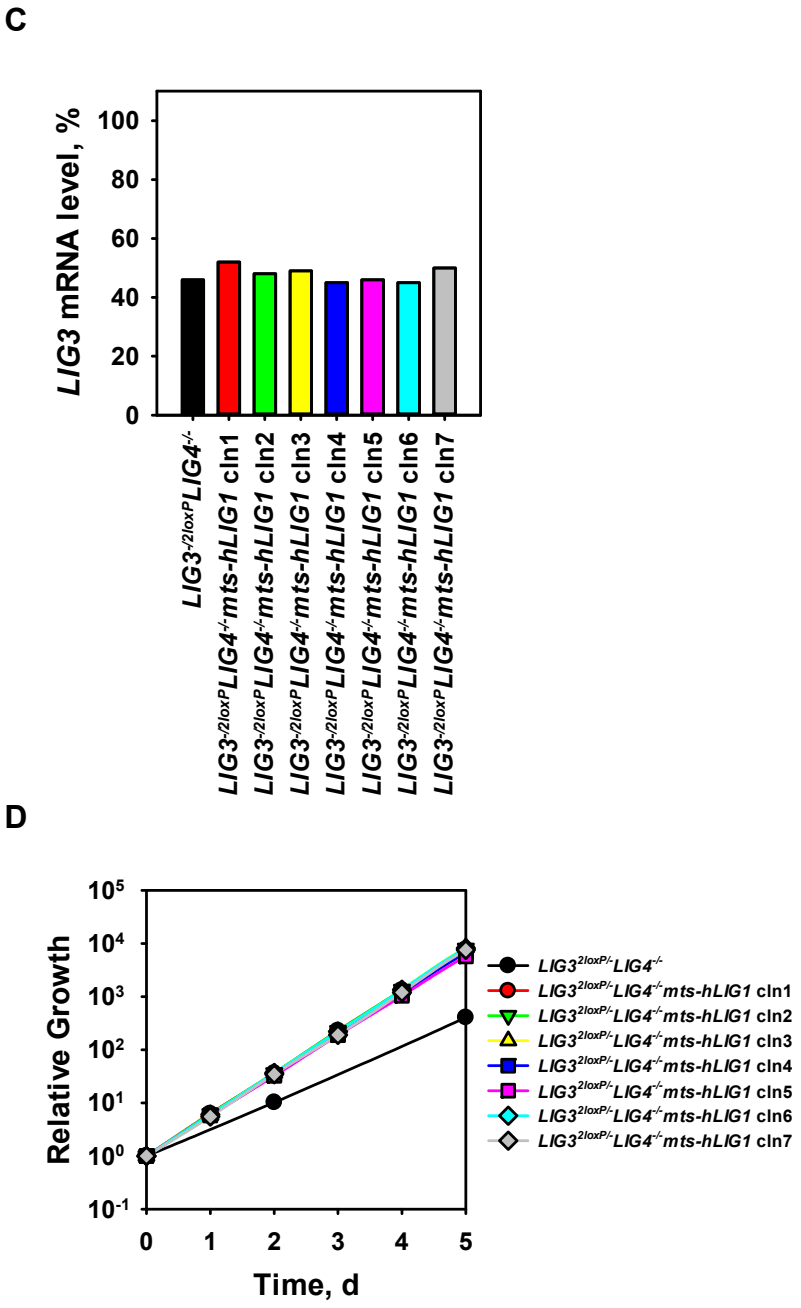

Figure 34: Characterization of *LIG3*$^{-/2loxP}$*LIG4*$^{-/-}$ cell clones ectopically expressing mts-hLig1 (Paul et al., 2013). (A) Human *LIG1* mRNA level measured by real-time PCR in clones 1-7 of *LIG3*$^{-/2loxP}$*LIG4*$^{-/-}$*mts-hLIG1* cells normalized to that measured in clone 3. Results of independent determinations with two primer pairs were used to calculate the indicated means and standard errors. (B) Western blot analysis of hLIG1 protein level in clones 1-7 of *LIG3*$^{-/2loxP}$*LIG4*$^{-/-}$*mts-hLIG1*, *LIG3*$^{-/2loxP}$*LIG4*$^{-/-}$ and Hela extracts. A mouse monoclonal antibody recognizing human but not chicken LIG1 was used. GAPDH is used as loading control. (kindly provided by E. Mladenov) (C) *LIG3* mRNA level measured by real-time PCR in clones 1-7 of *LIG3*$^{-/2loxP}$*LIG4*$^{-/-}$*mts-hLIG1* and parental *LIG3*$^{-/2loxP}$*LIG4*$^{-/-}$ cells normalized to the levels measured in wt cells. (D) Growth kinetics of *LIG3*$^{-/2loxP}$*LIG4*$^{-/-}$ cells and clones 1-7 expressing the mitochondrial version of hLig1, *LIG3*$^{-/2loxP}$*LIG4*$^{-/-}$*mts-hLIG1.* Cells were maintained in the exponential phase of growth by daily dilution in fresh growth medium.

In all seven clones, real time PCR, using primer pairs for hLIG1, shows comparable mRNA levels (Figure 34A); whereas western blotting analysis documents some variation in protein expression (Figure 34B). Since the used Anti-LIG1 Ab is not able to detect the endogenous chicken LIG1, we were able to selectively detect the overexpressed hLIG1. All seven clones show different but detectable LIG1 levels in comparison to the non-transfected control. hLIG1 apparently assists DNA replication in DT40 cells, as indicated by the improved growth characteristics of these clones, compared to the parental cell line *LIG3*$^{-/2loxP}$*LIG4*$^{-/-}$ (Paul et al., 2013).

In these clones one *LIG3* allele is completely eliminated, while the second allele is conditional. All of the examined clones show the expected reduction of *LIG3* mRNA, by 50%, as compared to the wt (Figure 34C) (Paul et al., 2013).

All seven *LIG3*$^{-/2loxP}$*LIG4*$^{-/-}$*mts-hLIG1* mutants show a marked increase in their growth characteristic, which is comparable to wt cells, again highlighting the function of overexpressed LIG1 in replication (Figure 34D) (Paul et al., 2013).

A further treatment of these clones with 4HT leads to the excision of the two loxP sites on the second allele and to the generation of *LIG3*$^{-/-}$*LIG4*$^{-/-}$ cells rescued by mitochondrial hLIG1. These mutants express only the endogenous chicken LIG1 and the overexpressed mitochondrial human LIG1 (Paul et al., 2013). Figure 35 shows the results of the characterization of the generated *LIG3*$^{-/-}$*LIG4*$^{-/-}$*mts-hLIG1* mutants.

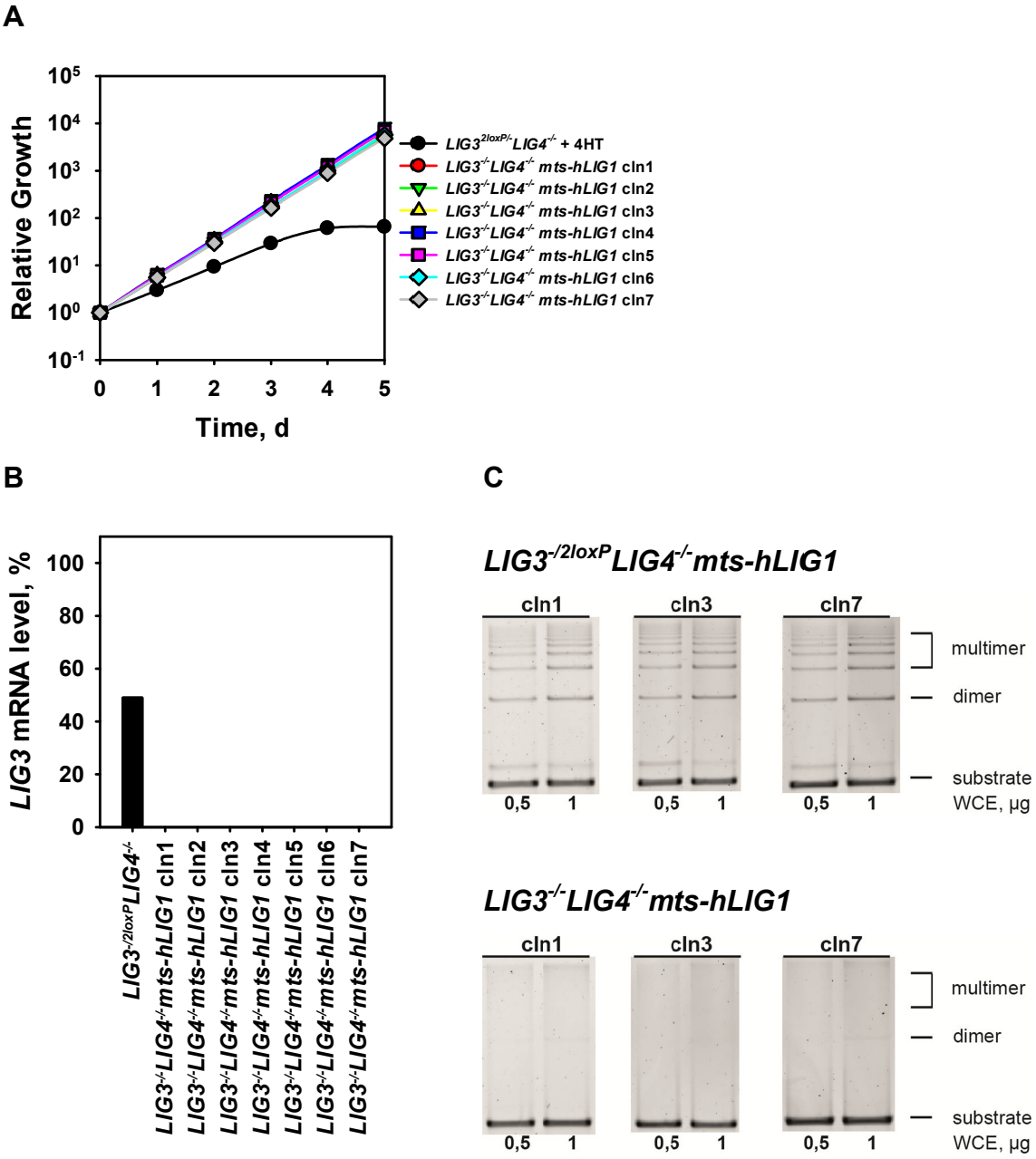

Figure 35: Characterization of LIG3$^{-/2loxP}$LIG4$^{-/-}$ cell clones ectopically expressing mts-hLig1 (Paul et al., 2013). A) Growth kinetics of *LIG3$^{-/2loxP}$LIG4$^{-/-}$mts-hLIG1* cell lines 5 days after 4HT treatment to become *LIG3$^{-/-}$LIG4$^{-/-}$mts-hLIG1*. The growth of *LIG3$^{-/2loxP}$LIG4$^{-/-}$* cells starting immediately after treatment with 4HT is also shown for comparison. Cells were maintained in the exponential phase of growth by daily dilution in fresh growth medium. B) *LIG3* mRNA level in clones 1-7 of *LIG3$^{-/2loxP}$LIG4$^{-/-}$mts-hLIG1* cells after treatment with 4HT for 5 days to generate their *LIG3$^{-/-}$LIG4$^{-/-}$mts-hLIG1* counterparts. *LIG3$^{-/2loxP}$LIG4$^{-/-}$* cells are used as controls and levels are normalized to the wt. C) *In vitro* DNA end-joining of *Sal*I linearized *pSP65* plasmid using whole cell extracts prepared from clones 1, 3 and 7 of the *LIG3$^{-/2loxP}$LIG4$^{-/-}$mts-hLIG1* mutant, before and after treatment with 4HT for 5 days. The linearized input substrate (linear) and the products of end-joining (dimers and multimers) are indicated.

The obtained mutants show no difference in growth characteristics in comparison to their untreated counterparts (Figure 35A), despite excision of the genomic *LIG3* segment between the loxP sites and a marked reduction in protein level (data not shown) and undetectable LIG3 mRNA levels (Figure 35B). In line with this observation, they demonstrate an undetectable *in vitro* end-joining capability as well (Figure 35C) (Paul et al., 2013). For reasons of simplification and since all seven clones show similar characteristics, in the next experiments we will focus only on clones 1, 3 and 7.

To elucidate the role of LIG1 in DSB repair in the generated mutants we performed a set of PFGE experiments. Figure 36 shows the results obtained.

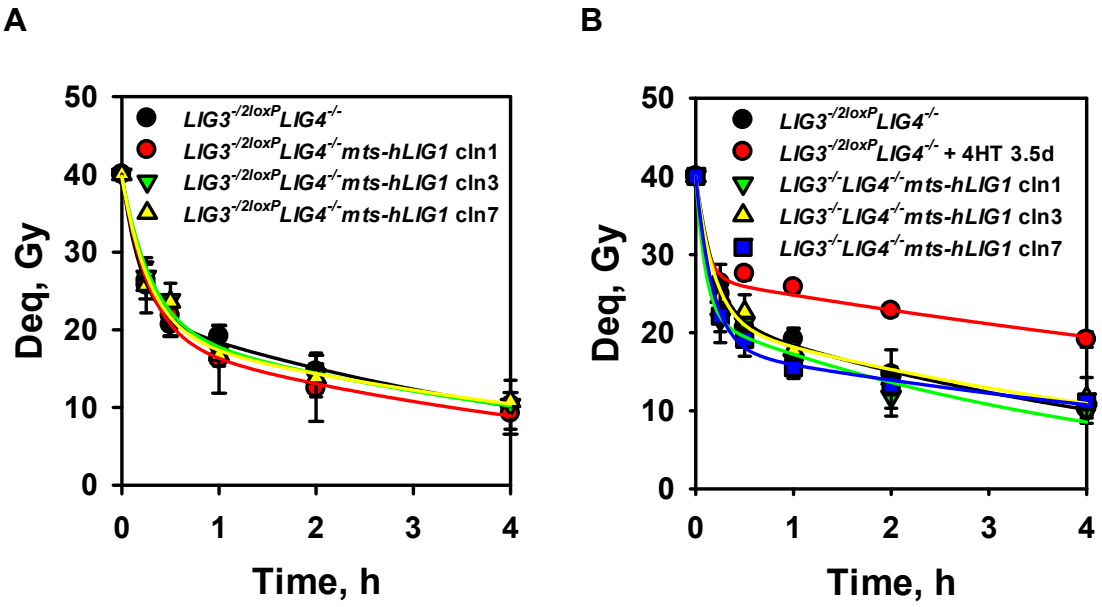

Figure 36: LIG1 is capable to support B-NHEJ in the absence of LIG3 (Paul et al., 2013). A) Kinetics of DSB repair in asynchronous *LIG3*$^{-/2loxP}$*LIG4*$^{-/-}$ and clones 1, 3 and 7 of *LIG3*$^{-/2loxP}$*LIG4*$^{-/-}$*mts-hLig1* cells. B) Kinetics of DSB repair in asynchronous *LIG3*$^{-/2loxP}$*LIG4*$^{-/-}$, clones 1, 3 and 7 of *LIG3*$^{-/-}$*Lig4*$^{-/-}$*mts-hLig1* cells and their counterparts after 3.5 days 4HT treatment, respectively. Results of at least three determinations from two independent experiments were used to calculate the indicated means and standard errors.

Analysis of DSB processing in clones 1, 3 and 4 shows that *LIG3*$^{-/2loxP}$*LIG4*$^{-/-}$ *mts-hLIG1* does not modulate DSB repair in any way in comparison to their parental cell line *LIG3*$^{-/2loxP}$*LIG4*$^{-/-}$. The same clones analyzed five days after treatment with 4HT to generate *LIG3*$^{-/-}$*LIG4*$^{-/-}$*mts-hLIG1* mutants show DSB processing with no difference in comparison to the untreated ones and better repair than the control cell line *LIG3*$^{-/2loxP}$*LIG4*$^{-/-}$ 3.5 days after treatment with 4HT (Paul et al., 2013).

We conclude that the endogenous chicken LIG1 in the nucleus can support B-NHEJ with efficiencies similar to that of LIG3. Of course, we cannot exclude that traces of the overexpressed mts-hLIG1 reach the cell nucleus and also support to B-NHEJ (Paul et al., 2013).

4.11 LIG3 and LIG1 support cell survival in D-NHEJ deficient cells exposed to IR albeit with lower efficiency than LIG4

As a final endpoint for DSB repair, radiosensitivity to killing was determined in the generated mutants using the colony formation assay (Paul et al., 2013). The survival curves obtained for all tested mutants are summarized in Figure 37.

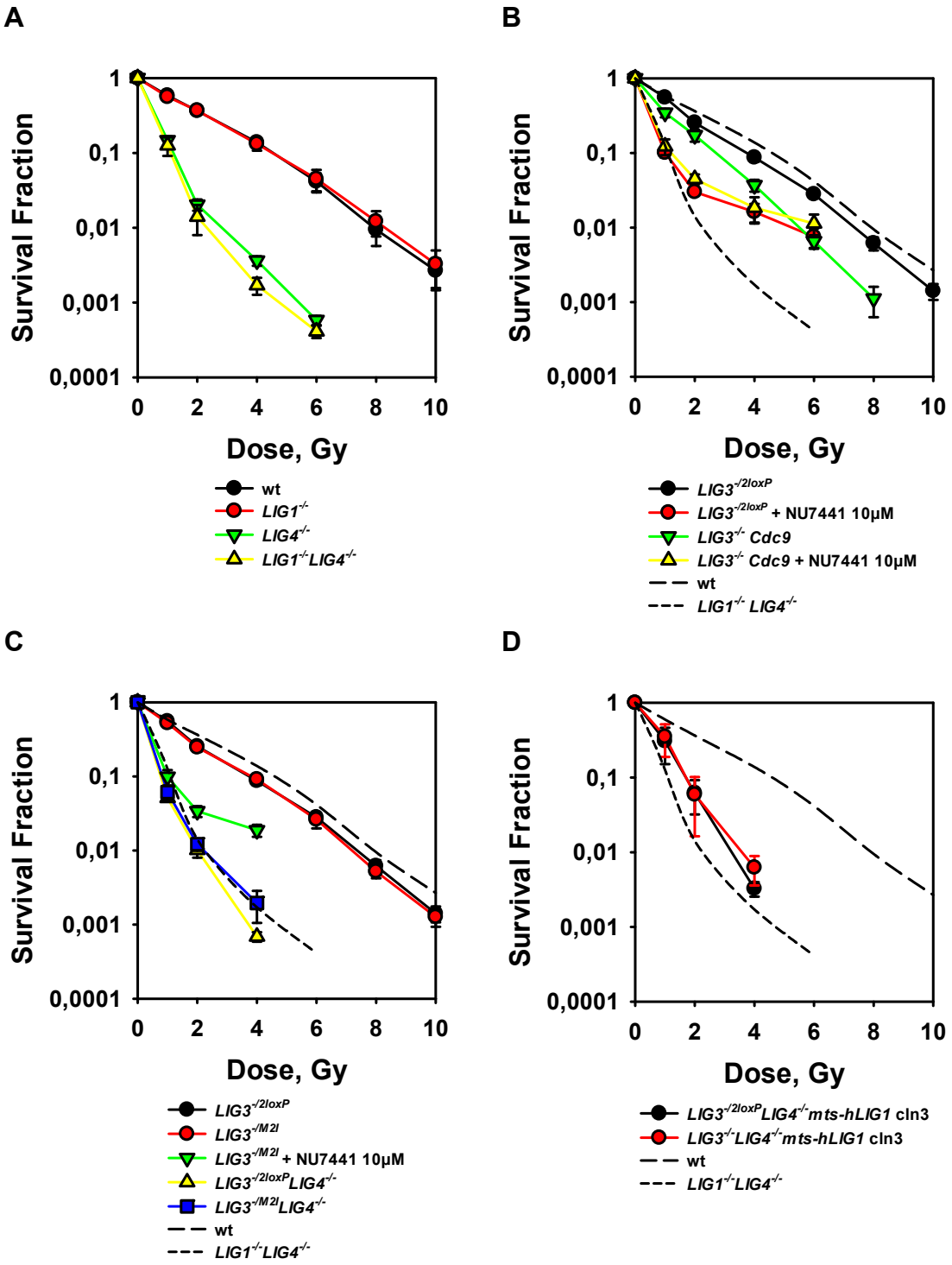

Figure 37: LIG1 and LIG3 contribute to the survival of cells exposed to IR (Paul et al., 2013). A) Cell survival measured by colony formation in wt, *Lig1*$^{-/-}$, *LIG4*$^{-/-}$ and *LIG1*$^{-/-}$*LIG4*$^{-/-}$ cells after exposure to increasing doses of X-rays. B). As in A for *LIG3*$^{-/2loxP}$, and *LIG3*$^{-/-}$*Cdc9* cells after treatment for 1h before and 4h after IR with 10 µM NU7441. The dashed lines trace for comparison the results of wt and *Lig1*$^{-/-}$*LIG4*$^{-/-}$ cells. C) As in B for *LIG3*$^{-/2loxP}$, *LIG3*$^{-/M2I}$, *LIG3*$^{-/2loxP}$*LIG4*$^{-/-}$, and *LIG3*$^{-/M2I}$*LIG4*$^{-/-}$ cells. D). As in B for clone 3 of *LIG3*$^{-/2loxP}$*LIG4*$^{-/-}$*mts-hLig1* and *LIG3*$^{-/-}$*LIG4*$^{-/-}$*mts-hLig1.* Results from at least two independent experiments were used to calculate the indicated means and standard errors.

Wt DT40 cells are modestly sensitive to IR, and exposure to 10 Gy kills about 99% of the population (Figure 37A). Deletion of LIG1 has no consequences for the radiosensitivity of the corresponding knockout mutant suggesting that LIG1 is not essential for the repair processes determining cell radiosensitivity to killing (Figure 37A). As expected, deletion of LIG4 causes a dramatic radiosensitization (Figure 37A). But this radiosensitization is not further impaired by deletion of LIG1 in the double mutant *Lig1*$^{-/-}$*LIG4*$^{-/-}$. In this mutant all ligation functions for the DNA metabolism including repair of all forms of radiation-induced DNA lesions are carried out by LIG3, the only remaining DNA ligase (Paul et al., 2013).

LIG3$^{-/2loxP-}$ cells display a radiosensitivity very similar to the wt and treatment with NU7441 radiosensitizes them to *LIG4*$^{-/-}$ levels (the radioresistant tail probably reflects ~5% of the cell population, which for unknown reasons is not responding to the drug) (Figure 37B). Notably, *LIG3*$^{-/-}$*Cdc9* cells are more radiosensitive than the wt (Figure 37B) pointing to a function of LIG3 in cell survival after exposure to IR even in the presence of LIG4, or to dominant negative effects exerted by the expression of *Cdc9*. However, after treatment with NU7441, *LIG3*$^{-/-}$Cdc9 cells become indistinguishable from the single *LIG4*$^{-/-}$ mutant (Figure 37B). These results clearly suggest that LIG1 can substitute for LIG3 in repair functions related to cell survival with similar efficiency (Paul et al., 2013).

Also *LIG3*$^{-/M2I}$ cells display radiosensitivity very similar to wt cells, indicating that nuclear LIG3 is not essential for cell survival after exposure to IR (Figure 37C). Treatment with NU7441 radiosensitizes this mutant to the same extent as the *LIG3*$^{-/2loxP}$ or *LIG3*$^{-/-}$Cdc9 cells, suggesting that the reduced level of nuclear LIG3 has in the presence of LIG1 no influence on cell radiosensitivity to killing, even when D-NHEJ is compromised (Paul et al., 2013).

The double mutants *LIG3*$^{-/2loxP}$*LIG4*$^{-/-}$ and *LIG3*$^{-/M2I}$*LIG4*$^{-/-}$ show radiosensitivity indistinguishable from that of *LIG4*$^{-/-}$ cells (Figure 37C), indicating that a strong reduction in LIG3 levels leaves the ability of DT40 to deal with lethal radiation lesions unchanged (Paul et al., 2013).

To further delineate the function of LIG1 on cell survival after exposure to IR, we examined clones ectopically expressing mts-hLIG1 either in the *LIG3*$^{-/2loxP}$*LIG4*$^{-/-}$ or the *LIG3*$^{-/-}$*LIG4*$^{-/-}$ genetic background (Figure 37D). Compared to *LIG3*$^{-/2loxP}$*LIG4*$^{-/-}$ cells, *LIG3*$^{-/-}$*LIG4*$^{-/-}$*mts-hLIG1* cells are slightly more radioresistant suggesting that overexpression of LIG1 provides a modest survival advantage to this mutant (Paul et al., 2013).

We conclude from the obtained results that both LIG3 and LIG1 efficiently support survival in DT40 cells (Paul et al., 2013).

5 Discussion

While LIG4 is solidly implicated in the D-NHEJ pathway of DSB repair, LIG1 is thought to play a central role in DNA replication by catalyzing Okazaki-fragment ligation at the replication fork on the lagging strand and in ligating the gaps generated during DSB repair by HR. On the other hand, LIG3 in vertebrates has been previously associated with the repair of single strand breaks and base damage, but now more and more publications implicate LIG3 as a major component of DSB repair by B-NHEJ (Audebert et al., 2004; Cotner-Gohara et al., 2010; Liang et al., 2008; Rosidi et al., 2008; Wang et al., 2005; Wang et al., 2006).

Although LIG1 was also implicated in the above repair pathway under certain conditions, it is still controversial whether LIG1 could substitute for the functions of LIG3 in the B-NHEJ repair pathway (Liang et al., 2008). However, the ligase responsible for B-NHEJ is less conclusively characterized, particularly because often the evidence was of biochemical nature and therefore of unknown physiological significance. For a conclusive elucidation of the function of LIG3 in B-NHEJ, here we focus on the contributions of LIG1 and LIG3 to DSB repair by studying the inherent functional flexibility of the ligase system, through the generation of a large set of knockout and knock-in mutants in the chicken DT40 cell system (summarized in Table 5) (Paul et al., 2013).

Our results confirm, in line with other studies from mouse systems (Gao et al., 2011; Simsek et al., 2011b), that *LIG3* knockout lethality can be rescued by expression of a ligase endowed with a mitochondria specific targeting signal. We could show that the mitochondria specific function of DT40 LIG3 can be supported by Cdc9, the yeast homolog of LIG1, and by human LIG1 with a mitochondrial targeting signal (mts-hLIG1). This has also very recently been demonstrated in mouse cells, where it could be shown that any member of the ligase family is able to support mitochondria function, if it carries an mitochondria specific targeting signal (Simsek et al., 2011b). Thus, it was possible for us to study nuclear specific DSB repair functions supported by

other ligases than LIG3, while mitochondria functionality was maintained by different ligases (Paul et al., 2013).

Noteworthy is that in other cell systems cell survival for several generations is possible after *LIG3* knockout (Gao et al., 2011). This raises the question as to why DT40 cells die immediately after a significant reduction in LIG3 levels. As DT40 cells are chicken B cell lymphocytes they are more prone to apoptosis. In addition, due to their high proliferation rate of ~10 h doubling time, their mitochondria content may be higher than usual. Since mitochondria store a set of apoptotic cell-suicide proteins (Wang and Youle, 2009), the induced mitochondrial malfunction by *LIG3* depletion may cause the release of these proteins and the inception of apoptosis (Paul et al., 2013).

Remarkably, peripheral blood monocytes (PBMCs) lack the DNA repair proteins XRCC1, LIG3α, PARP1 and DNA-PKcs but have intact mitochondria. PBMCs are non-dividing cells and consequently hypersensitive to DNA damage. Monocyte differentiation generates macrophages and dendritic cells, and interestingly these cells have restored XRCC1 and LIG3α protein levels and are resistant to methylating agents (Bauer et al., 2012).

Notably, it is possible to generate cells that lack mitochondria by long-term treatment with low levels of ethidium bromide (Leibowitz, 1971). These cells are then resistant to apoptosis and cell death (Ferraresi et al., 2008; Park et al., 2004). This observation indicates that DT40 specific parameters generate the response observed upon LIG3 depletion and requires further studies.

In the present work and for the first time we were able to demonstrate in a clean genetic background an impressive and not previously appreciated potential of LIG3 to substitute for other ligases in all essential aspects of the DNA metabolism. The obtained PFGE results show that, while repair of DSBs is severely compromised in the absence of LIG4, efficient DSB rejoining is still possible, albeit with slower kinetics. Since this rejoining remains unchanged in the double *LIG1*$^{-/-}$*LIG4*$^{-/-}$ mutant, where LIG3 is the sole remaining ligase, the contribution of LIG3 in DSB repair is unequivocally shown. Similar conclusions could be drawn from γ-H2AX foci kinetic data and survival curve data to conclusively implicate LIG3 in B-NHEJ (Paul et al., 2013).

Since alternative pathways of NHEJ operating as backup have been associated with various functions of the immune system and in telomere maintenance, the results also implicate LIG3 in genomic stability (McVey and Lee, 2008; Nussenzweig and Nussenzweig, 2007). LIG3 via B-NHEJ is predominantly responsible for the formation of chromosome translocations (Simsek et al., 2011a), although this outcome is not a universal finding for LIG3 (Boboila et al., 2012). Also the observation that in several cancer cell lines LIG3 is overexpressed, e.g. CML cell lines that are positive for BCR-ABL translocation (Chen et al., 2008), indicates an increased usage of LIG3 and B-NHEJ for DSB repair in this context (Sallmyr et al., 2008; Tobin et al., 2012a; Tobin et al., 2012b). Possible functions of LIG3 in DSB repair are also supported by the impressive substrate flexibility of LIG3 (Tomkinson and Mackey, 1998) and its special domain structure. The N-terminal zinc finger domain of LIG3 normally serves as a nick sensor and mediates together with the catalytic core an intermolecular ligation (Cotner-Gohara et al., 2010).

It is commonly thought that XRCC1 is a protein partner of LIG3 (Caldecott et al., 1994) and that both molecules operate in a complex as they form a heterodimer through their BRCT domains (Caldecott, 2003). However, cells deficient in XRCC1 fail to show decreased usage of B-NHEJ as indicated by increased usage of microhomology (Verkaik et al., 2002). Interestingly, several recent reports uncoupled the function of LIG3 from XRCC1 in certain cellular functions (Gao et al., 2011; Simsek et al., 2011b) including repair of DSBs induced during Ig heavy chain class switch recombination by alternative end-joining; they conclude that XRCC1 is not a prerequisite factor for B-NHEJ (Boboila et al., 2012).

Therefore, we consider possible that in DT40 cells LIG3 operates in B-NHEJ without need for XRCC1. Additionally, in mammalian mitochondria XRCC1 is absent, indicating that LIG3 within the mitochondria does not require XRCC1 for function. In line with this, an interaction of LIG3α with mitochondrial polymerase γ has been shown (De and Campbell, 2007). Since we were not able to identify a XRCC1 homolog in the known DT40 chicken genome, we are not in a position to conclusively address the question as to whether in DT40 cells LIG3 requires XRCC1 for some of its functions (Paul et al., 2013).

Our investigations revealed that LIG3, as sole cellular DNA ligase, supports repair of DSBs in a *LIG1*$^{-/-}$*LIG4*$^{-/-}$ background. In these mutants deletion of LIG4 compromises D-NHEJ, allowing DSB processing by LIG3 via B-NHEJ (Mladenov and Iliakis, 2011). Similarly, robust DSB repair via B-NHEJ is observed in *LIG3*$^{-/-}$*LIG4*$^{-/-}$ mutants rescued with mts-hLIG1. In this mutant LIG1 is the only remaining DNA ligase and covers for all ligation requirements of DSB repair, while the *LIG4* knockout shifts DSB processing from D-NHEJ to B-NHEJ. In line with this, *LIG3*$^{-/-}$*Cdc9* cells, treated with NU7441 to compromise D-NHEJ, also showed an involvement of LIG1 in DSB repair via B-NHEJ which confirms the above findings. Together with the survival curve data the results point to a remarkable ability of LIG1 and LIG3 to support DSB repair by B-NHEJ with similar efficiency and in an apparently interchangeable manner (Paul et al., 2013).

Our results extend and modify earlier biochemical observations for LIG3 (Audebert et al., 2004; Cotner-Gohara et al., 2010; Liang et al., 2008; Rosidi et al., 2008; Wang et al., 2006), which favored the function of the protein in B-NHEJ, although LIG1 was also implicated under certain conditions (Liang et al., 2008). The similarity between the protein structures of LIG1 and LIG3 offers an explanation of the functional overlap between these two enzymes (Pascal et al., 2004). However, the shown interchangeability of LIG1 and LIG3 in B-NHEJ does not exclude a functional differentiation deriving from differences in their protein domain structure, as both ligases have different interaction partner proteins, which modulate their capability for certain ligation functions in the DNA metabolism. One can argue that in the case of X-rays a large variety of biochemically distinct DSBs is induced and raises the possibility that certain types of DSBs are more efficiently processed by a particular ligase than others (Paul et al., 2013).

It has been proposed that different alternative pathways of DSB repair exist, as LIG1 and LIG3 are differently involved in the formation of chromosome translocations initiated by I-*Sce*I induced DSBs (Simsek et al., 2011a). Indeed, our results also suggest slight differences in the contribution of LIG1 and LIG3 in B-NHEJ. Since *LIG3*$^{-/M2I}$*LIG4*$^{-/-}$ cells, or *LIG3*$^{-/-}$*Cdc9* cells after treatment with NU7441, show a further enhanced defect DSB repair capability in comparison

to *LIG4*$^{-/-}$ or *LIG1*$^{-/-}$*LIG4*$^{-/-}$ cells, perhaps a small subset of IR-induced DSBs is more efficiently processed by LIG3 than by LIG1. We assume only one existing B-NHEJ, which may use the proteins in a sequential manner, depending on their presence. This directly influences its outcome and whether microhomology is used, or not. It might be just convenient using it, but it is not a necessity (Mansour et al., 2010). We also like to point out that differences in the functions and use of LIG1 and LIG3 in B-HNEJ may be species specific, as in a mouse model system depletion of LIG1 generated a more severe effect than depletion of LIG3 (Gao et al., 2011) (Paul et al., 2013).

However, from our results it is clear that the slight advantage of LIG3 in B-NHEJ can be compensated by overexpression of mts-hLIG1, which solidly integrates this ligase into B-NHEJ (Paul et al., 2013). Results from yeast, which generally lack LIG3, and from other eukaryotes, further support a function of LIG1 in B-NHEJ. In yeast, deletion of Dnl4, the homolog of LIG4, or its accessory factor Nej1 reduces DSB repair capability by an alternative pathway to ~50% but does not completely compromise it. These results are consistent with a role of LIG1 in alternative end-joining (Boulton and Jackson, 1996; Lee and Lee, 2007; Ma et al., 2003). In human cells, LIG1 has also been shown to be involved in alternative DSB repair (Liang et al., 2008), and also results obtained in B cells performing Ig class switch recombination indicate a role of LIG1 in alternative end-joining (Boboila et al., 2012).

In the beginning it was thought that LIG3 is restricted to vertebrates, but recent phylogenetic tree studies based on comparisons on the DBD-CC for all three ligases, found *LIG3* in ~30% of the eukaryotes and 4 of the 6 ancestral eukaryotic groups, respectively. Usually the mitochondrial targeting signal (MTS) of LIG3 is used to predict the presence of this ligase in mitochondria. But in some organisms a PCNA-interacting peptide (PIP) box at the N-terminus of LIG1, where no obvious MTS is present in LIG3, makes it difficult to predict which ligase may be localized in the mitochondria of the investigated organism (Simsek and Jasin, 2011).

Since in lower eukaryotes replication and maintenance of mitochondria DNA is part of *LIG1* functions, it will be interesting to consider the evolutionary advantages that are associated with the transfer of this function to *LIG3* in vertebrates. Genome sequencing revealed that LIG3 arose much earlier in eukaryotic evolution than previously suspected. It follows that the absence of LIG3 from many eukaryotes suggests that LIG3 was also lost at several instances during evolution. As a result, closely related organisms can differ in the presence of LIG3 (Simsek and Jasin, 2011).

The results in aggregate suggest that LIG1 and LIG3 operate flexibly in B-NHEJ. This enhances further the flexibility of B-NHEJ in the usage of participating factors (Paul et al., 2013). The apparent adaptability in participating factor selection of B-NHEJ is in stark contrast to the rigid repertoire of factors participating in D-NHEJ and may reflect its primordial nature (DiBiase et al., 2000).

Despite the potential deleterious consequences of B-NHEJ function, little is known about the underlying mechanism of B-NHEJ, its regulation, integration into the cellular DNA DSB processing apparatus and its interaction with components of D-NHEJ and HRR. Therefore, it could be possible that in certain cases, even in repair proficient cells, D-NHEJ fails in some way and thereby permits B-NHEJ to substitute for it. Likewise, it has been found that DNA end-resection, which generates single stranded DNA regions might facilitate the use of microhomology during B-NHEJ and leaves possible interdependencies between B-NHEJ and HRR open (Mladenov and Iliakis, 2011). Since DNA end-processing and the use of homology is an important component of HRR, it would be of great interest to investigate the extent to which irregular HRR events allow, or even initiate the function of B-NHEJ.

In summary, the results outlined above provide the first solid genetic proof for an independent and robust function of both, LIG1 and LIG3 to DSB repair via B-NHEJ. They demonstrate an impressive and previously unrecognized potential interplay of LIG1 and LIG3 to participate interchangeably in DNA metabolisms (Paul et al., 2013). Recently published results in other cell systems (Boboila et al., 2012; Gao et al., 2011; Simsek et al., 2011b) confirm the restricted function of LIG4 in D-NHEJ. Together with our recent results on the ligation requirements of LIG3 in semi-conservative DNA replication (Arakawa et al., 2012), these findings suggest a functional redundancy between LIG1 and LIG3 in DNA replication, NER, and HRR, and a hierarchical relationships between LIG4, LIG3 and LIG1 in DSB repair that should contribute to the stability of vertebrate genomes. It is intriguing that such relationships developed only after the evolutionary appearance of *LIG3,* as *LIG1* and *LIG4* family members have well separated functions in lower eukaryotes.

6 Summary

Among the variety of lesions that are induced by ionizing radiation, the most critical one is the DNA double strand break (DSB). DSBs are highly cytotoxic lesions and if left unrepaired or are misrepaired can lead to chromosomal aberrations and induction of apoptosis or can result in mutations, genomic instability and carcinogenesis. Cells of higher eukaryotes use two major repair pathways to repair their DSBs: homologous recombination repair (HRR) and non-homologous end-joining (NHEJ). Previous biochemical and genetic studies from our lab support the view that vertebrates remove DSBs from their genomes predominantly by two non-homologous end joining (NHEJ) pathways, termed D-NHEJ and B-NHEJ. While D-NHEJ depends on the well characterized activities of DNA-dependent protein kinase (DNA-PK) and LIG4/XRCC4/XLF complexes, the activities and the mechanisms of the alternative, backup NHEJ are less well characterized. Previous studies from our laboratory implicated LIG3 together with PARP in B-NHEJ and histone H1 as an alignment factor. Notably, the contribution of LIG1 to B-NHEJ remains conjectural and although biochemical, cytogenetic and genetic experiments implicate LIG3, this contribution has not been formally demonstrated.

DNA ligase III (LIG3) is beside DNA ligases I (LIG1) and IV (LIG4) one of three mammalian DNA ligases, unique in that it is restricted to vertebrates. The *LIG3* gene of higher eukaryotes generates four distinct DNA ligase polypeptides that serve nuclear and mitochondrial functions. The mitochondrial and nuclear versions LIG3α are synthesized from LIG3 mRNA by an alternative translation initiation mechanism. This N-terminal mitochondrial leader sequence is a unique characteristic of LIG3 that is not shared by any of the other remaining ligases.

To conclusively examine the function of LIG3 in B-NHEJ we generated a series of knockouts in the DT40 system system in cooperation with Hiroshi Arakawa from Helmholtz Center Munich. While *LIG1*$^{-/-}$ and *LIG4*$^{-/-}$ mutants are viable and grow normally, LIG3 knockout is lethal. Therefore, conditional knockout models were developed and combined with knockouts of all other DNA ligases to study the functions of LIG1 and LIG3 in DSB repair.

To study the role of LIG1 in DSB repair we knocked out this ligase in wt and *LIG4*$^{-/-}$ genetic background to generate cells deficient in *LIG1*$^{-/-}$ and double mutants deficient in *LIG1*$^{-/-}$*LIG4*$^{-/-}$. There is no effect on the repair of DSBs measured by PFGE in *LIG1*$^{-/-}$ cells suggesting that this ligase has no measurable contribution to the repair of this form of DNA lesion. *LIG4*$^{-/-}$ cells show a pronounced defect in DSB repair due to the inhibition of D-NHEJ. However, these cells are capable of repairing the majority of IR induced DSBs using B-NHEJ. The repair of the generated double *LIG1*$^{-/-}$*LIG4*$^{-/-}$ knockout mutant was indistinguishable from that of *LIG4*$^{-/-}$ cells providing thus conclusive evidence that a. LIG1 is not required for the repair of DSBs either by B-NHEJ or D-NHEJ, if LIG3 is present and functional and b. that LIG3, the only remaining DNA ligase in this mutant, is an integral component of B-NHEJ. The results were confirmed at low doses in γ-H2AX foci kinetics and in cell survival assays.

In addition, our results confirm, that *LIG3* is essential for survival of higher eukaryotic cells due to its function in the mitochondria. In line with other studies, the *LIG3* knockout lethality can be rescued by expression of a ligase endowed with a mitochondria specific targeting sequence. To conclusively determine the role of LIG1 in DSB repair, we took advantage of these findings and developed a genetic system devoid of LIG3. Therefore we generated cells expressing hLIG1 with a mitochondrial targeting sequence (mts-hLIG1) in the *LIG3*$^{-/-}$*LIG4*$^{-/-}$ genetic background. DSB repair studies of the generated *LIG3*$^{-/-}$*LIG4*$^{-/-}$*mts-hLIG1* mutants show a DSB processing with no difference in comparison to double *LIG1*$^{-/-}$*LIG4*$^{-/-}$ knockout mutants. Since these mutants express only the endogenous chicken LIG1 and the overexpressed mitochondrial human LIG1, we can conclude that also LIG1 is able to support DSB repair by B-NHEJ.

In summary, the results obtained expand the functions of LIG1 to alternative NHEJ and demonstrate a remarkable ability for LIG3 to backup DSB repair by B-NHEJ, in addition to its essential function in the mitochondria. Together with our recent results on DNA replication, these observations uncover a remarkable and previously unappreciated functional flexibility and interchangeability between LIG1 and LIG3 in B-NHEJ.

7 References

Aboussekhra, A., Biggerstaff, M., Shivji, M.K.K., Vilpo, J.A., Moncollin, V., Podust, V.M., Protic, M., Huebscher, U., Egly, J.-M., and Wood, R.D. (1995). Mammalian DNA nucleotide excision repair reconstituted with purified protein components. Cell *80*, 859-868.

Ackland, S.P., Schilsky, R.L., Beckett, M.A., and Weichselbaum, R.R. (1988). Synergistic cytoxicity and DNA strand break formation by bromodeoxyuridine and bleomycin in human tumor cells. Cancer Res *48*, 4244-4249.

Ahnesorg, P., Smith, P., and Jackson, S.P. (2006). XLF Interacts with the XRCC4-DNA Ligase IV Complex to Promote DNA Nonhomologous End-Joining. Cell *124*, 301-313.

Arakawa, H., Bednar, T., Wang, M., Paul, K., Mladenov, E., Bencsik-Theilen, A.A., and Iliakis, G. (2012). Functional redundancy between DNA ligases I and III in DNA replication in vertebrate cells. Nucleic acids research *40*, 2599-2610.

Arakawa, H., Hauschild, J., and Buerstedde, J.-M. (2002). Requirement of the Activation-Induced Deaminase (AID) Gene for Immunoglobulin Gene Conversion. Science *295*, 1301-1306.

Arakawa, H., Lodygin, D., and Buerstedde, J.-M. (2001). Mutant lox P vectors for selectable marker recycle and conditional knockouts. BMC Biotechnology *1*, 7.

Arakawa, H., Saribasak, H., and Buerstedde, J.-M. (2004). Activation-Induced Cytidine Deaminase Initiates Immunoglobulin Gene Conversion and Hypermutation by a Common Intermediate. PLoS Biol *2*, 967-974.

Arnaudeau, C., Lundin, C., and Helleday, T. (2001). DNA double-strand breaks associated with replication forks are predominantly repaired by homologous

recombination involving an exchange mechanism in mammalian cells. J Mol Biol *307*, 1235-1245.

Audebert, M., Salles, B., and Calsou, P. (2004). Involvement of Poly(ADP-ribose) Polymerase-1 and XRCC1/DNA Ligase III in an Alternative Route for DNA Double-strand Breaks Rejoining. J Biol Chem *279*, 55117-55126.

Baba, T.W., Giroir, B.P., and Humphries, E. (1985). Cell lines derived from avian lymphomas exhibit two distinct phenotypes. Virology *144*, 139-151.

Ballarini, F., Alloni, D., Facoetti, A., and Ottolenghi, A. (2008). Heavy-ion effects: from track structure to DNA and chromosome damage. New Journal of Physics *10*, doi:10.1088/1367-2630/1010/1087/075008.

Barnes, D.E., Stamp, G., Rosewell, I., Denzel, A., and Lindahl, T. (1998). Targeted disruption of the gene encoding DNA ligase IV leads to lethality in embryonic mice. Curr Biol *8*, 1395-1398.

Barnes, D.E., Tomkinson, A.E., Lehmann, A.R., Webster, A.D.B., and Lindahl, T. (1992). Mutations in the DNA ligase 1 gene of an individual with immunodeficiencies and cellular hypersensitivity to DNA-damaging agents. Cell *69*, 495-503.

Bassing, C.H., Swat, W., and Alt, F.W. (2002). The Mechanism and Regulation of Chromosomal V(D)J Recombination. Cell *109*, S45-S55.

Bauer, M., Goldstein, M., Heylmann, D., and Kaina, B. (2012). Human Monocytes Undergo Excessive Apoptosis following Temozolomide Activating the ATM/ATR Pathway While Dendritic Cells and Macrophages Are Resistant. PLoS One *7*, e39956.

Baumann, P., Benson, F.E., and West, S.C. (1996). Human Rad51 protein promotes ATP-dependent homologous pairing and strand transfer reactions in vitro. Cell *87*, 757-766.

Bennardo, N., Cheng, A., Huang, N., and Stark, J.M. (2008). Alternative-NHEJ Is a Mechanistically Distinct Pathway of Mammalian Chromosome Break Repair. PLoS Genet *4*, e1000110.

Bentley, D.J., Harrison, C., Ketchen, A.-M., Redhead, N.J., Samuel, K., Waterfall, M., Ansell, J.D., and Melton, D.W. (2002). DNA ligase I null mouse cells show normal DNA repair activity but altered DNA replication and reduced genome stability. J Cell Sci *115*, 1551-1561.

Bentley, D.J., Selfridge, J., Millar, J.K., Samuel, K., Hole, N., Ansell, J.D., and Melton, D.W. (1996). DNA ligase I is required for fetal liver erythropoiesis but is not essential for mammlian cell viability. Nat Genet *13*, 489-491.

Boboila, C., Oksenych, V., Gostissa, M., Wang, J.H., Zha, S., Zhang, Y., Chai, H., Lee, C.-S., Jankovic, M., Saez, L.-M.A*., et al.* (2012). Robust chromosomal DNA repair via alternative end-joining in the absence of X-ray repair cross-complementing protein 1 (XRCC1). Proc Natl Acad Sci USA *109*, 2473-2478.

Boulton, S.J., and Jackson, S.P. (1996). *Saccharomyces cerevisiae* Ku70 potentiates illegitimate DNA double-strand break repair and serves as a barrier to error-prone repair pathways. EMBO J *15*, 5093-5103.

Caldecott, K., Tucker, J.D., Stanker, L.H., and Thompson, L.H. (1995). Characterization of the XRCC1-DNA ligase III complex in vitro and its absence from mutant hamster cells. Nucleic acids research *23*, 4836-4843.

Caldecott, K.W. (2003). XRCC1 and DNA strand break repair. DNA Repair *2*, 955-969.

Caldecott, K.W., McKeown, C.K., Tucker, J.D., Ljungquist, S., and Thompson, L.H. (1994). An Interaction between the Mammalian DNA Repair Protein XRCC1 and DNA Ligase III. Mol Cell Biol *14*, 68-76.

Cardoso, M.C., Joseph, C., Rahn, H.-P., Reusch, R., Nadal-Ginard, B., and Leonhardt, H. (1997). Mapping and Use of a Sequence that Targets DNA Ligase I to Sites of DNA Replication In Vivo. J Cell Biol *139*, 579-587.

Chen, X., Zhong, S., Zhu, X., Dziegielewska, B., Ellenberger, T., Wilson, G.M., MacKerell, A.D., Jr., and Tomkinson, A.E. (2008). Rational Design of Human DNA Ligase Inhibitors that Target Cellular DNA Replication and Repair. Cancer Res *68*, 3169-3177.

Chen, Y., Cairns, R., Papandreou, I., Koong, A., and Denko, N.C. (2009). Oxygen Consumption Can Regulate the Growth of Tumors, a New Perspective on the Warburg Effect. PLoS One *4*, e7033.

Corneo, B., Wendland, R.L., Deriano, L., Cui, X., Klein, I.A., Wong, S.-Y., Arnal, S., Holub, A.J., Weller, G.R., Pancake, B.A.*, et al.* (2007). Rag mutations reveal robust alternative end joining. Nature *449*, 483-486.

Cotner-Gohara, E., Kim, I.-K., Hammel, M., Tainer, J.A., Tomkinson, A.E., and Ellenberger, T. (2010). Human DNA Ligase III Recognizes DNA Ends by Dynamic Switching between Two DNA-Bound States. Biochemistry *49*, 6165-6176.

Cotner-Gohara, E., Kim, I.-K., Tomkinson, A.E., and Ellenberger, T. (2008). Two DNA-binding and Nick Recognition Modules in Human DNA Ligase III. J Biol Chem *283*, 10764-10772.

Critchlow, S.E., Bowater, R.P., and Jackson, S.P. (1997). Mammalian DNA double-strand break repair protein XRCC4 interacts with DNA ligase IV. Curr Biol *7*, 588-598.

Davies, A.J., and Chen, D.J. (2010). A role for ATM kinase activity and Mre11 in microhomology-mediated end-joining. Cell Cycle *9*, 3147-3148.

De, A., and Campbell, C. (2007). A novel interaction between DNA ligase III and DNA polymerase γ plays an essential role in mitochondrial DNA stability. Biochem J *402*, 175-186.

Deriano, L., Stracker, T.H., Baker, A., Petrini, J.H.J., and Roth, D.B. (2009). Roles for NBS1 in Alternative Nonhomologous End-Joining of V(D)J Recombination Intermediates. Mol Cell *34*, 13-25.

Desjardins, P., Frost, E., and Morais, R. (1985). Ethidium Bromide-Induced Loss of Mitochondrial DNA from Primary Chicken Embryo Fibroblasts. Mol Cell Biol *5*, 1163-1169.

DiBiase, S.J., Zeng, Z.-C., Chen, R., Hyslop, T., Curran, W.J., Jr., and Iliakis, G. (2000). DNA-dependent protein kinase stimulates an independently active, nonhomologous, end-joining apparatus. Cancer Res *60*, 1245-1253.

Dinkelmann, M., Spehalski, E., Stoneham, T., Buis, J., Wu, Y., Sekiguchi, J.M., and Ferguson, D.O. (2009). Multiple functions of MRN in end-joining pathways during isotype class switching. Nat Struct Mol Biol *16*, 808-813.

Dore, A.S., Furnham, N., Davies, O.R., Sibanda, B.L., Chirgadze, D.Y., Jackson, S.P., Pellegrini, L., and Blundell, T.L. (2006). Structure of an Xrcc4-DNA ligase IV yeast ortholog complex reveals a novel BRCT interaction mode. DNA Repair *5*, 362-368.

Dulic, A., Bates, P.A., Zhang, X., Martin, S.R., Freemont, P.S., Lindahl, T., and Barnes, D.E. (2001). BRCT Domain Interactions in the Heterodimeric DNA Repair Protein XRCC! - DNA Ligase III. Biochemistry *40*, 5906-5913.

Elledge, S.J. (1996). Cell cycle checkpoints: Preventing an identity crisis. Science *274*, 1664-1672.

Ellenberger, T., and Tomkinson, A.E. (2008). Eukaryotic DNA Ligases: Structural and Functional Insights. Ann Rev Biochem *77*, 313-338.

Elmroth, K., Nygren, J., Martensson, S., Ismail, I.H., and Hammarsten, O. (2003). Cleavage of cellular DNA by calicheamicin γI. DNA Repair *2*, 363-374.

Essers, J., van Steeg, H., de Wit, J., Swagemakers, S.M., Vermeij, M., Hoeijmakers, J.H., and Kanaar, R. (2000). Homologous and non-homologous recombination differentially affect DNA damage repair in mice. EMBO J *19*, 1703-1710.

Feldmann, E., Schmiemann, V., Goedecke, W., Reichenberger, S., and Pfeiffer, P. (2000). DNA double-strand break repair in cell-free extracts from Ku80-deficient cells: implications for Ku serving as an alignment factor in non-homologous DNA end joining. Nucleic acids research *28*, 2585-2596.

Ferraresi, R., Troiano, L., Pinti, M., Roat, E., Lugli, E., Quaglino, D., Taverna, D., Bellizzi, D., Passarino, G., and Cossarizza, A. (2008). Resistance of mtDNA-Depleted Cells to Apoptosis. Cytometry *73A*, 528-537.

Ferrari, G., Rossi, R., Arosio, D., Vindigni, A., Biamonti, G., and Montecucco, A. (2003). Cell Cycle-dependent Phosphorylation of Human DNA Ligase I at the Cyclin-dependent Kinase Sites. J Biol Chem *278*, 37761-37767.

Frank, K.M., Sekiguchi, J.M., Seidl, K.J., Swat, W., Rathbun, G.A., Cheng, H.-L., Davidson, L., Kangaloo, L., and Alt, F.W. (1998). Late embryonic lethality and impaired *V*(D)*J* recombination in mice lacking DNA ligase IV. Nature *396*, 173-177.

Frank, K.M., Sharpless, N.E., Gao, Y., Sekiguchi, J.M., Fergson, D.O., Zhu, C., Manis, J.P., Horner, J., DePinho, R.A., and Alt, F.W. (2000). DNA ligase IV deficiency in mice leads to defective neurogenesis and embryonic lethality via the p53 pathway. Mol Cell *5*, 993-1002.

Frankenberg, D. (1969). A ferrous sulphate dosemeter independent of photon energy in the range from 25 ke v up to 50 mev. Physics in Medicine and Biology *14*, 597-605.

Frosina, G., Fortini, P., Rossi, O., Carrozzino, F., Raspaglio, G., Cox, L.S., Lane, D.P., Abbondandolo, A., and Dogliotti, E. (1996). Two Pathways for Base Excision Repair in Mammalian Cells. J Biol Chem *271*, 9573-9578.

Gao, Y., Katyal, S., Lee, Y., Zhao, J., Rehg, J.E., Russell, H.R., and McKinnon, P.J. (2011). DNA ligase III is critical for mtDNA integrity but not Xrcc1-mediated nuclear DNA repair. Nature *471*, 240-244.

Goodhead, D.T. (1994). Initial events in the cellular effects of ionizing radiations: clustered damage in DNA. Int J Radiat Biol *65*, 7-17.

Goodhead, D.T. (1995). Molecular and cell models of biological effects of heavy ion radiation. Radiat Environm Biophys *34*, 67-72.

Goodhead, D.T., and Nikjoo, H. (1989). Track structure analysis of ultrasoft X-rays compared to high- and low-LET radiations. Int J Radiat Biol *55*, 513-529.

Grawunder, U., Wilm, M., Wu, X., Kulesza, P., Wilson, T.E., Mann, M., and Lieber, M.R. (1997). Activity of DNA ligase IV stimulated by complex formation with XRCC4 protein in mammalian cells. Nature *388*, 492-495.

Gu, J., Lu, H., Tippin, B., Shimazaki, N., Goodman, M.F., and Lieber, M.R. (2007). XRCC4: DNA ligase IV can ligate incompatible DNA ends and can ligate across gaps. EMBO J *26*, 1010-1023.

Hall, E.J., and Giaccia, A.J. (2006). Radiobiology for the Radiologist, Sixth Edition edn (Philadelphia, Baltimore, New York, London, Buenos Aires, Hong Kong, Sydney, Tokyo, Lippincott Williams & Wilkins).

Hartwell, L.H. (1974). Saccharomyces cerevisiae cell cycle. Bacteriological Reviews *38*, 164-198.

Helleday, T., Lo, J., van Gent, D.C., and Engelward, B.P. (2007). DNA double-strand break repair: From mechanistic understanding to cancer treatment. DNA Repair *6*, 923-935.

Henderson, L.M., Arlett, C.F., Harcourt, S.A., Lehmann, A.R., and Broughton, B.C. (1985). Cells from an immunodeficient patient (46BR) with a defect in DNA ligation are hypomutable but hypersensitive to the induction of sister chromatid exchanges. Proc Natl Acad Sci USA *82*, 2044-2048.

Heyer, W.-D., Ehmsen, K.T., and Liu, J. (2010). Regulation of Homologous Recombination in Eukaryotes. Annual Review of Genetics *44*, 113-139.

Iliakis, G. (2009). Backup pathways of NHEJ in cells of higher eukaryotes: Cell cycle dependence. Radiother Oncol *92*, 310-315.

Iliakis, G., Blöcher, D., Metzger, L., Okayasu, R., Pantelias, G., and Cicilioni, O. (1991). Measurement of DNA double strand breaks in mammalian cells: Comparison between pulsed field gel electrophoresis and non-unwinding filter elution. NATO ASI Series *H54*, 55-69.

Iliakis, G., Rosidi, B., Wang, M., and Wang, H. (2005). Plasmid-Based Assays for DNA End-Joining In Vitro. In Methods in Molecular Biology: DNA Repair Protocols: Mammalian Systems, D.S. Henderson, ed. (Totowa, N.M., Humana Press Inc.), pp. 123-131.

Iliakis, G., Wang, H., Perrault, A.R., Boecker, W., Rosidi, B., Windhofer, F., Wu, W., Guan, J., Terzoudi, G., and Pantelias, G. (2004). Mechanisms of DNA double strand break repair and chromosome aberration formation. Cytogenetic and Genome Research *104*, 14-20.

Jackson, S.P. (2002). Sensing and repairing DNA double-strand breaks. Carcinogenesis *23*, 687-696.

Jeggo, P.A. (1998). Identification of genes involved in repair of DNA double-strand breaks in mammalian cells. Radiat Res *150 (Suppl)*, S80-S91.

Johnson, R.D., and Jasin, M. (2000). Sister chromatid gene conversion is a prominent double-strand break repair pathway in mammalian cells. EMBO J *19*, 3398-3407.

Johnston, L.H. (1979). The DNA Repair Capability of *cdc9*, the *Saccharomyces cerevisiae* Mutant Defective in DNA Ligase. Molecular & General Genetics *170*, 89-92.

Johnston, L.H., and Nasmyth, K.A. (1978). *Saccharomyces cerevisiae* cell cycle mutant *cdc9* is defective in DNA ligase. Nature *274*, 891-893.

Jones, J., and Simkus, C. (2009). The roles of the RAG1 and RAG2 “non-core” regions in V(D)J recombination and lymphocyte development. Archivum Immunologiae et Therapiae Experimentalis *57*, 105-116.

Kadhim, M.A., Hill, M.A., and Moore, S.R. (2006). Genomic instability and the role of radiation quality. Radiation Protection Dosimetry *122*, 221-227.

Karran, P. (2000). DNA double strand break repair in mammalian cells. Current Opinion in Genetics & Development *10*, 144-150.

Khanna, K.K., and Jackson, S.P. (2001). DNA double-strand breaks: signaling, repair and the cancer connection. Nat Genet *27*, 247-254.

Kinner, A., Wu, W., Staudt, C., and Iliakis, G. (2008). γ-H2AX in recognition and signaling of DNA double-strand breaks in the context of chromatin. Nucleic acids research *36*, 5678-5694.

Konkow, S. (2012). Functions of the MRE11-RAD50-NBS1 complex in DNA double strand break repair. DuEPublico *Ph.D. thesis*.

Krüger, I., Rothkamm, K., and Löbrich, M. (2004). Enhanced fidelity for rejoining radiation-induced DNA double-strand breaks in the G_2 phase of Chinese hamster ovary cells. Nucleic acids research *32*, 2677-2684.

Kulczyk, A.W., Yang, J.-C., and Neuhaus, D. (2004). Solution Structure and DNA Binding of the Zinc-finger Domain from DNA Ligase IIIα. J Mol Biol *341*, 723-738.

Lafleur, M.V.M., Woldhuis, J., and Loman, H. (1979). Alkali-labile sites and post-irradiation effects in gamma-irradiated biologically active double-stranded DNA in aqueous solution. Int J Radiat Biol *36*, 241-247.

Lakshmipathy, U., and Campbell, C. (1999). The Human DNA Ligase III Gene Encodes Nuclear and Mitochondrial Proteins. Mol Cell Biol *19*, 3869-3876.

Leber, R., Wise, T.W., Mizuta, R., and Meek, K. (1998). The XRCC4 gene product is a target for and interacts with the DNA-dependent protein kinase. J Biol Chem *273*, 1794-1801.

Lee, G.S., Neiditch, M.B., Salus, S.S., and Roth, D.B. (2004). RAG Proteins Shepherd Double-Strand Breaks to a Specific Pathway, Suppressing Error-Prone Repair, but RAG Nicking Initiates Homologous Recombination. Cell *117*, 171-184.

Lee, K., and Lee, S.E. (2007). Saccharomyces cerevisiae Sae2- and Tel1-Dependent Single-Strand DNA Formation at DNA Break Promotes Microhomology-Mediated End Joining. Genetics *176*, 2003-2014.

Lee, S.E., Mitchell, R.A., Cheng, A., and Hendrickson, E.A. (1997). Evidence for DNA-PK-dependent and -independent DNA double-strand break repair pathways in mammalian cells as a function of the cell cycle. Mol Cell Biol *17*, 1425-1433.

Lee, Y., Barnes, D.E., Lindahl, T., and McKinnon, P.J. (2000). Defective neurogenesis resulting from DNA ligase IV deficiency requires Atm [In Process Citation]. Genes & Development *14*, 2576-2580.

Leibowitz, R.D. (1971). The effect of ethidium bromide on mitochondrial DNA synthesis and mitochondrial DNA structure in HeLa cells. J Cell Biol *51*, 116-122.

Leung, C.C.Y., and Glover, J.N.M. (2011). BRCT domains: Easy as one, two, three. Cell Cycle *10*, 2461-2470.

Levin, D.S., McKenna, A.E., Motycka, T.A., Matsumoto, Y., and Tomkinson, A.E. (2000). Interaction between PCNA and DNA ligase I is critical for joining of Okazaki fragments and long-patch base-excision repair. Curr Biol *10*, 919-922, S911-S912.

Liang, L., Deng, L., Nguyen, S.C., Zhao, X., Maulion, C.D., Shao, C., and Tischfield, J.A. (2008). Human DNA ligases I and III, but not ligase IV, are required for microhomology-mediated end joining of DNA double-strand breaks. Nucleic acids research *36*, 3297-3310.

Lieber, M.R. (2008). The Mechanism of Human Nonhomologous DNA End Joining. J Biol Chem *283*, 1-5.

Lieber, M.R. (2010). The Mechanism of Double-Strand DNA Break Repair by the Nonhomologous DNA End-Joining Pathway. Ann Rev Biochem *79*, 1.1-1.31.

Lieber, M.R., Ma, Y., Pannicke, U., and Schwarz, K. (2003). Mechanism and regulation of human non-homologous DNA end-joining. Nat Rev Mol Cell Biol *4*, 712-720.

Limbo, O., Chahwan, C., Yamada, Y., de Bruin, R.A.M., Wittenberg, C., and Russell, P. (2007). Ctp1 Is a Cell-Cycle-Regulated Protein that Functions with Mre11 Complex to Control Double-Strand Break Repair by Homologous Recombination. Mol Cell *28*, 134-146.

Lindahl, T., and Barnes, D.E. (1992). Mammalian DNA ligases. Ann Rev Biochem *61*, 251-281.

Lönn, U., Lönn, S., Nylen, U., and Winblad, G. (1989). Altered formation of DNA replication intermediates in human 46 BR fibroblast cells hypersensitive to 3-aminobenzamide. Carcinogenesis *10*, 981-985.

Ma, J.-L., Kim, E.M., Haber, J.E., and Lee, S.E. (2003). Yeast Mre11 and Rad1 Proteins Define a Ku-Independent Mechanism To Repair Double-Strand Breaks Lacking Overlapping End Sequences. Mol Cell Biol *23*, 8820-8828.

Ma, Y., Lu, H., Tippin, B., Goodman, M.F., Shimazaki, N., Koiwai, O., Hsieh, C.-L., Schwarz, K., and Lieber, M.R. (2004). A Biochemically Defined System for Mammalian Nonhomologous DNA End Joining. Mol Cell *16*, 701-713.

Ma, Y., Pannicke, U., Schwarz, K., and Lieber, M.R. (2002). Hairpin Opening and Overhang Processing by an Artemis/DNA-Dependent Protein Kinase Complex in Nonhomologous End Joining and V(D)J Recombination. Cell *108*, 781-794.

Mackey, Z.B., Ramos, W., Levin, D.S., Walter, C.A., McCarrey, J.R., and Tomkinson, A.E. (1997). An Alternative Splicing Event Which Occurs in Mouse Pachytene Spermatocytes Generates a Form of DNA Ligase III with Distinct Biochemical Properties That May Function in Meiotic Recombination. Mol Cell Biol *17*, 989-998.

Mansour, W.Y., Rhein, T., and Dahm-Daphi, J. (2010). The alternative end-joining pathway for repair of DNA double-strand breaks requires PARP1 but is not dependent upon microhomologies. Nucleic acids research *38*, 6065-6077.

McKinnon, P.J., and Caldecott, K.W. (2007). DNA Strand Break Repair and Human Genetic Disease. Annual Review of Genomics and Human Genetics *8*, 37-55.

McVey, M., and Lee, S.E. (2008). MMEJ repair of double-strand breaks (director's cut): deleted sequences and alternative endings. Trends Genet *24*, 529-538.

Mimori, T., and Hardin, J.A. (1986). Mechanism of Interaction between Ku Protein and DNA. J Biol Chem *261*, 10375-10379.

Mladenov, E., and Iliakis, G. (2011). Induction and Repair of DNA Double Strand Breaks: The Increasing Spectrum of Non-homologous End Joining Pathways. Mutation Research/Fundamental and Molecular Mechanisms of Mutagenesis *711*, 61-72.

Montecucco, A., Rossi, R., Levin, D.S., Gary, R., Park, M.S., Motycka, T.A., Ciarrocchi, G., Villa, A., Biamonti, G., and Tomkinson, A.E. (1998). DNA ligase I is recruited to sites of DNA replication by an interaction with proliferating cell nuclear antigen: identification of a common targeting mechanism for the assembly of replication factories. EMBO J *17*, 3786-3795.

Montecucco, A., Savini, E., Weighardt, F., Rossi, R., Ciarrocchi, G., Villa, A., and Biamonti, G. (1995). The N-terminal domain of human DNA ligase I contains the nuclear localization signal and directs the enzyme to sites of DNA replication. EMBO J *14*, 5379-5386.

Moser, J., Kool, H., Giakzidis, I., Caldecott, K., Mullenders, L.H.F., and Fousteri, M.I. (2007). Sealing of Chromosomal DNA Nicks during Nucleotide Excision Repair Requires XRCC1 and DNA Ligase III[alpha] in a Cell-Cycle-Specific Manner. Mol Cell *27*, 311-323.

Mothersill, C., and Seymour, C. (2006). Radiation-Induced Bystander Effects: Evidence for an Adaptive Response to Low Dose Exposures? Dose-Response *4*, 283-290.

Moynahan, M.E., and Jasin, M. (2010). Mitotic homologous recombination maintains genomic stability and suppresses tumorigenesis. Nat Rev Mol Cell Biol *11*, 196-207.

Nash, R.A., Caldecott, K.W., Barnes, D.E., and Lindahl, T. (1997). XRCC1 Protein Interacts with One of Two Distinct Forms of DNA Ligase III. Biochemistry *36*, 5207-5211.

Niida, H., and Nakanishi, M. (2006). DNA damage checkpoints in mammals. Mutagenesis *21*, 3-9.

Nikjoo, H., Charlton, D.E., and Goodhead, D.T. (1994). Monte Carlo Track Structure Studies of Energy Deposition and Calculation of Initial DSB and RBE. Advances in Space Research *14*, 10161-10180.

Nikjoo, H., and Goodhead, D.T. (1991). Track structure analysis illustrating the prominent role of low-energy electrons in radiobiological effects of low-LET radiations. Physics in Medicine and Biology *36*, 229-238.

Nimonkar, A.V., Özsoy, A.Z., Genschel, J., Modrich, P., and Kowalczykowski, S.C. (2008). Human exonuclease 1 and BLM helicase interact to resect DNA and initiate DNA repair. Proc Natl Acad Sci USA *105*, 16906-16911.

Nussenzweig, A., and Nussenzweig, M.C. (2007). A Backup DNA Repair Pathway Moves to the Forefront. Cell *131*, 223-225.

Okano, S., Lan, L., Caldecott, K.W., Mori, T., and Yasui, A. (2003). Spatial and Temporal Cellular Responses to Single-Strand Breaks in Human Cells. Mol Cell Biol *23*, 3974-3981.

Okano, S., Lan, L., Tomkinson, A.E., and Yasui, A. (2005). Translocation of XRCC1 and DNA ligase IIIα from centrosomes to chromosomes in response to DNA damage in mitotic human cells. Nucleic acids research *33*, 422-429.

Olive, P.L. (1998). The Role of DNA Single- and Double-Strand Breaks in Cell Killing by Ionizing Radiation. Radiat Res *150 (Suppl.)*, S42-S51.

Paap, B., Wilson III, D.M., and Sutherland, B.M. (2008). Human abasic endonuclease action on multilesion abasic clusters: implications for radaition-induced biological damage. Nucleic acids research *36*, 2717-2727.

Park, S.Y., Chang, I., Kim, J.-Y., Kang, S.W., Park, S.-H., Singh, K., and Lee, M.-S. (2004). Resistance of Mitochondrial DNA-depleted Cells against Cell Death. J Biol Chem *279*, 7512-7520.

Pascal, J.M., O'Brien, P.J., Tomkinson, A.E., and Ellenberger, T. (2004). Human DNA ligase I completely encircles and partially unwinds nicked DNA. Nature *432*, 473-478.

Paul, K., Wang, M., Mladenov, E., Bencsik-Theilen, A.A., Bednar, T., Wu, W., Arakawa, H., and Iliakis, G. (2013). DNA ligases I and III cooperate in alternative non-homologous end-joining in vertebrates. PLoS One *8*, e59505.

Perez-Jannotti, R.M., Klein, S.M., and Bogenhagen, D.F. (2001). Two Forms of Mitochondrial DNA Ligase III Are Produced in Xenopus laevis Oocytes. J Biol Chem *276*, 48978-48987.

Perrault, R., Wang, H., Wang, M., Rosidi, B., and Iliakis, G. (2004). Backup Pathways of NHEJ Are Suppressed by DNA-PK. J Cell Biochem *92*, 781-794.

Petersen, S., Casellas, R., Reina-San-Martin, B., Chen, H.T., Difilippantonio, M.J., Wilson, P.C., Hanitsch, L., Celeste, A., Muramatsu, M., Pilch, D.R.*, et al.* (2001). AID is required to initiate Nbs1/γ-H2AX focus formation and mutations at sites of class switching. Nature *414*, 660-665.

Petrini, J.H.J., Xiao, Y., and Weaver, D.T. (1995). DNA Ligase I Mediates Essential Functions in Mammalian Cells. Mol Cell Biol *15*, 4303-4308.

Puebla-Osorio, N., Lacey, D.B., Alt, F.W., and Zhu, C. (2006). Early Embryonic Lethality Due to Targeted Inactivation of DNA Ligase III. Mol Cell Biol *26*, 3935-3941.

Rai, R., Zheng, H., He, H., Luo, Y., Multani, A., Carpenter, P.B., and Chang, S. (2010). The function of classical and alternative non-homologous end-joining pathways in the fusion of dysfunctional telomeres. EMBO J *29*, 2598-2610.

Rass, E., Grabarz, A., Plo, I., Gautier, J., Bertrand, P., and Lopez, B.S. (2009). Role of Mre11 in chromosomal nonhomologous end joining in mammalian cells. Nat Struct Mol Biol *16*, 819-825.

Riballo, E., Kühne, M., Rief, N., Doherty, A., Smith, G.C.M., Recio, M.-J., Reis, C., Dahm, K., Fricke, A., Krempler, A.*, et al.* (2004). A pathway of double-strand break rejoining dependent upon ATM, artemis, and proteins locating to γ-H2AX foci. Mol Cell *16*, 715-724.

Richardson, C., Horikoshi, N., and Pandita, T.K. (2004). The role of the DNA double-strand break response network in meiosis. DNA Repair *3*, 1149-1164.

Rosidi, B., Wang, M., Wu, W., Sharma, A., Wang, H., and Iliakis, G. (2008). Histone H1 functions as a stimulatory factor in backup pathways of NHEJ. Nucleic acids research *36*, 1610-1623.

Rossi, R., Villa, A., Negri, C., Scovassi, I., Ciarrocchi, G., Biamonti, G., and Montecucco, A. (1999). The replication factory targeting sequence/PCNA-binding site is required in G_1 to control the phosphorylation status of DNA ligase I. EMBO J *18*, 5745-5754.

Rothkamm, K., Krüger, I., Thompson, L.H., and Löbrich, M. (2003). Pathways of DNA Double-Strand Break Repair during the Mammalian Cell Cycle. Mol Cell Biol *23*, 5706-5715.

Rothkamm, K., and Löbrich, M. (2003). Evidence of a lack of DNA double-strand break repair in human cells exposed to very low X-ray doses. Proc Natl Acad Sci USA *100*, 5057-5062.

Sallmyr, A., Tomkinson, A.E., and Rassool, F.V. (2008). Up-regulation of WRN and DNA ligase IIIα in chronic myeloid leukemia: consequences for the repair of DNA double-strand breaks. Blood *112*, 1413-1423.

Sancar, A., Lindsey-Boltz, L.A., Ünsal-Kacmaz, K., and Linn, S. (2004). Molecular Mechanisms of Mammalian DNA Repair and the DNA Damage Checkpoints. Ann Rev Biochem *73*, 39-85.

Sartori, A.A., Lukas, C., Coates, J., Mistrik, M., Fu, S., Bartek, J., Baer, R., Lukas, J., and Jackson, S.P. (2007). Human CtIP promotes DNA end resection. Nature *450*, 509-514.

Sato, K., Hieda-Shiomi, N., and Hama-Inaba, H. (1983). X-ray-sensitive mutant mouse cells with various sensitivities to chemical mutagens. Mutat Res *121*, 281-285.

Schär, P., Herrmann, G., Daly, G., and Lindahl, T. (1997). A newly identified DNA ligase of Saccharomyces cerevisiae involved in RAD52-independent repair of DNA double-strand breaks. Genes & Development *11*, 1912-1924.

Sekiguchi, J.M., Ferguson, D.O., Chen, H.T., Yang, E.M., Earle, J., Frank, K., Whitlow, S., Gu, Y., Xu, Y., Nussenzweig, A.*, et al.* (2001). Genetic interactions between ATM and the nonhomologous end-joining factors in genomic stability and development. Proc Natl Acad Sci USA *98*, 3243-3028.

Shuman, S. (2009). DNA Ligases: Progress and Prospects. J Biol Chem *284*, 17365-17369.

Shuman, S., and Glickman, M.S. (2007). Bacterial DNA repair by non-homologous end joining. Nature Reviews Microbiology *5*, 852-861.

Simsek, D., Brunet, E., Wong, S.Y.-W., Katyal, S., Gao, Y., McKinnon, P.J., Lou, J., Zhang, L., Li, J., Rebar, E.J.*, et al.* (2011a). DNA Ligase III Promotes Alternative Nonhomologous End-Joining during Chromosomal Translocation Formation. PLoS Genet *7*, e1002080.

Simsek, D., Furda, A., Gao, Y., Artus, J., Brunet, E., Hadjantonakis, A.-K., Van Houten, B., Shuman, S., McKinnon, P.J., and Jasin, M. (2011b). Crucial role for DNA ligase III in mitochondria but not in Xrcc1-dependent repair. Nature *471*, 245-248.

Simsek, D., and Jasin, M. (2011). DNA ligase III: A spotty presence in eukaryotes, but an essential function where tested. Cell Cycle *10*, 3636-3644.

Singh, S.K., Wu, W., Wu, W., Wang, M., and Iliakis, G. (2009). Extensive Repair of DNA Double-Strand Breaks in Cells Deficient in the DNA-PK Dependent Pathway of NHEJ after Exclusion of Heat-Labile Sites. Radiat Res *172*, 152-164.

Sleeth, K.M., Sorensen, C.S., Issaeva, N., Dziegielewski, J., Bartek, J., and Helleday, T. (2007). RPA Mediates Recombination Repair During Replication Stress and Is Displaced from DNA by Checkpoint Signalling in Human Cells. J Mol Biol *373*, 38-47.

Song, W., Levin, D.S., Varkey, J., Post, S., Bermudez, V.P., Hurwitz, J., and Tomkinson, A.E. (2007). A Conserved Physical and Functional Interaction between the Cell Cycle Checkpoint Clamp Loader and DNA Ligase I of Eukaryotes. J Biol Chem *282*, 22721-22730.

Soulas-Sprauel, P., Le Guyader, G., Rivera-Munoz, P., Abramowski, V., Olivier-Martin, C., Goujet-Zalc, C., Charneau, P., and de Villartay, J.-P. (2007). Role for DNA repair factor XRCC4 in immunoglobulin class switch recombination. J Exp Med *204*, 1717-1727.

Sri Krishna, S., Majumdar, I., and Grishin, N.V. (2003). Structural classification of zinc fingers. Nucleic acids research *31*, 532-550.

Stamato, T.D., and Denko, N. (1990). Asymmetric field inversion gel electrophoresis: A new method for detecting DNA double-strand breaks in mammalian cells. Radiat Res *121*, 196-205.

Sutherland, B.M., Bennett, P.V., Sidorkina, O., and Laval, J. (2000). Clustered DNA damages induced in isolated DNA and in human cells by low doses of ionizing radiation. Proc Natl Acad Sci USA *97*, 103-108.

Symington, L.S. (2002). Role of Rad52 epistasis group genes in homologous recombination and double-strand break repair. Microbiology and Molecular Biology Reviews:MMBR *66*, 630-670.

Takeda, S., Nakamura, K., Taniguchi, Y., and Paull, T.T. (2007). Ctp1/CtIP and the MRN Complex Collaborate in the Initial Steps of Homologous Recombination. Mol Cell *28*, 351-352.

Tamulevicius, P., Wang, M., and Iliakis, G. (2007). Homology-Directed Repair is Required for the Development of Radioresistance during S Phase: Interplay between Double-Strand Break Repair and Checkpoint Response. Radiat Res *167*, 1-11.

Teo, S.-H., and Jackson, S.P. (1997). Identification of *Saccharomyces cerevisiae* DNA ligase IV: involvement in DNA double-strand break repair. EMBO J *16*, 4788-4795.

Tobin, L.A., Robert, C., Nagaria, P., Chumsri, S., Twaddell, W., Ioffe, O.B., Greco, G.E., Brodie, A.H., Tomkinson, A.E., and Rassool, F.V. (2012a). Targeting Abnormal DNA Repair in Therapy-Resistant Breast Cancers. Mol Cancer Res *10*, 96-107.

Tobin, L.A., Robert, C., Rapoport, A.P., Gojo, I., Baer, M.R., Tomkinson, A.E., and Rassool, F.V. (2012b). Targeting abnormal DNA double-strand break repair in tyrosine kinase inhibitor-resistant chronic myeloid leukemias. Oncogene *in press*.

Tomkinson, A.E., and Mackey, Z.B. (1998). Structure and function of mammalian DNA ligases. Mutat Res *407*, 1-9.

Tomkinson, A.E., Vijayakumar, S., Pascal, J.M., and Ellenberger, T. (2006). DNA Ligases: Structure, Reaction Mechanism, and Function. Chemical Reviews *106*, 687-699.

Valerie, K., and Povirk, L.F. (2003). Regulation and mechanisms of mammalian double-strand break repair. Oncogene *22*, 5792-5812.

van Gent, D.C., Hoeijmakers, J.H.J., and Kanaar, R. (2001). Chromosomal stability and the DNA double-stranded break connection. Nature Reviews Genetics *2*, 196-206.

Verkaik, N.S., Esveldt-van Lange, R.E.E., van Heemst, D., Brüggenwirth, H.T., Hoeijmakers, J.H.J., Zdzienicka, M.Z., and van Gent, D.C. (2002). Different types of V(D)J recombination and end-joining defects in DNA double-strand break repair mutant mammalian cells. European Journal of Immunology *32*, 701-709.

Walker, J.R., Corpina, R.A., and Goldberg, J. (2001). Structure of the Ku heterodimer bound to DNA and its implications for double-strand break repair. Nature *412*, 607-614.

Wang, C., and Youle, R.J. (2009). The Role of Mitochondria in Apoptosis. Annual Review of Genetics *43*, 95-118.

Wang, H., Perrault, A.R., Takeda, Y., Qin, W., Wang, H., and Iliakis, G. (2003). Biochemical evidence for Ku-independent backup pathways of NHEJ. Nucleic acids research *31*, 5377-5388.

Wang, H., Rosidi, B., Perrault, R., Wang, M., Zhang, L., Windhofer, F., and Iliakis, G. (2005). DNA Ligase III as a Candidate Component of Backup Pathways of Nonhomologous End Joining. Cancer Res *65*, 4020-4030.

Wang, H., Zeng, Z.-C., Bui, T.-A., Sonoda, E., Takata, M., Takeda, S., and Iliakis, G. (2001a). Efficient rejoining of radiation-induced DNA double-strand breaks in vertebrate cells deficient in genes of the RAD52 epistasis group. Oncogene *20*, 2212-2224.

Wang, H., Zhao-Chong, Z., Perrault, A.R., Cheng, X., Qin, W., and Iliakis, G. (2001b). Genetic evidence for the involvement of DNA ligase IV in the DNA-PK-dependent pathway of non-homologous end joining in mammalian cells. Nucleic acids research *29*, 1653-1660.

Wang, M., Wu, W., Wu, W., Rosidi, B., Zhang, L., Wang, H., and Iliakis, G. (2006). PARP-1 and Ku compete for repair of DNA double strand breaks by distinct NHEJ pathways. Nucleic acids research *34*, 6170-6182.

Wang, Y.-G., Nnakwe, C., Lane, W.S., Modesti, M., and Frank, K.M. (2004). Phosphorylation and Regulation of DNA Ligase IV Stability by DNA-dependent Protein Kinase. J Biol Chem *279*, 37282-37290.

Ward, J.F. (1988). DNA damage produced by ionizing radiation in mammalian cells: Identities, mechanisms of formation, and reparability. Progress in Nucleic Acid Research *35*, 95-125.

Ward, J.F. (1990). The yield of DNA double-strand breaks produced intracellularly by ionizing radiation: a review. Int J Radiat Biol *57*, 1141-1150.

Webster, A.D.B., Barnes, D.E., Arlett, C.F., Lehmann, A.R., and Lindahl, T. (1992). Growth retardation and immunodeficiency in a patient with mutations in the DNA ligase 1 gene. Lancet *339*, 1508-1509.

Wei, Y.-F., Robins, P., Carter, K., Caldecott, K., Pappin, D.J.C., Yu, G.-L., Wang, R.-P., Shell, B.K., Nash, R.A., Schar, P.*, et al.* (1995). Molecular cloning and expression of human cDNAs encoding a novel DNA ligase IV and DNA ligase III, an enzyme active in DNA repair and recombination. Mol Cell Biol *15*, 3206-3216.

Weterings, E., and Chen, D.J. (2008). The endless tale of non-homologous end-joining. Cell Res *18*, 114-124.

Weterings, E., and van Gent, D.C. (2004). The mechanism of non-homologous end-joining: a synopsis of synapsis. DNA Repair *3*, 1425-1435.

Wilson, T.E., Grawunder, U., and Lieber, M.R. (1997). Yeast DNA ligase IV mediates non-homologous DNA end joining. Nature *388*, 495-498.

Windhofer, F., Wu, W., and Iliakis, G. (2007a). Low Levels of DNA Ligases III and IV Sufficient for Effective NHEJ. Journal of Cellular Physiology *213*, 475-483.

Windhofer, F., Wu, W., Wang, M., Singh, S.K., Saha, J., Rosidi, B., and Iliakis, G. (2007b). Marked dependence on growth state of backup pathways of NHEJ. Int J Radiat Oncol Biol Phys *68*, 1462-1470.

Witter, R.L., Bose, H.R., and Calnek, B.W. (1979). A proposed method for designating avian cell lines and transplantable tumours. Avian Pathology *8*, 487-498.

Wold, M.S. (1997). Replication Protein A: A heterotrimeric, single-stranded DNA-binding protein required for eukaryotic DNA metabolism. Ann Rev Biochem *66*, 61-92.

Wu, W., Wang, M., Wu, W., Singh, S.K., Mussfeldt, T., and Iliakis, G. (2008). Repair of radiation induced DNA double strand breaks by backup NHEJ is enhanced in G2. DNA Repair *7*, 329-338.

Yan, C.T., Boboila, C., Souza, E.K., Franco, S., Hickernell, T.R., Murphy, M., Gumaste, S., Geyer, M., Zarrin, A.A., Manis, J.P.*, et al.* (2007). IgH class switching and translocations use a robust non-classical end-joining pathway. Nature *449*, 478-482.

Zhang, Y., Hefferin, M.L., Chen, L., Shim, E.Y., Tseng, H.-M., Kwon, Y., Sung, P., Lee, S.E., and Tomkinson, A.E. (2007). Role of Dnl14-Lif1 in nonhomologous end-joining repair complex assembly and suprresion of homologous recombination. Nat Struct Mol Biol *14*, 639-646.

Zhang, Y., Riesterer, C., Ayrall, A.M., Sablitzky, F., Littlewood, T.D., and Reth, M. (1996). Inducible site-directed recombination in mouse embryonic stem cells. Nucleic acids research *24*, 543-548.

List of figures

List of tables

Lebenslauf

Der Lebenslauf ist in der veröffentlichten Version aus Gründen des Datenschutzes nicht enthalten.